

博士論文(要約)

**Workflow Innovations in Natural Product Chemistry  
with the Crystalline Sponge Method**

(結晶スポンジ法による天然物化学研究のワークフロー刷新)

和田 直樹

## Contents

### Chapter 1

<b>General introduction.....</b>	<b>1</b>
1.1 Structural Analysis in Natural Product Chemistry	
1.2 The Crystalline Sponge Method	
1.3 Structural Determination of Natural Products by the Crystalline Sponge Method	
1.4 Overview of This Thesis	
1.5 Reference	

### Chapter 2

<b>Rapid Structural Analysis of Red Algal Halogenated Terpenoids in Minute Quantities .....</b>	<b>21</b>
2.1 Introduction	
2.2 Crystalline Sponge Affinity Screening of Individual Components in Red Algal Crude Extract	
2.3 Absolute Stereochemical Determination of Halogenated Terpenoids by the Crystalline Sponge Method	
2.4 Summary	
2.5 Experimental section	
2.6 References	

### Chapter 3

<b>Stereochemical Analysis of Steroids Using Polar Solvents .....</b>	<b>75</b>
3.1 Introduction	
3.2 Structural Analysis of Cholesterol with the Conventional Soaking Procedures	
3.3 Establishment of New Solvent Conditions Available in the Crystalline Sponge Method	
3.4 Stereochemical Analysis of Hydroxy Steroids	
3.5 Summary	
3.6 Experimental section	
3.7 References	

### Chapter 4

<b>Complete Structural Determination of Trace Amounts of Enzyme Products Produced by Terpene Cyclases of Red Algal Origin.....</b>	<b>113</b>
4.1 Introduction	
4.2 Heterologous Expression of a Putative Sesquiterpene Cyclase LphTPS-C	
4.3 Isolation and Structural Elucidation of a Novel Sesquiterpenol: Haraldol	
4.4 Isolation and Structural Elucidation of a Novel Sesquiterpene <i>epi</i> -germacrene E from a Putative Sesquiterpene Cyclase LphTPS-B	
4.5 Structural Elucidation of a Chlorine Adduct	
4.6 Summary	
4.7 Experimental section	
4.8 Reference	

### Chapter 5

<b>Summary and Perspective.....</b>	<b>162</b>
<b>List of Publications.....</b>	<b>166</b>
<b>Acknowledgements.....</b>	<b>167</b>



# Chapter 1

## General Introduction

### 1.1 Structural Analysis in Natural Product Chemistry

Living things (organisms) produce a wide variety of chemical substances, ranging from primary metabolites which are vital for all organisms such as deoxyribonucleic acid (DNA), ribonucleic acid (RNA), amino acids, and proteins, to secondary metabolites (hereinafter referred to as natural products) derived from biosynthetic pathways unique to each species. Although the biological role of natural products on each organism (bioactivities) are still largely undiscovered, some natural products are known to exhibit specific bioactivities as pheromones,<sup>[1]</sup> repellents,<sup>[2]</sup> or toxins.<sup>[3]</sup> Humans have been aware of the mysterious functions

of natural products since long before the development of chemistry as an academic field, and have used living materials containing natural products as folk medicines,<sup>[4]</sup> and sometimes even as luxury items<sup>[5]</sup> or poisons.<sup>[6]</sup> As of 2019, 23.4% of all new approved drugs were natural products or their derivatives,<sup>[7]</sup> thus humans have been enjoying extraordinary benefits from natural products.

Attempts to explore valuable natural products from organisms follows the development of natural product chemistry, in which scientists extract and purify compounds of interest, perform structural analysis of chemical substances, evaluate bioactivities, establish synthetic routes to natural products with chemical reactions (total synthesis), and recently elucidate biosynthetic machineries based on genomic information.<sup>[8]</sup> The development of analytical tools in structural analysis has been greatly promoted by the needs to analyze chemical structures in natural product chemistry. For instance, infrared (IR) spectroscopy, mass spectrometry (MS), and nuclear magnetic resonance (NMR) spectroscopy are considered as the standard tools in contemporary research in natural product chemistry. Since the 1950s, when computers became available at universities and other research institutes, single crystals of natural products have been frequently subjected to single crystal X-ray diffraction (SCXRD) experiments, to obtain atomic images of natural products by mathematically processing diffraction spots that correspond to electron density images.<sup>[9]</sup> Recently, the electron cryo-microscopy (cryoEM) method microcrystal electron diffraction (MicroED) was applied to elucidate the structures of small organic molecules from very tiny crystals (typically ca.  $1 \times 2 \mu\text{m}^2$  size in contrast to  $100 \times 100 \times 100 \mu\text{m}^3$  used in conventional SCXRD experiments).<sup>[10]</sup> Though MicroED was initially proposed as a measurement method in protein crystallography,

the everlasting motivations to analyze chemical structures led to its applications in natural product chemistry.<sup>[11]</sup>

I would like to briefly summarize the history of SCXRD. In 1912, Laue discovered that irradiation of X-ray beams on a single crystal generated diffraction images, and in 1913, William Henry Bragg and his son Lawrence Bragg analyzed the crystal structures by X-ray diffraction. Hodgkin elucidated the three-dimensional structures of penicillin and vitamin B<sub>12</sub> by SCXRD.<sup>[12]</sup> With the dissemination of electronic computers, various analyses can now be performed on personal computers, therefore the users of SCXRD are no longer limited to crystallographers, but SCXRD is used by many researchers engaged in materials science. The softwares for SCXRD (the SHELX packages) developed by Sheldrick since the 1970s are widely used for crystallographic analysis of small molecules today.<sup>[13]</sup>

Since a pair of optical isomers often exhibit different bioactivities, structural determination including absolute configurations is an important topic in natural product chemistry. Before the development of two-dimensional NMR measurements and the Mosher methods,<sup>[14]</sup> which can provide detailed information on stereochemical structures including absolute configurations, SCXRD was the only method that could determine absolute configurations of natural products directly. In SCXRD, Flack and Parsons conceived a crystallographic parameter (what is called “the Flack parameter”) to assess precision of absolute structural assignment based on X-ray diffraction intensities.<sup>[15]</sup> While SCXRD directly provides information on three-dimensional structures of analytes, NMR stereochemical determination is achieved through measurement and interpretations of complicated spectra, thus the assignments by NMR are considered to be less clear and reliable. Indeed, there are many examples of

incorrect structural assignments of natural products caused by misinterpretation of NMR spectra.<sup>[16]</sup> Although MicroED can give the three-dimensional structures of natural products from samples in very tiny scales, it cannot be applied to determination of absolute configurations because the anomalous scattering effects are not observed at the optical wavelengths used in electron diffraction experiments. Electronic circular dichroism (ECD) and vibrational circular dichroism (VCD) spectroscopy are also often used to determine absolute configurations by comparing calculated and measured spectra.<sup>[17]</sup> The two methods are, however, difficult to apply to natural products with conformational flexibility or with multiple chiral centers.

To summarize, it is important to accurately determine chemical structures including absolute configurations in natural product chemistry. Among the various tools in structural analysis, SCXRD plays an extremely important role in determining absolute configurations. On the other hand, there are also some cases where SCXRD cannot be integrated in the workflow of structural analysis of natural products: Crystallization trials to grow single crystals suitable for SCXRD need natural product samples in at least milligram scales and much research period and efforts, therefore those often end in vain. Moreover, non-crystalline (oily, gaseous, or amorphous) natural products should be derivatized to crystalline compounds through organic synthesis. These drawbacks of SCXRD had forced scientists to conduct scale-up experiments to complete structural analysis of natural products, deteriorating efficiency of the research workflow. In the next section, I will explain a novel method, the crystalline sponge method, that solved several significant issues of SCXRD.

## 1.2 The Crystalline Sponge Method

In 2013, Inokuma *et al.* reported a SCXRD analysis that does not require crystallization of analytes, namely the crystalline sponge (CS) method.<sup>[18]</sup> In the CS method, single crystals of the porous coordination complexes are soaked in sample solutions to form the host-guest structures, and chemical structures of the included samples are elucidated by SCXRD (Fig. 1–1A). Though there are a wide variety of CS lineups,<sup>[19]</sup> the most commonly used host complexes would be  $[(\text{ZnI}_2)_3(\mathbf{1})_2 \cdot x(\text{solvent})]_n$  (**2A**),<sup>[20]</sup>  $[(\text{ZnBr}_2)_3(\mathbf{1})_2 \cdot x(\text{solvent})]_n$  (**2B**)<sup>[21]</sup> and  $[(\text{ZnCl}_2)_3(\mathbf{1})_2 \cdot x(\text{solvent})]_n$  (**2C**)<sup>[21–22]</sup> prepared from zinc halides and tris-(4-pyridyl)-1,3,5-triazine (tpt = **1**) (Fig. 1–1B).

**2A–2C** possess several ideal properties as CS:<sup>[23]</sup> The size of the pores ( $5 \times 8 \text{ \AA}^2$ ) is appropriate for accommodation of common organic molecules; The hydrophobic nature of the pores allows inclusion and binding of the guests; The symmetry is so low that symmetrical operations do not often generate statistical disorders of included compounds; **2A–2C** are able to form multiple intermolecular interactions with guest molecules via electron-rich halogen nodes,  $\pi$ - $\pi$  interaction sites and hydrogen bonding sites at ligand **1**; The interpenetrated network structure can be deformed to fit (induced-fit) the guest molecules, giving it excellent molecular recognition capabilities; The single crystals are stable both chemically and physically so guests and solvents inside the cavity can be exchanged without losing crystallinity. After the original report, various guidelines and technical improvements were suggested to enhance the practicability and crystallographic data quality of the CS method,<sup>[22, 24]</sup> that are also explained in detail in chapter 3–1.

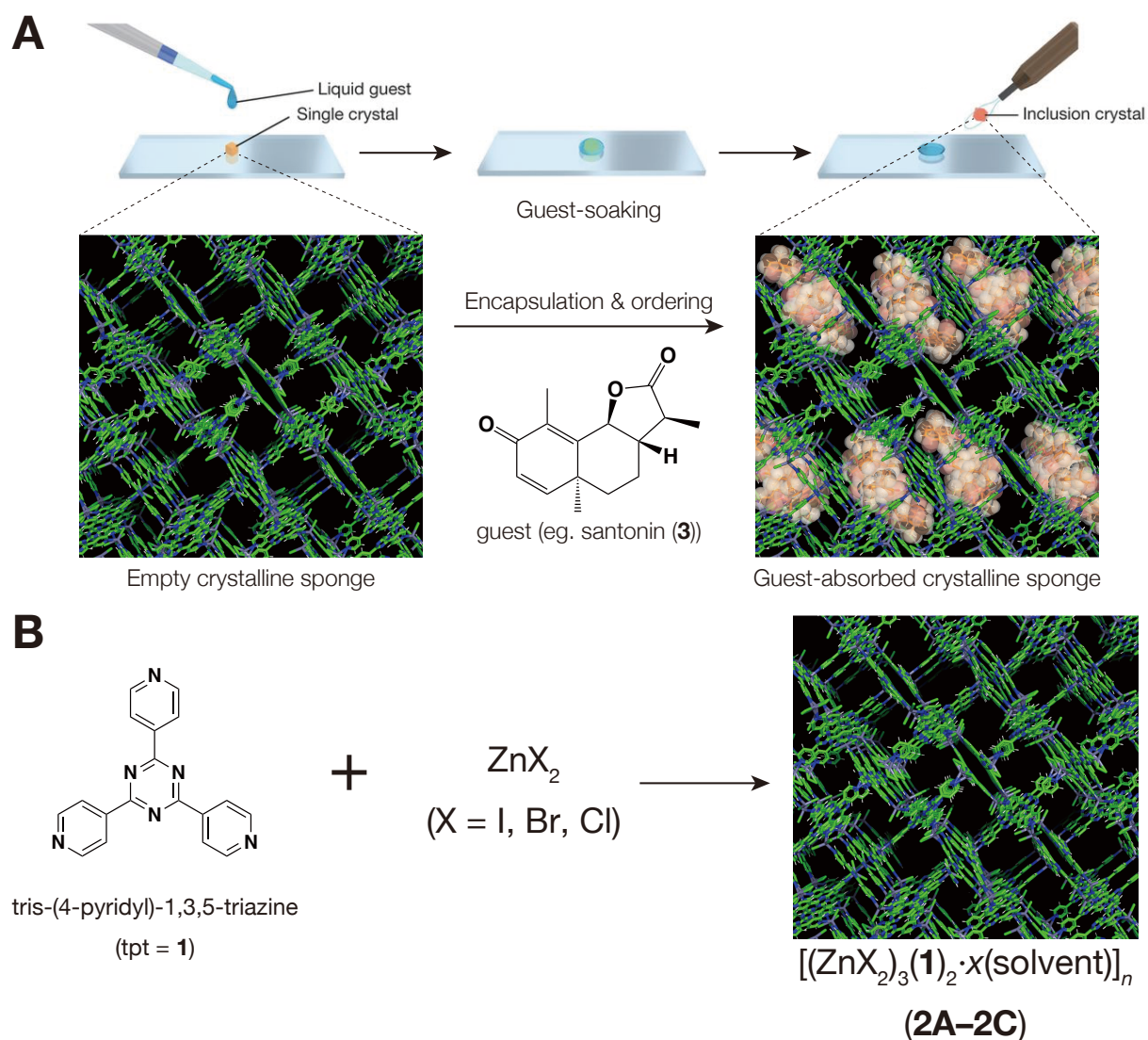


**Fig. 1-1** (A) Schematic representation of the crystalline sponge method. (B) Preparation of single crystals of the crystalline sponges  $[(\text{ZnX}_2)_3(\mathbf{1})_2 \cdot x(\text{solvent})]_n$  (X = I, Br, Cl; **2A-2C**) from ligand **1** and zinc halides. (A) Adapted by permission from Springer Nature: Y. Inokuma *et al.*, *Nature* **2013**, 495, 461-466.<sup>[18]</sup>

The first step in the CS method is to synthesize single crystals of the crystalline sponge. Several methods have been reported for the preparation of the crystalline sponge **2A**, including those using test tubes and multiwell microplates.<sup>[24a, 25]</sup> In the method using test tubes,

single crystals of **2A–2C** are usually obtained by liquid–liquid diffusion crystallization of ligand **1** and zinc halides in a mixture of nitrobenzene and methanol, or chloroform and methanol (Fig. 1–2A). Usually, a nitrobenzene or chloroform solution of **1** is added as the lower layer, and a methanolic solution of zinc halide is gently poured to form the upper layer. The single crystals with appropriate size (ca. 100  $\mu\text{m}$  large) for SCXRD will form in the boundary region of the layers from 3 days to 1 week. Subsequently, solvent in the tubes is replaced with an inert solvent (eg. *n*-hexane and cyclohexane). Except in the cases that sample amount is abundant and target compounds are better guests than solvent, this solvent exchange step should not be omitted.<sup>[24b]</sup> The guest soaking process is sometimes performed in glass tubes and glass plates, but mostly in small vials to allow slow evaporation (Fig. 1–2B). A tiny CS crystal is placed in the bottom of a vial with a small portion of solvent and a guest solution. The vial is then capped and equipped with a needle to allow slow evaporation of the solvent. The guest-soaking process is typically performed over 1 to 2 days at 50 °C, though users of the CS method should be aware that optimization of the guest-soaking process is crucial for successful analysis of each analyte. Generally, four factors need to be varied in optimization: guest concentration, temperature, time, and solvent (investigated in detail in chapter 3). Crystals after the guest-soaking are visually inspected under a microscope with a polarizer. The crystals that retain crystallinity show rainbow-like polarization, whereas the bad crystals do not show polarization and sometimes gather numerous cracks.

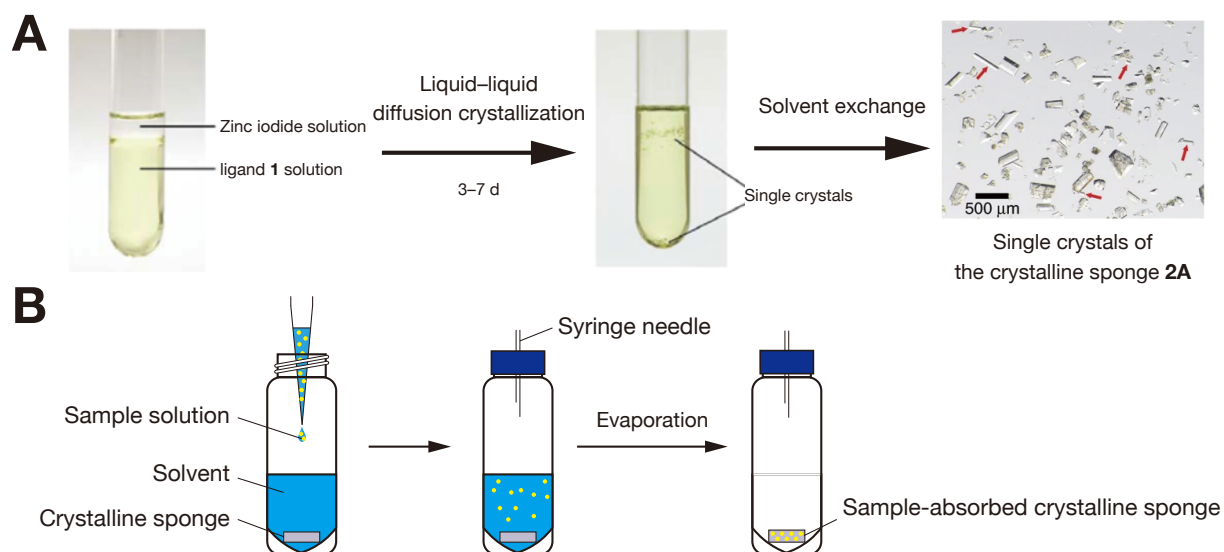


**Fig. 1–2** (A) The synthesis of the crystalline sponge **2A** by liquid–liquid diffusion crystallization. Red arrows indicate crystals suitable for the guest-soaking. (B) Schematic representation of the guest-soaking in small vials. (A) Adapted by permission from Springer Nature: Y. Inokuma *et al.*, *Nat. Protoc.* **2014**, 9, 246-252.<sup>[24a]</sup>

After completion of the guest-soaking, the single crystals of CS are subjected to SCXRD measurements. In the screening step, users of the CS method should pay attention to shapes and resolution limits of diffraction spots, and changes in crystallographic parameters of the unit cells. Elongation of a cell length or expansion of a cell volume are good indication of the guest inclusion. Diffraction images are collected at cryogenic temperatures, integrated, and scaled with crystallographic software. Initial structures can be calculated with the softwares in the SHELX packages (eg. SHELXS and SHELXT<sup>[26]</sup> programs). Since the initial structures possess numerous chemical and crystallographic errors (misassignment of the framework atoms, untreated disorders, and unlocated guests and solvents), crystal structures should be corrected manually by the least-square refinements with SHELXL<sup>[27]</sup> program. In many cases, zinc halide moiety tends to need disorder treatment. Solvents are not usually found in initial



structures and can overlap with the guest molecules. Occupancies of solvents and guests should be appropriately estimated to obtain crystal structures with acceptable crystallographic parameters. In the CS method, guests are mildly (non-covalently) trapped by the framework and crystallographic site-occupancies of the guest molecules frequently become less than 100%. Therefore, atomic displacement parameters (ADPs) can be relatively larger compared to those in routine crystal structures and the users need geometrical restraints to model guest structures. In any case, the users should keep in mind not to use excess numbers of geometrical restraints because that leads to “fabricate” structures of the guest molecules. Inspection of electron densities on the modelled structures is needed throughout the refinement process. I strongly desire the refinement process becomes automated in the future to disseminate the CS method as commonplace as NMR and MS.

The benefit of the CS method is the ability to determine absolute configurations of target compounds with a minimal amount and without introducing heavy atoms. The guest-soaking process in the vials can be performed with only micrograms of the sample per each crystal. The presence of heavy atoms (typically zincs and halides) in the frameworks induces strong anomalous scattering when chiral guests are periodically ordered within the cavity with high occupancies. It is often the case that SCXRD analysis of small organic compounds consisting of light atoms (H, C, N, O, etc.) cannot provide absolute structures because light atoms do not absorb X-ray beams considerably. In such a case, the Flack parameter does not converge to a reasonable value (between 0 and 0.5) or remains close to 0.5, which means that the absolute structures could not be determined from the dataset. Santonin (**3**), consisting of C, H, and O, was the first molecule that the CS method provided the absolute configuration from only 5  $\mu\text{g}$  (Fig. 1–1A). Moreover, it contributed to determination of absolute configurations of

synthetic compounds bearing chiral quaternary carbons<sup>[28]</sup> and with axial chirality,<sup>[29]</sup> of which structural characterization would be recalcitrant by conventional analytical techniques.

Since the original report in 2013, the CS method has contributed to structural analysis of many compounds with structural complexity. The application scope is not limited to natural product chemistry, but also to synthetic chemistry, agrochemistry, medicinal chemistry and food industry. In the next section, I specifically describe the applications in natural product chemistry, where this thesis also aims to contribute.

### 1.3 Structural Determination of Natural Products by the Crystalline Sponge Method

Structural analysis of natural products can be performed more accurately, rapidly, and in smaller scales by the introduction of the CS method. A novel sesterterpene astellifadiene (**4**) isolated from *Aspergillus oryzae* NSAR1 expressing a gene from *Emericella varicolor* NBRC 32302 is an oily compound with a 6-8-6-5-fused ring system.<sup>[30]</sup> Crystallization failures and difficulty in chemical derivatizations had hampered the authors from determining the absolute configuration of **4**. On the other hand, the CS method could provide the absolute structure of **4** from just 10 µg of the sample without any chemical derivatization (Fig. 1–3). Elatenyne (**5**) is a marine natural product that was isolated from the marine red alga, *Laurencia elata*, in 1986 by Hall and co-workers, while the absolute configuration of **5** remained unknown for over 30 years.<sup>[31]</sup> The total synthesis did not seem to reveal the absolute configuration, because **5** shows almost no specific rotation value resulting from the pseudo-*meso* core scaffold. In 2016, the CS method was employed to confirm the absolute structure of **5** and successfully revealed the stereochemistry of six chiral centers on the 2,2'-bifuranyl skeleton, together its

click-derivative.<sup>[32]</sup> Structures of cycloelatanenes A and B (**6** and **7**) isolated from the same alga were also investigated, and the CS method could revise the structures previously determined by incomplete NMR analysis.<sup>[33]</sup> Moreover, the correct structure of fuliginone (**8**), that was originally considered to be a phenyl substituted phenalenone, was unequivocally elucidated by the CS method.<sup>[34]</sup> Li *et al.* could determine the absolute configuration of asarinin (**9**) isolated from a Chinese medicinal plant, *Asarum heterotropoides* var. *mandshuricum*, by taking advantages of high-flux synchrotron radiations (Fig. 1–4).<sup>[35]</sup> Structures of volatile organic compounds in essential oil mixtures (**10** from *Acorus Tatarinowii* and **11–16** from peppermint oil) were elucidated by the combination of the CS method with preparative high performance liquid chromatography (HPLC) or gas chromatography (GC).<sup>[36]</sup> The structure of diterpenoid **17** of which NMR signals were broadened was successfully elucidated by the CS method.<sup>[37]</sup>

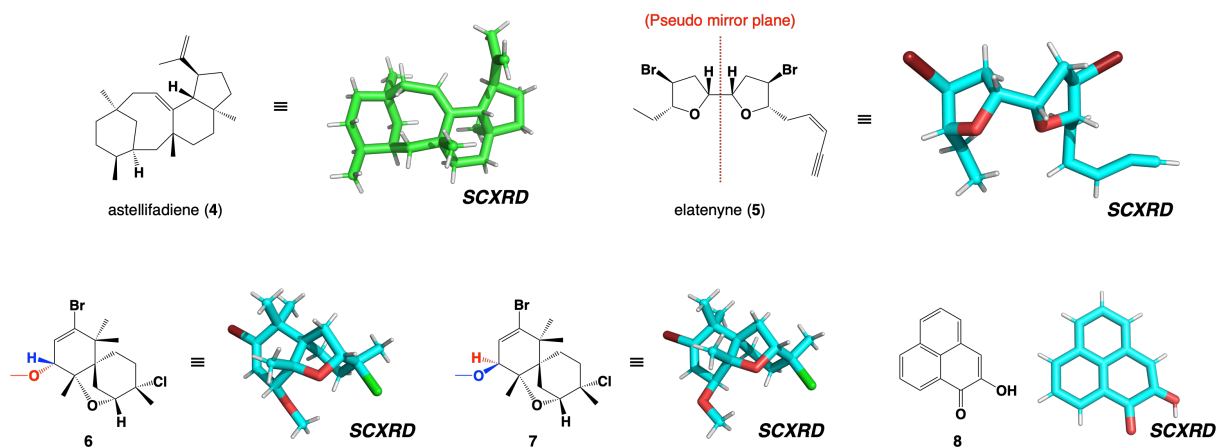


**Fig. 1–3** Chemical structures and crystal structures of **4–8** elucidated by the crystalline sponge method.

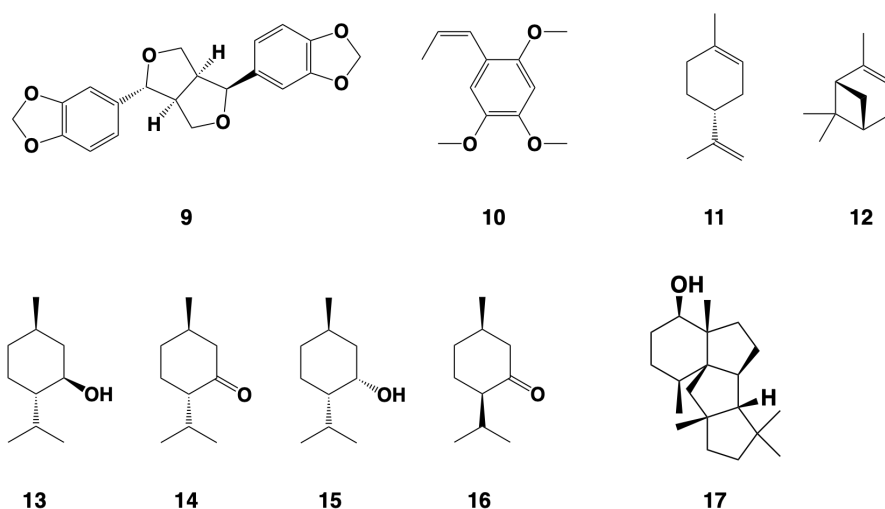


**Fig. 1–4** Chemical structures of **9–17**.

Natural product chemists pay great attention to bacteria, since they are rich sources of bioactive natural products due to their diversity as species. However, isolation and structural analysis of bacterial natural products normally involves cultivation in large (e.g. >10 L for broth cultures) scales, that has been a burden for scientists in this field and often ends in failure due to the scarcity of natural products in microbial weights. Here, the CS method, that requires isolated compounds in only microgram-to-nanogram scales, is expected to downsize the experimental scales of microbial cultivations. As a proof of concept, the CS method was applied to structural analysis of metabolites obtained by enzymatic reduction with baker's yeast. In all three cases tested, chemical structures of the product metabolites (**18–20**) were determined with isolated samples in microgram quantities, including absolute configurations for **19** and **20** (Fig. 1–5).<sup>[38]</sup>

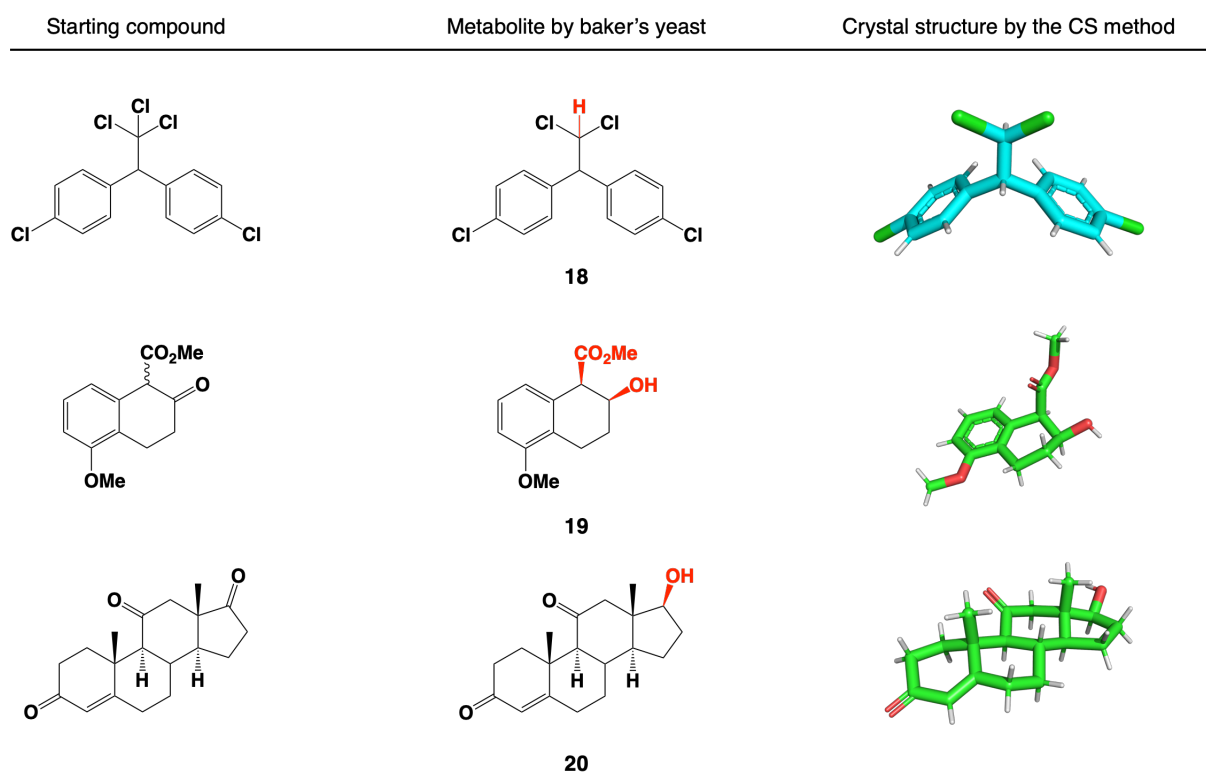


**Fig. 1–5** Chemical structures and crystal structures of metabolites **18–20** elucidated by the crystalline sponge method.

Relative configurations of cycloadducts prepared from collimonins A (**21**) and B (**22**), that were isolated from the fungus-feeding bacterium *Collimonas fungivorans* Ter331, were determined by the CS method (Fig. 1–6).<sup>[39]</sup> Tenebrathin (**23**), a new compound with a nitroaryl moiety isolated from *Streptoalloteichus tenebrarius* NBRC 16177, was characterized including the double-bond geometry and the absolute configuration of the epoxide stereocenter.<sup>[40]</sup> Ariefa *et al.* confirmed the absolute configurations of four new spiroketals, colletofurans B–E (**24–27**) from fungal strain *Colletotrichum boninense* AM-12–2, by the CS method.<sup>[41]</sup>

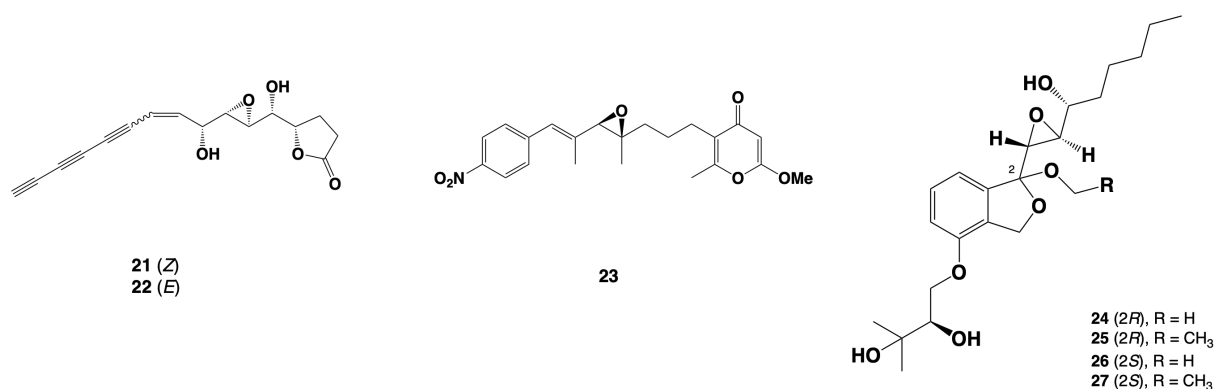


**Fig. 1–6** Chemical structures of 21–27.

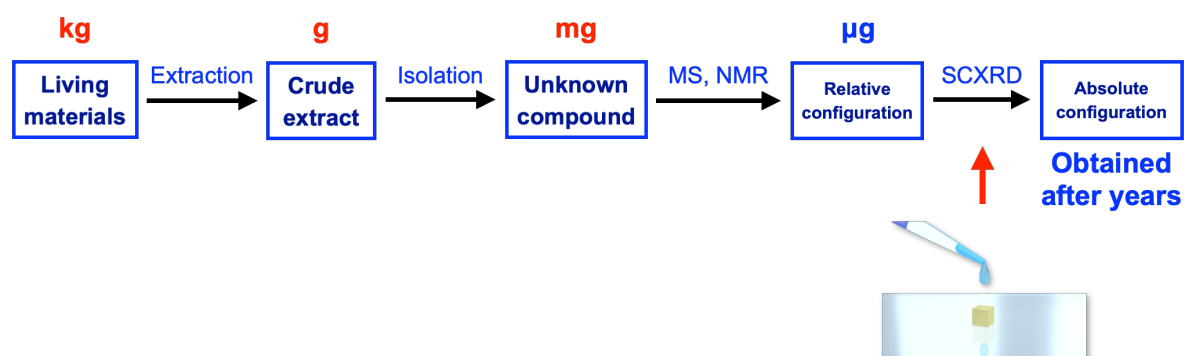
## 1.4 Overview of This Thesis

Isolation and structural determination of natural products from organisms is significant not only from the chemical point of view of evaluating compounds, but also from the medicinal point of view of drug discovery. In general, samples of at least dozens of milligrams are required for accurate structural analysis of natural products. In isolating natural products, it is often the case that bulk quantities (kilogram scales) of biological samples yield only a small amount (microgram scales) of the target natural products, thus scale-up experiments are often necessary. However, it is not always possible to scale up experiments due to limited availability of biological samples or low yield of natural products in bacterial cultivation. As a result, time and cost required for optimization of the isolation and extraction processes has reduced the overall efficiency in structural determination of natural products.

Recently, it has been shown that the amount of sample necessary for structural determination of natural products can be reduced by orders of magnitude with the CS method. However, in the previous studies, the natural products were still obtained in an obsolete research workflow where each analyte is isolated from bulk quantities of biological samples, which did not provide sufficient scale-down effects in the workflow of natural product chemistry. In

addition, there were many cases in which structural analysis by the CS method was abandoned because of the incompatibility between the guest and the host-framework after numerous efforts to isolate pure samples.

### Conventional Workflow



### This Workflow

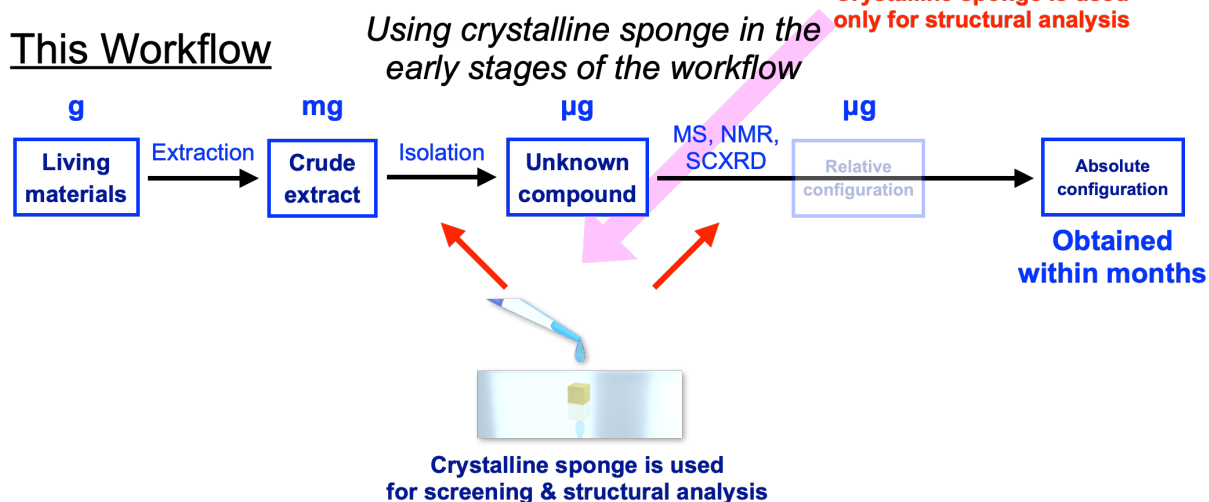


**Fig. 1–7** The schematic illustration of this study. In the conventional workflow by which they utilized the CS method for structural analysis of natural products, the CS method was applied in the last step to elucidate absolute structures of the natural products after structural analysis by the other spectroscopic methods such as MS and NMR. Thus, milligrams scales of the compound samples had to be prepared by processing grams of crude extract obtained from kilograms of living materials to conduct accurate structural analysis. This study proposed a

novel research workflow in natural product chemistry by utilizing the crystalline sponge in the early stages of the workflow. In this workflow, crystalline sponge is firstly used over crude extract to screen compounds and over microgram scales of isolated compounds for structural analysis. This workflow that premises the use of the CS method can downsize the preparation scales of living materials, crude extracts, and isolated compounds necessary for absolute structural elucidation by orders of magnitudes and accelerate the research period that typically lasts several years to be completed within months.

This study aimed to establish a novel research workflow that truly streamlines structural analysis of natural products by the introduction of the CS method.

In chapter 2, I proposed the procedure of Crystalline Sponge Affinity Screening (CSAS) in which we can assess the applicability of the CS method (and possibly the proper soaking conditions) for unknown natural products prior to compound isolation.

Chapter 3 focuses on technical improvements in the CS method, intending to facilitate structural analysis of steroidal natural products. In this chapter, I discovered that polar solvents (ketones and esters) can promote ordering of the guest compounds in the CS cavity. With the updated protocol, I could determine chemical structures of several steroids with high fidelity.

Chapter 4 includes an application of the CS method in a genome-based biosynthetic study. I demonstrated that it is possible to determine chemical structures of novel compounds rapidly and reliably from unprecedented tiny amounts of isolated samples.

Chapter 5 summarizes this thesis and proposes the future perspectives originating from this work.



## 1.5 References

- [1] K. Li, T. J. Buchinger and W. Li, *Nat. Prod. Rep.* **2018**, *35*, 501-513.
- [2] M. F. Maia and S. J. Moore, *Malar. J.* **2011**, *10*, S11.
- [3] a) R. Schoental, *Fd Cosmet. Toxicol.* **1965**, *3*, 609-620; b) S. O. Duke, C. L. Cantrell, K. M. Meepagala, D. E. Wedge, N. Tabanca and K. K. Schrader, *Toxins* **2010**, *2*, 1943-1962.
- [4] H. Yuan, Q. Ma, L. Ye and G. Piao, *Molecules* **2016**, *21*, 559.
- [5] J. Berman, U. Zorrilla-López, G. Farré, C. Zhu, G. Sandmann, R. M. Twyman, T. Capell and P. Christou, *Phytochem. Rev.* **2014**, *14*, 727-743.
- [6] D. K. Semwal, R. B. Semwal, I. Vermaak and A. Viljoen, *J. Ethnopharmacol.* **2014**, *155*, 1011-1028.
- [7] D. J. Newman and G. M. Cragg, *J. Nat. Prod.* **2020**, *83*, 770-803.
- [8] a) J. Jiang, X. He and D. E. Cane, *J. Am. Chem. Soc.* **2006**, *128*, 8128-8129; b) T. Pluskal, M. P. Torrens-Spence, T. R. Fallon, A. De Abreu, C. H. Shi and J. K. Weng, *Nat. Plants* **2019**, *5*, 867-878; c) R. S. Nett, W. Lau and E. S. Sattely, *Nature* **2020**, *584*, 148-153.
- [9] K. Tsuda, *J. Synth. Org. Chem. Jpn.* **1965**, *23*, 203-212.
- [10] C. G. Jones, M. W. Martynowycz, J. Hattne, T. J. Fulton, B. M. Stoltz, J. A. Rodriguez, H. M. Nelson and T. Gonen, *ACS Cent. Sci.* **2018**, *4*, 1587-1592.
- [11] a) L. J. Kim, M. Xue, X. Li, Z. Xu, E. Paulson, B. Mercado, H. M. Nelson and S. B. Herzon, *J. Am. Chem. Soc.* **2021**, *143*, 6578-6585; b) L. J. Kim, M. Ohashi, Z. Zhang, D. Tan, M. Asay, D. Cascio, J. A. Rodriguez, Y. Tang and H. M. Nelson, *Nat. Chem. Biol.* **2021**, *17*, 872-877.
- [12] D. C. Hodgkin, J. Kamper, M. Mackay, J. Pickworth, K. N. Trueblood and J. G. White, *Nature* **1956**, *178*, 64-66.
- [13] G. M. Sheldrick, *Acta Cryst. A* **2008**, *64*, 112-122.

- [14] a) J. A. Dale and H. S. Mosher, *J. Am. Chem. Soc.* **1973**, *95*, 512-519; b) I. Ohtani, T. Kusumi, Y. Kashman and H. Kakisawa, *J. Am. Chem. Soc.* **1991**, *113*, 4092-4096.
- [15] S. Parsons, H. D. Flack and T. Wagner, *Acta Cryst. B* **2013**, *69*, 249-259.
- [16] K. C. Nicolaou and S. A. Snyder, *Angew. Chem. Int. Ed.* **2005**, *44*, 1012-1044.
- [17] L.-Y. Kong and P. Wang, *Chin. J. Nat. Med.* **2013**, *11*, 193-198.
- [18] Y. Inokuma, S. Yoshioka, J. Ariyoshi, T. Arai, Y. Hitora, K. Takada, S. Matsunaga, K. Rissanen and M. Fujita, *Nature* **2013**, *495*, 461-466.
- [19] a) O. Ohmori, M. Kawano and M. Fujita, *Angew. Chem. Int. Ed.* **2005**, *44*, 1962-1964; b) G. H. Ning, K. Matsumura, Y. Inokuma and M. Fujita, *Chem. Commun.* **2016**, *52*, 7013-7015; c) Y. Inokuma, K. Matsumura, S. Yoshioka and M. Fujita, *Chem. Asian J.* **2017**, *12*, 208-211; d) E. Sanna, E. C. Escudero-Adan, A. Bauza, P. Ballester, A. Frontera, C. Rotger and A. Costa, *Chem. Sci.* **2015**, *6*, 5466-5472; e) J. S. Qin, S. Yuan, A. Alsalmé and H. C. Zhou, *ACS Appl. Mater. Interfaces* **2017**, *9*, 33408-33412; f) E. Sanna, A. Bauzá, E. C. Escudero-Adán, C. Rotger, A. Frontera and A. Costa, *Cryst. Growth Des.* **2017**, *17*, 3611-3615; g) X.-Y. Yang, S. Yuan, J.-S. Qin, C. Lollar, A. Alsalmé and H.-C. Zhou, *Mater. Chem. Front.* **2017**, *1*, 1764-1767; h) S.-Y. Zhang, C.-X. Yang, W. Shi, X.-P. Yan, P. Cheng, L. Wojtas and M. J. Zaworotko, *Chem* **2017**, *3*, 281-289; i) W. de Poel, P. Tinnemans, A. L. L. Duchateau, M. Honing, F. Rutjes, E. Vlieg and R. De Gelder, *Chem. Eur. J.* **2019**, 14999-15003.
- [20] a) K. Biradha and M. Fujita, *Angew. Chem. Int. Ed.* **2002**, *41*, 3392-3395; b) K. Biradha, Y. Hongo and M. Fujita, *Angew. Chem. Int. Ed.* **2002**, *41*, 3395-3398.
- [21] T. R. Ramadhar, S. L. Zheng, Y. S. Chen and J. Clardy, *Chem. Commun.* **2015**, *51*, 11252-11255.
- [22] F. Sakurai, A. Khutia, T. Kikuchi and M. Fujita, *Chem. Eur. J.* **2017**, *23*, 15035-15040.

- [23] N. Zigon, V. Duplan, N. Wada and M. Fujita, *Angew. Chem. Int. Ed.* **2021**, *60*, 25204-25222.
- [24] a) Y. Inokuma, S. Yoshioka, J. Ariyoshi, T. Arai and M. Fujita, *Nat. Protoc.* **2014**, *9*, 246-252; b) M. Hoshino, A. Khutia, H. Xing, Y. Inokuma and M. Fujita, *IUCrJ* **2016**, *3*, 139-151; c) T. R. Ramadhar, S. L. Zheng, Y. S. Chen and J. Clardy, *Acta Crystallogr. A* **2015**, *71*, 46-58; d) Y. Taniguchi, R. Matsumoto and T. Kadota, *Chem. Eur. J.* **2020**, *26*, 15799-15803.
- [25] G. W. Waldhart, N. P. Mankad and B. D. Santarsiero, *Org. Lett.* **2016**, *18*, 6112-6115.
- [26] G. M. Sheldrick, *Acta Cryst. A* **2015**, *71*, 3-8.
- [27] G. M. Sheldrick, *Acta Cryst. C* **2015**, *71*, 3-8.
- [28] a) S. Sairenji, T. Kikuchi, M. A. Abozeid, S. Takizawa, H. Sasai, Y. Ando, K. Ohmatsu, T. Ooi and M. Fujita, *Chem. Sci.* **2017**, *8*, 5132-5136; b) M. A. Abozeid, S. Sairenji, S. Takizawa, M. Fujita and H. Sasai, *Chem. Commun.* **2017**, *53*, 6887-6890.
- [29] S. Yoshioka, Y. Inokuma, M. Hoshino, T. Sato and M. Fujita, *Chem. Sci.* **2015**, *6*, 3765-3768.
- [30] Y. Matsuda, T. Mitsuhashi, S. Lee, M. Hoshino, T. Mori, M. Okada, H. Zhang, F. Hayashi, M. Fujita and I. Abe, *Angew. Chem. Int. Ed.* **2016**, *55*, 5785-5788.
- [31] D. A. Dias and S. Urban, *Phytochemistry* **2011**, *72*, 2081-2089.
- [32] S. Urban, R. Brkljaca, M. Hoshino, S. Lee and M. Fujita, *Angew. Chem. Int. Ed.* **2016**, *55*, 2678-2682.
- [33] S. Lee, M. Hoshino, M. Fujita and S. Urban, *Chem. Sci.* **2017**, *8*, 1547-1550.
- [34] R. Brkljaca, B. Schneider, W. Hidalgo, F. Otalvaro, F. Ospina, S. Lee, M. Hoshino, M. Fujita and S. Urban, *Molecules* **2017**, *22*, 211.
- [35] K. Li, D. S. Yang, X. F. Gu and B. Di, *Fitoterapia* **2019**, *134*, 135-140.

- [36] a) X. F. Gu, Y. Zhao, K. Li, M. X. Su, F. Yan, B. Li, Y. X. Du and B. Di, *J. Chromatogr. A* **2016**, *1474*, 130-137; b) N. Zigon, T. Kikuchi, J. Ariyoshi, Y. Inokuma and M. Fujita, *Chem. Asian J.* **2017**, *12*, 1057-1061.
- [37] T. Mitsuhashi, T. Kikuchi, S. Hoshino, M. Ozeki, T. Awakawa, S. P. Shi, M. Fujita and I. Abe, *Org. Lett.* **2018**, *20*, 5606-5609.
- [38] Y. Inokuma, T. Ukegawa, M. Hoshino and M. Fujita, *Chem. Sci.* **2016**, *7*, 3910-3913.
- [39] K. Kai, M. Sogame, F. Sakurai, N. Nasu and M. Fujita, *Org. Lett.* **2018**, *20*, 3536-3540.
- [40] S. Hoshino, T. Mitsuhashi, T. Kikuchi, C. P. Wong, H. Morita, T. Awakawa, M. Fujita and I. Abe, *Org. Lett.* **2019**, *21*, 6519-6522.
- [41] N. R. Ariefta, M. Azim, T. Aboshi, T. Koseki, Y. Taniguchi, M. Fujita and Y. Shiono, *Org. Lett.* **2020**, *22*, 3161-3165.

## **Chapter 2**

# **Rapid Structural Analysis of Red Algal Halogenated Terpenoids in Minute Quantities**

### **2.1 Introduction**

In the studies involving natural product (NP) isolation followed by structural elucidation, scientists need to collect and handle large quantity of samples derived from living organism such as plants, animals, and fungi, including algae that I aim to focus on in this chapter. It is common that only microgram-scale samples, that would be beyond the applicable scopes of standard tools in structural analysis, are obtained after lengthy extraction, sample processing, and chromatographic separations. This has been a major bottleneck that slows down the efficiency of compound isolation and structural characterization in NP chemistry. Here, I

envisioned that the whole experimental scales would be downsized by integrating the crystalline sponge method into the workflow in NP chemistry. Considering the fact that more than 20% of the newly approved drugs from 1981 to 2019 are of NP origin,<sup>[1]</sup> streamlining the workflow would also contribute to stable supply of lead compounds for new drug development.

Before I propose the novel usage of the crystalline sponge in the workflow of NP chemistry, I herein would like to illustrate historical backgrounds in structural elucidation of natural products derived from the red algal genus *Laurencia*. Halide ions are present in high concentrations in seawater; it includes 19,000 mg/L of chloride ions, 65 mg/L of bromide ions, 1.3 mg/L of fluoride ions, and 0.06 mg/L of iodide ions.<sup>[2]</sup> It is not difficult to imagine that NPs incorporating halide ions are collected from marine organisms. Indeed, many halogenated NPs have been found in the genus *Laurencia* and its predators such as starfish and jellyfish.<sup>[3]</sup> It is also known that many of the NPs show bioactivity (eg. anti-inflammatory and antibacterial effects), and are classified as sesquiterpenes (terpenes possessing 15 carbon atoms) (Fig. 2–1).

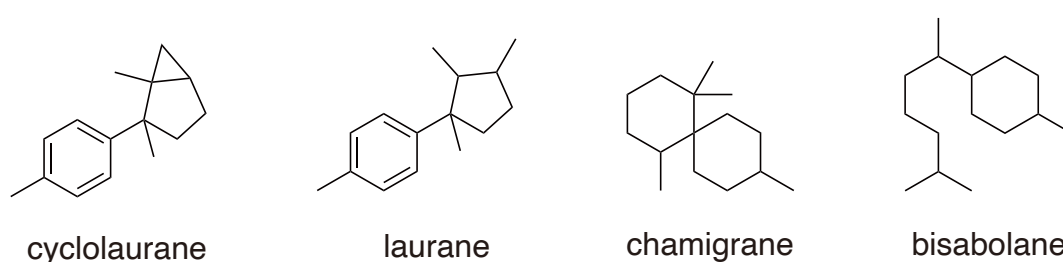


**Fig. 2–1** Representative scaffolds of the sesquiterpenoids isolated from the genus *Laurencia* and its predators.

Brominated sesquiterpenoids have long attracted much attention from NP chemists since the 1950s (Fig. 2–2). In 1959, Tanaka *et al.* discovered the first NP containing a bromine

atom in an extract of the sea hare *Aplysia kurodai*.<sup>[4]</sup> In 1963, Yamamura *et al.* isolated two brominated sesquiterpenoids, aplysin (**1**) and aplysinol (**2**), from the same species.<sup>[5]</sup> In 1966, Irie *et al.* isolated laurinterol (**3**) from *Laurencia intermedia* YAMADA, and accidentally obtained **1** by derivatization with tosylic acid, which suggested that **3** is an intermediate of **1** produced by the red algae and chemically converted in its predator.<sup>[6]</sup> Because of the non-crystalline nature of **3**, Irie *et al.* was unable to determine the absolute stereochemistry of **3**. Structural characterization of **3** by single-crystal X-ray diffraction (SCXRD) analysis was performed with its derivative, laurinterol acetate (**4**), in 1967.<sup>[7]</sup> In the 1970s and 1980s, there were a series of reports on the isolation of brominated sesquiterpenoids. In 1971, Sims *et al.* firstly isolated a multi-halogenated sesquiterpenoid, pacifenol (**5**), which contains a bromine and two chlorines, along with **3** from *Laurencia pacifica*, and determined the absolute stereochemistry of **5** by SCXRD analysis.<sup>[8]</sup> Fronczek *et al.* re-examined the crystal structure of **5** in 1986, since that by Sims *et al.* had crystallographical problems such as occurrence of unnatural bond lengths and the absolute structure not determined by the Bijvoet method.<sup>[9]</sup> In 1972, Sims *et al.* isolated johnstonol (**6**) from *Laurencia johnstonii*, showing structural similarity to **5**, and determined the absolute structure by SCXRD analysis.<sup>[10]</sup> In 1973, Sims *et al.* reported that **5** may be an artifact resulting from acid isomerization of prepacifenol (**7**) occurred during silica gel column chromatography.<sup>[11]</sup> Because of the non-crystalline nature of **7**, SCXRD analysis of **7** has never been performed up to the present time (note; this is achieved in this work). In 1976, deoxyprepacifenol (**8**) was isolated from *Aplysia californica*,<sup>[12]</sup> and 2,10-dibromo-3-chlorochamigran-7-en-9-ol (**9**) was isolated from *L. pacifica*.<sup>[13]</sup> SCXRD analysis of **8** was performed just after isolation to determine the absolute stereochemistry, whereas absolute stereochemical determination of non-crystalline **9** had to wait until 1988, when a ketone derivative **10** was characterized by SCXRD analysis.<sup>[14]</sup>

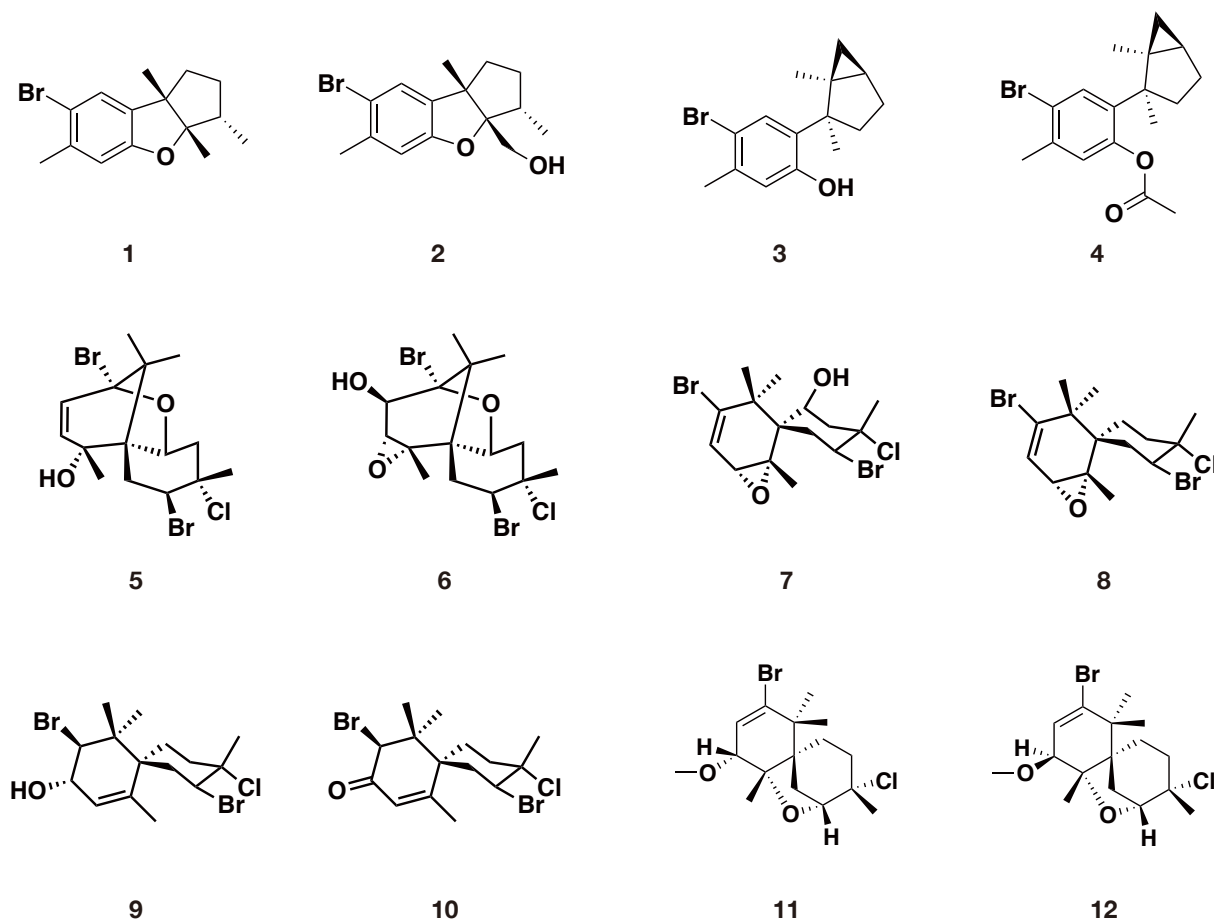


**Fig. 2–2** Brominated sesquiterpenoids 1–3, 5–9, 11–12 and derivatives 4 and 10.

As illustrated chemical structures in Fig. 2–2, many of the halogenated sesquiterpenoids of red algal origin possess complicated ring-fused scaffolds, that often disturb precise structural determination. Relative structures of cycloelatanenes A and B (**11** and **12**) from *Laurencia elata*, of which proposed structures were incorrectly interconverted by Urban *et al.*, were revised by the crystalline sponge method.<sup>[15]</sup> This was due to incorrect assignments in the <sup>1</sup>H NMR spectral analysis and misinterpretation of noise signals in the NOESY NMR analysis. As shown in Fig. 2–3, aldingenins A–D (**13**–**16**) seemingly isolated from *Laurencia aldingensis*<sup>[16]</sup> were later identified to be either known NPs or related compounds by total synthesis and



computationally driven reassignment of  $^{13}\text{C}$  NMR chemical shifts.<sup>[17]</sup> It is speculated that the misinterpretation of mass spectra led to the false isolation reports of **13**–**16**. Moreover, in 2017, as many as 16 chemical structures of halogenated NPs were revised by parametric corrections to DFT-computed  $^{13}\text{C}$  NMR chemical shifts and spin–spin coupling constants.<sup>[18]</sup>

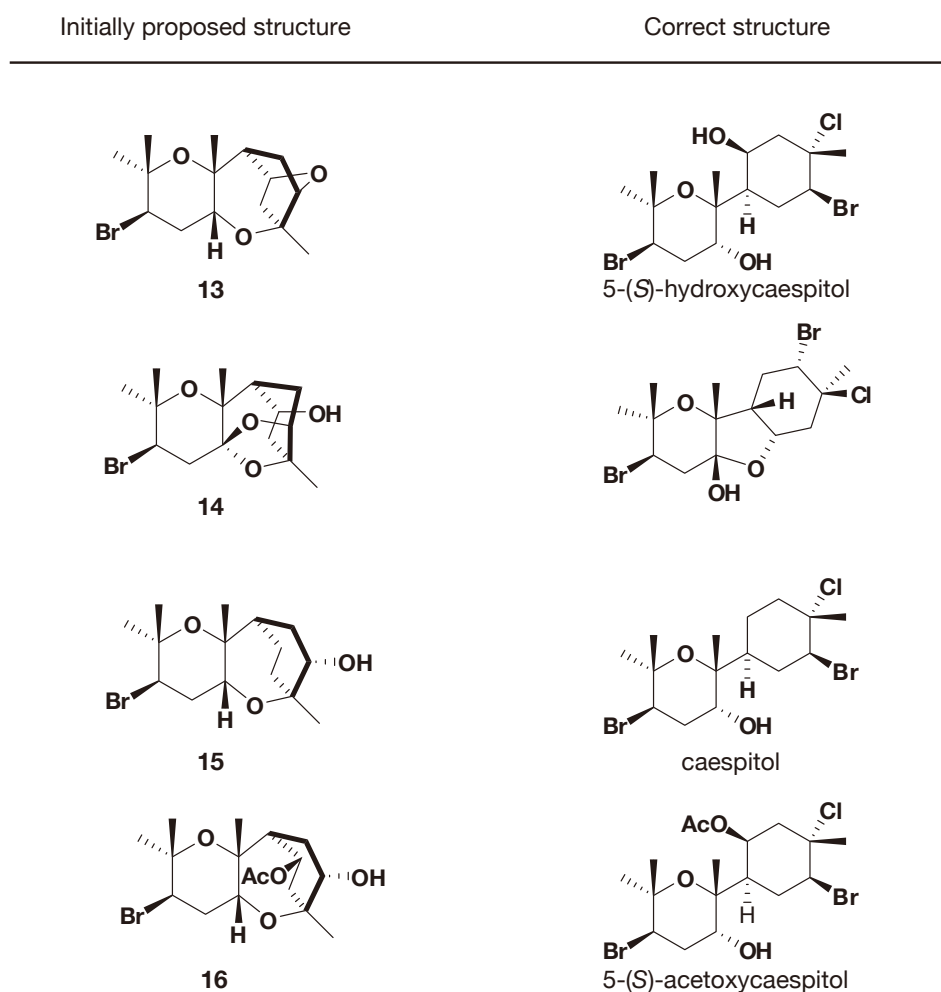


**Fig. 2–3** Chemical structures of aldigenins A–D (**13**–**16**), that had been initially assumed to be novel compounds, but were later proven to be nonexistent compounds.

Total synthesis of NPs plays a critical role in correcting chemical structures that have been incorrectly proposed. However, total synthesis of halogenated sesquiterpenoids is often hard to be accomplished due to the complex fused-ring scaffold and presence of multiple

halogen substituents. For instance, many of the halogenated sesquiterpenoids listed above possess a chamigrane scaffold. As of November 2018, there are only 4 examples of accomplished asymmetric total synthesis of halogenated chamigrane-type natural products (Fig. 2–4), and solely (+)–elatol (**17**) has multiple halogen atoms.<sup>[19]</sup> Although there are several attempts to establish novel synthetic routes for NPs chemoenzymatically, there are only a limited number of discovered enzymes responsible for biosynthesis of halogenated sesquiterpenoids from the genus *Laurencia*, such as terpene cyclases and vanadium haloperoxidases.<sup>[20]</sup>

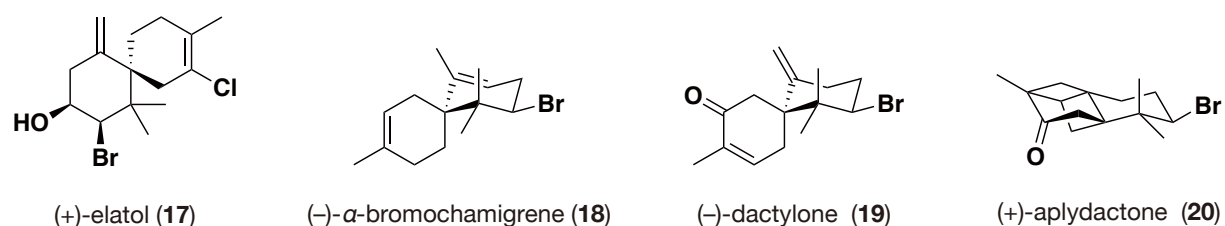


**Fig. 2–4** Examples of asymmetric total synthesis of halogenated sesquiterpenoids **17–20** possessing a chamigrane scaffold.

In summary, although halogenated sesquiterpenoids have been attracting targets of structural analysis for more than 60 years, the structural complexity has hindered rapid and accurate structural elucidation. If a novel workflow utilizing the crystalline sponges is introduced in this field, it is expected that the experimental scales are reduced from gram-to-milligram scales to nano-to-microgram scales and the output speed of this field will be accelerated than ever before. To demonstrate this, I aim to establish a workflow for rapid NP structural determination using the crystalline sponges.

## **2.2 Crystalline Sponge Affinity Screening of Individual Components in Red Algal Crude Extract**

Limited quantity of biological samples has been a rate-limiting factor in the number of reported cases of compound isolation and structural characterization in NP chemistry. One solution to this problem demonstrated in the previous works is to utilize the crystalline sponge method at the structural analysis step after NP isolation, that offers absolute stereochemistry of target compounds from nanogram-to-microgram scales.<sup>[21]</sup> The NPs of analytical targets in the previous works were, however, obtained in a conventional workflow that involves extraction and purification from bulk (typically kilogram-scales) quantities of living materials. Therefore, the time and cost required for NP isolation remains a major bottleneck in NP chemistry. In addition, researchers had to devote much futile efforts to optimize soaking conditions for each NP analytes that are poorly absorbed by the crystalline sponges.

Therefore, I designed a new protocol, crystalline sponge affinity screening (CSAS), to prescreen NPs showing good affinity with the crystalline sponges from crude extract before compound isolation as shown in Fig. 2–5.

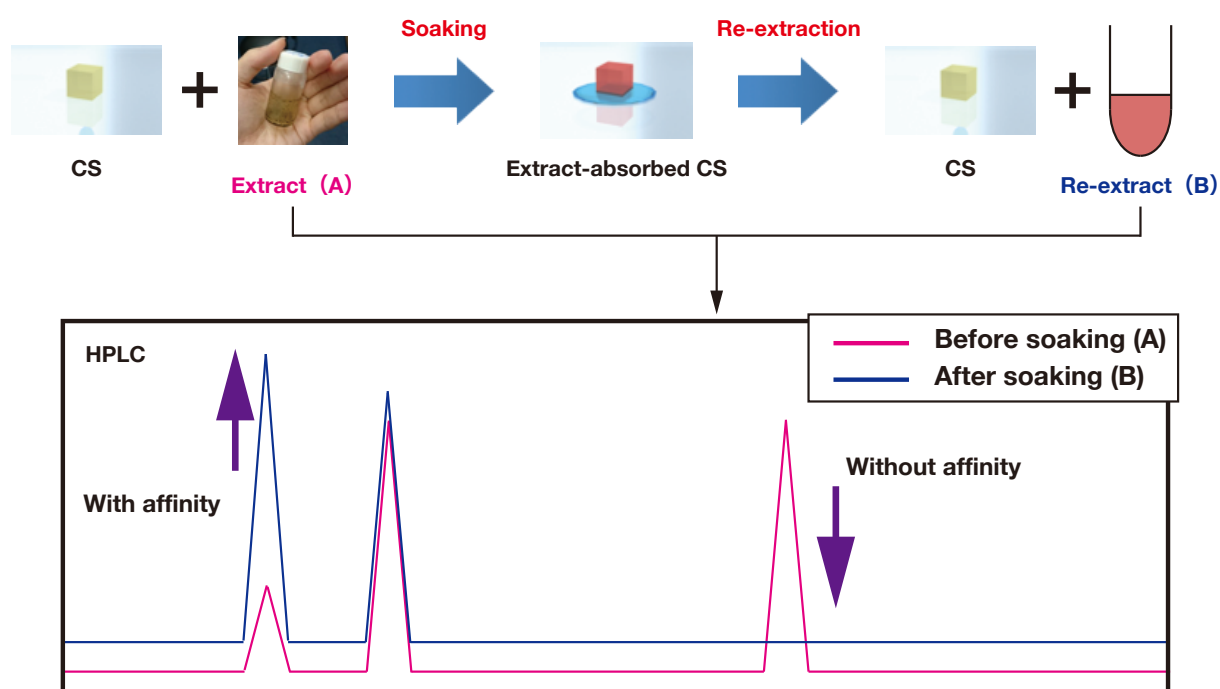


**Fig. 2–5** A schematic representation of crystalline sponge affinity screening (CSAS).

The procedures of CSAS are as follows. Firstly, components in crude extract (A) are separated by high-performance liquid chromatography (HPLC) to obtain information on the number of components in the sample and the peak area ratio of each component. Secondly, the crude extract is dissolved in an appropriate organic solvent and the guest soaking is performed with a single crystal of crystalline sponges. During this process, components with high affinity to the crystalline sponges are expected to be abundantly incorporated, while components with low affinity are poorly absorbed. Upon the completion of the guest soaking, the crystalline sponges are dissolved or soaked in fresh solvents to obtain re-extract (B). In re-extract, the ratio of each component should change due to different degrees of the affinity with the crystalline sponges. HPLC analysis of re-extract (B) and comparison of the peak ratio before and after the guest soaking should indicate that components with increased or constant peak areas have affinity with the crystalline sponge without purifying NPs from crude extract (A).

A few dozen milligrams of methanolic extract derived from *L. pacifica* were provided by collaborators from the Jing-Ke Weng Group (Whitehead Institute for Biomedical Research, the United States). Considering that conventional NP structural analysis starts from crude extract in gram scales, accomplishing structural elucidation of NPs from this limited sample will demonstrate the scale-down effects by one-hundredth to one-thousandth scales. HPLC-UV analysis of this extract showed that it is composed of at least 9 compounds (peaks **a–i**) in Fig. 2–6A (See experimental section for detail analytical condition). To assess the affinity of peaks **a–i** with the crystalline sponges and prioritize target components that should be investigated with the crystalline sponge method, the extract was absorbed with the crystalline sponge complex,  $[(\text{ZnI}_2)_3(\text{tpt})_2 \cdot x(\text{cyclohexane})]_n$  (**21**; tpt = 2,4,6-tris(4-pyridyl)-1,3,5-triazine).<sup>[22]</sup> Five single crystals of **21** were infiltrated in a mixture of cyclohexane and 1,2-dichloroethane (DCE) (9:1 v/v) containing 25  $\mu\text{g}$  of the extracted extract and allowed to stand at 50 °C for 6 days. The crystals were then picked up, transferred to a new glass vial, and allowed to stand in 0.1 mL cyclohexane for 4 days at room temperature to obtain re-extract from **21**. HPLC-UV analysis of the re-extract showed the existence of 6 compounds (peaks **a**, **b**, **c**, **e**, **g**, **i**), that are highly expected to be characterized by the crystalline sponge method (Fig. 2–6B). The relative peak areas of **a**, **b**, **c**, and **e** increased after inclusion (Fig. 2–6C), indicating that these interact strongly with complex **21**. No significant change was observed for the relative peak area of **i**. Although the relative peak area of **g** decreased after inclusion, it still showed an affinity with complex **21**. On the other hand, the peaks of **d**, **f**, and **h** disappeared after inclusion, indicating their low affinity with **21**. Based on the results of CSAS, I speculated that structural analysis of **a**, **b**, **c**, **e**, **g**, and **i** could be performed by the crystalline sponge method. For the peaks **d**, **f**, and **h**, changing the soaking conditions (the type of the crystalline sponge, temperature,

concentrations, solvents, etc.) may enhance the affinity between the compounds and the crystalline sponges.

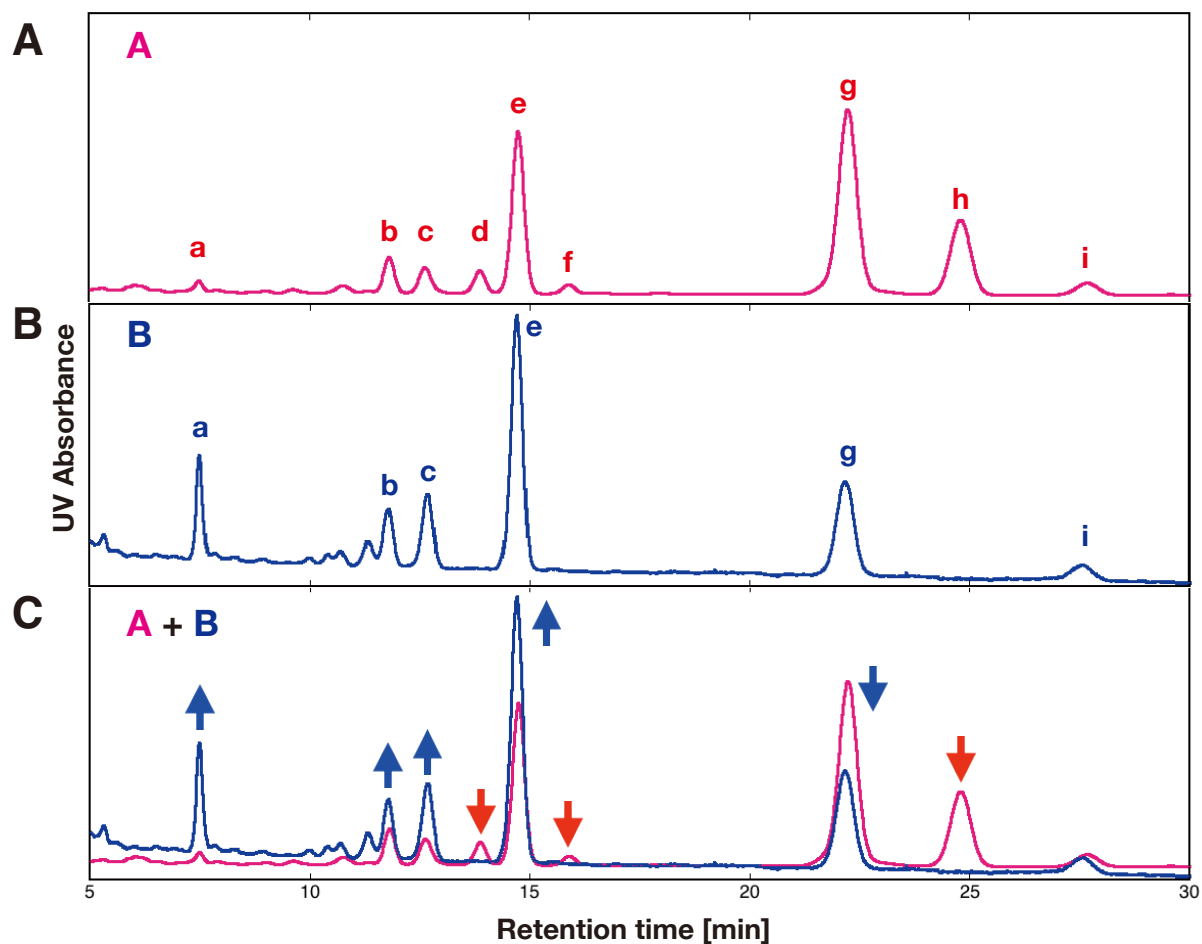


**Fig. 2–6** CSAS using the crude extract of *L. pacifica* for analytical prioritization. A) Outline of the HPLC profiling experiments (B) before (magenta, extract A) and (C) after (blue, extract B) contact with the CS **21**. (C) Overlay of the profiles of A and B. The intensity is normalized so that summation of the peak areas (a–i) is constant. The arrows indicate the increase or decrease in percentage before and after inclusion (upward indicates an increase, downward indicates a decrease).

### 2.3 Absolute Stereochemical Determination of Halogenated Terpenoids by the Crystalline Sponge Method

To confirm whether **a**, **b**, **c**, **e**, **g**, and **i**, which passed CSAS in chapter 2.2 are suitable for the crystalline sponge method, we firstly attempted preparative HPLC purification of each component and structural analysis with mass spectrometry (MS) and nuclear magnetic resonance (NMR) spectroscopy. I isolated the target components from 10 mg of the crude extract with preparative HPLC equipped with an octadecylsilyl (ODS) column in a semi-preparative scale. The isolated yield was less than 1 mg for all components. High-resolution mass spectrometry (HRMS) analysis indicated that **a**, **b**, **c**, and **e** are halogenated sesquiterpenoids, that contain 15 carbon atoms, 2 bromine atoms, and 1 chlorine atom. Similarly, HRMS analysis indicated that **g** is a halogenated sesquiterpenoid, that contains 15 carbon atoms, 1 bromine atom, and 1 oxygen atom.  $^1\text{H}$  NMR measurements were performed on all isolated components, and 2D NMR measurements (HMQC, HMBC, COSY, NOESY, etc.) were also performed on **e** and **g**, which were relatively abundantly isolated (Tables 2–1 to 2–6, Figs. 2–25 to 2–40).

Firstly, I analyzed the structure of **e**, which was the most abundant component (0.7 mg). **E** was suggested to have a molecular formula of  $\text{C}_{15}\text{H}_{21}\text{O}_2\text{ClBr}_2$  by HRMS analysis. In addition,  $^1\text{H}$ , COSY, HSQC, HMBC and other NMR measurements revealed the presence of three halogen atoms and one three-membered ring in the chamigrane scaffold (Fig. 2–7A). Although it is known that  $^{13}\text{C}$  NMR chemical shifts of carbon atoms bonded to bromine and chlorine atoms exhibit isotopic shifts, the sample scarcity hindered me from obtaining NMR spectra showing sufficient signal intensities to recognize isotopic shifts in the HSQC spectrum. Therefore, it was difficult to determine the position of each hetero atom by NMR. Next, I performed structural analysis with the crystalline sponge method. **E** was dissolved in DCE at a

concentration of 1 mg/mL. One single crystal of the crystalline sponge  $[(\text{ZnI}_2)_3(\text{tpt})_2 \cdot x(\text{cyclohexane})]_n$  (**21**) placed at the bottom of a glass vial was immersed in 45  $\mu\text{L}$  of cyclohexane and 5  $\mu\text{L}$  of the guest solution. To increase the occupancy of the guest molecules in the crystalline sponge as high as possible, the following guest soaking conditions were adopted. The septum of the lid was punctured with a syringe needle, and the vial was placed at 50 °C for 9 h to concentrate the solution. Afterwards, the lid was replaced with a new one, and the vial was kept at 50 °C for 2 days without piercing the septum with a syringe needle. After 5 days of the soaking, good single crystals suitable for SCXRD measurements were obtained as shown in Fig. 2–7B. Crystallographic analysis clearly revealed the structure of prepacifenol (**7**)<sup>[11]</sup> as shown in Fig. 2–7C. With the information on the position of hetero atoms by NMR analysis as a clue, I identified the exact position of the atoms in **7** by the crystalline sponge method. The Flack parameter  $x$  calculated by the Parsons' method<sup>[23]</sup> was converged to 0.046(3), that allowed me to determine the absolute structure of **7** with high fidelity (Fig. 2–7D). The NMR chemical shift values of **7** are consistent with literature values, and the NOESY correlation supports the chemical structure elucidated by the crystalline sponge method (Fig. 2–7E). In the previous study, the absolute configuration of the non-crystalline **7** was tentatively assigned based on the absolute configuration of its derivative **5**, whereas this study showed the absolute configuration of **7** for the first time. **7** was forming halogen bonding with iodides and hydrogen bonding with the tpt ligands present in **21** (Fig. 2–7F). These intermolecular interactions may account for the strong affinity of **7** with the crystalline sponge **21**. Actually, from the single crystal soaked with the crude extract, **7** was observable in crystallographic analysis.



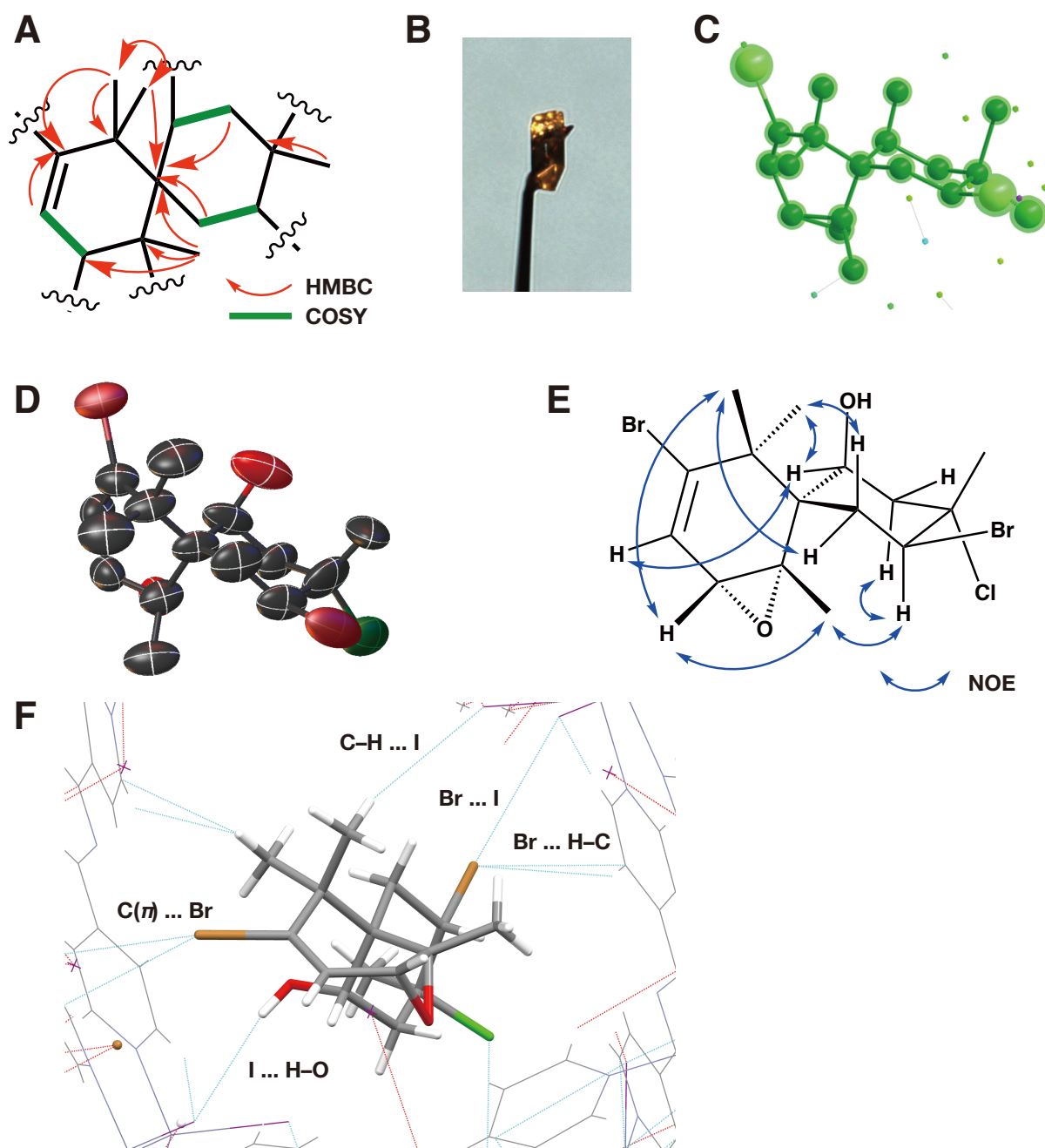


**Fig. 2-7** (A) Partial NMR structure of **7** elucidated from  $^1\text{H}$ , and 2D (HSQC, HMBC, and COSY) NMR analyses. (B) The photograph of **21** after the guest soaking with **7**. (C) Crystallographic model for **7** before least square refinement. Oxygen and carbon atoms are not clearly discriminated at this stage. (D) Thermal ellipsoid plot of **7** with 30% probability. Hydrogen atoms are not shown for clarity. (E) Key NOESY correlations observed in **7**. (F)

Intermolecular interactions between **7** and **21**. The captions indicate the atoms involving in the interactions.

Secondly, I analyzed the structure of **g**, which was the second most abundant component. HRMS analysis indicated the chemical formula of  $C_{15}H_{19}OBr$  and NMR analysis readily revealed the planar structure of laurinterol (**3**) (Fig. 2–8A). Independently, the crystalline sponge method was applied to structural analysis of **3** with a good single crystal (Fig. 2–8B), and elucidated the absolute structure (Fig. 2–8C) with the Flack parameter  $x$  as low as 0.053(6). The NMR chemical shift values of **3** are consistent with literature values, and the NOESY correlation supports the chemical structure elucidated by the crystalline sponge method (Fig. 2–8D). As illustrated in chapter 2.1, the previous study assigned the absolute configuration of **3** based on the crystal structure of derivative **4**, but in this study, the absolute structure of **3** was determined without derivatization. Interestingly, the intermolecular interaction between **21** and **3** was quite easily formed (Fig. 2–8E) so that as many as twelve crystallographically-independent molecules of **3** were observed in an asymmetric unit of the crystalline sponge and filled the void of **21** (Fig. 2–8F).

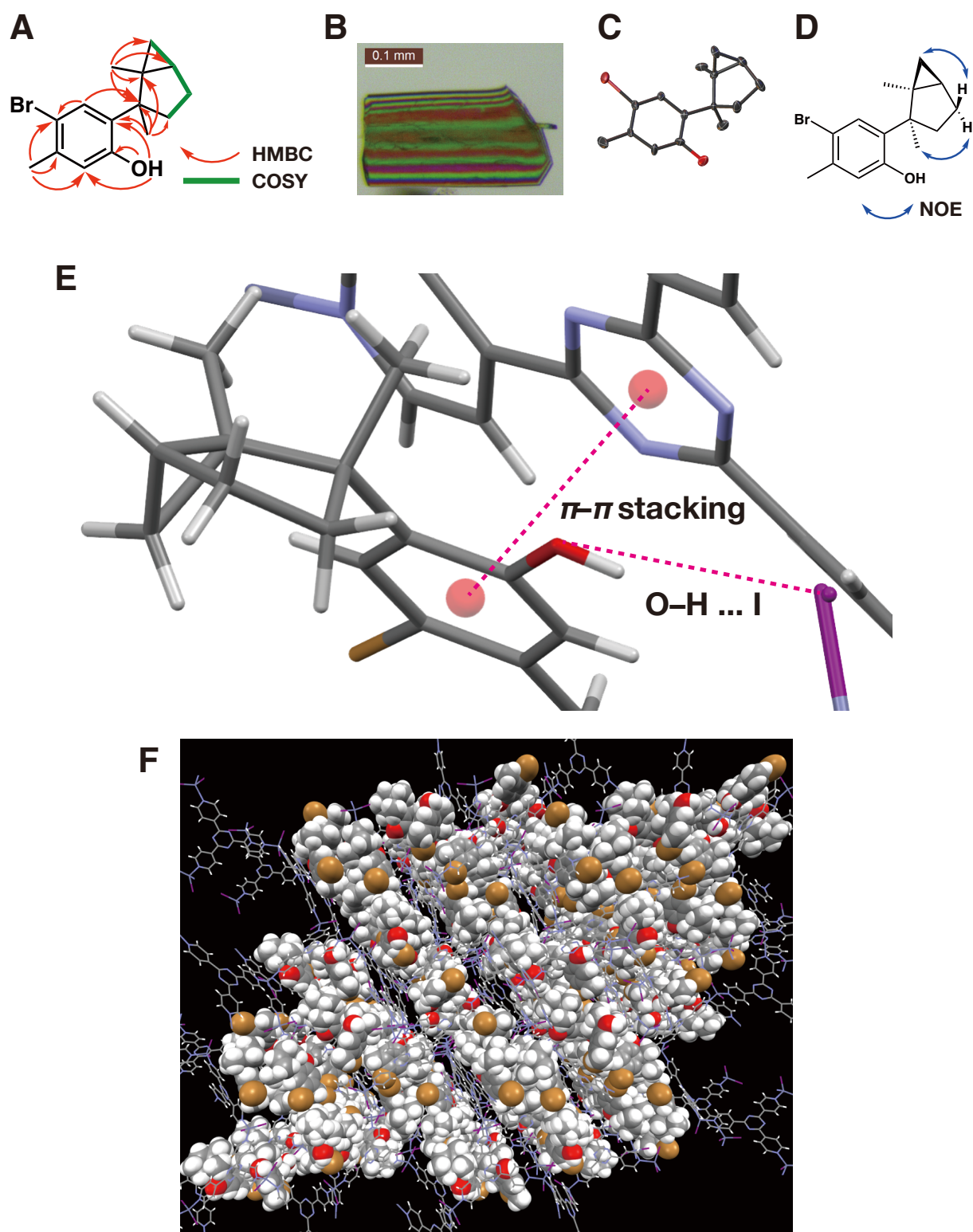


**Fig. 2-8** (A) NMR structure of **g** elucidated from  $^1\text{H}$ , and 2D (HMQC, HMBC, and COSY) NMR analyses. (B) The photograph of **21** after the guest soaking with **3**. (C) Thermal ellipsoid

plot of **3** with 30% probability. Hydrogen atoms are not shown for clarity. (D) Key NOESY correlations observed in **3**. (E) An example of intermolecular interactions between **3** and **21**. The captions indicate the atoms involving in the interactions. The red spheres indicate the centroids of the aromatic rings. (F) The packing structure of **21** filled with **3**.

I analyzed the structure of **a**, which showed significant absorption by the crystalline sponge in CSAS as shown in Fig. 2–9A. Due to the scarcity of isolated amount (0.04 mg), 2D NMR measurements could not be performed. Although such components may be easily overlooked in the conventional workflow for NP structural determination due to the small peak area of in the chromatograms, this workflow based on the crystalline sponges clearly pointed out that they have a high affinity and are suitable targets for the crystalline sponge method. As shown in Fig. 2–9B, structural analysis by the crystalline sponge method clearly revealed the absolute structure of johnstonol (**6**) [ $x = 0.126(7)$ ], and the NMR chemical shift values of **6** are consistent with literature values. As in the case of **7** that structurally resembles **6**, there is an intermolecular interaction between **21** and **6** via bromine atoms in the crystal structure (Fig. 2–9C).

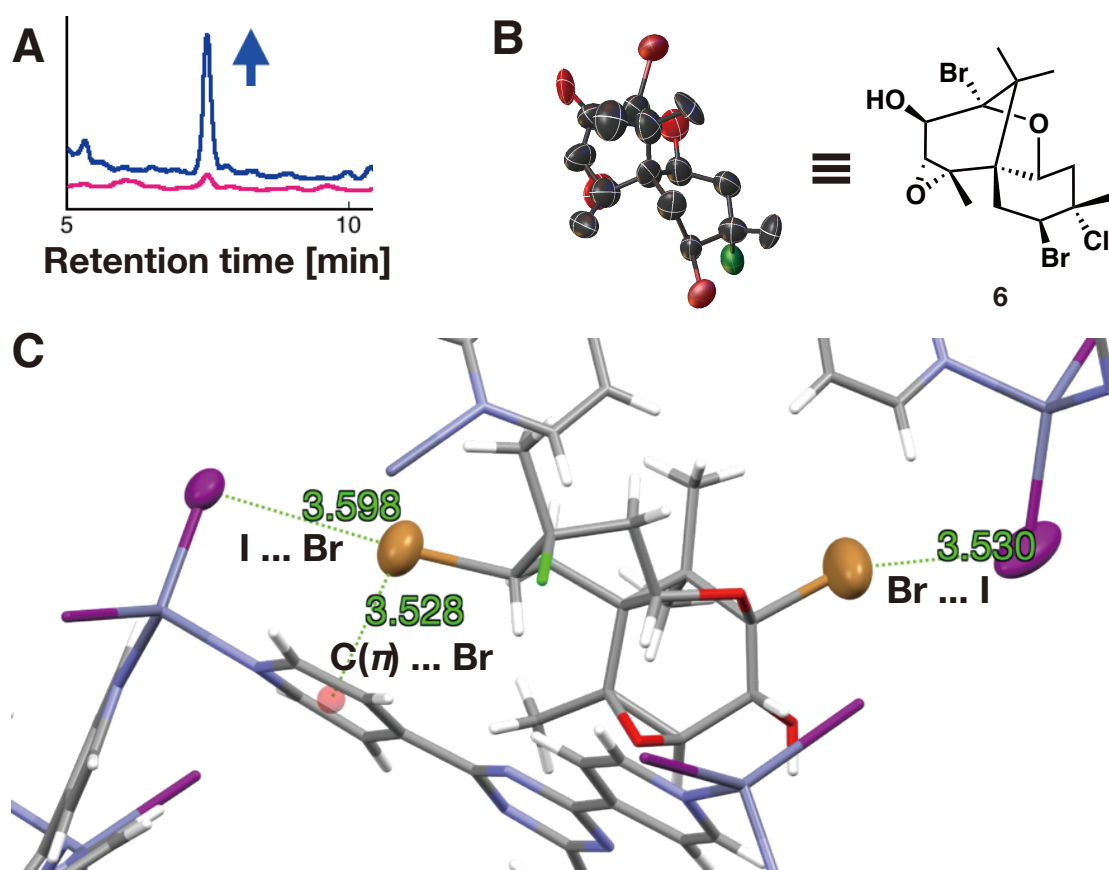


**Fig. 2–9** (A) Peak area amplification of **a** in CSAS. (B) Thermal ellipsoid plot of **6** with 30% probability. Hydrogen atoms are not shown for clarity. (C) An example of intermolecular interactions between **6** and **21**. The captions indicate the atoms involving in the interactions. Iodide and bromine atoms are represented in thermal ellipsoid plot. The red spheres indicate the centroids of the aromatic rings. The values indicate atom distances highlighted with dashed lines and in angstroms (Å).

Structural analysis of **b** with the crystalline sponge method revealed the absolute structure of 2,10-dibromo-3-chlorochamigran-7-en-9-ol (**9**) as shown in Fig. 2–10A [ $x = 0.053(4)$ ], and the NMR chemical shift values of **9** are consistent with literature values. The previous study speculated the *anti* configuration of bromine and hydroxy substituents in **9** based on the derivatization to **10** and the  $J$  coupling constants in  $^1\text{H}$  NMR spectrum.<sup>[14]</sup> In this study,

the absolute configuration of **9** was determined for the first time from only 0.07 mg of the isolates sample and supported the previous conclusion (Fig. 2–10B). In the Jones Oxidation product **10**, epimerization of a chiral center bonded to a bromine atom could have occurred via keto-enol tautomerization, that decreases the reliability of the previous conclusion on the stereochemical assignment.

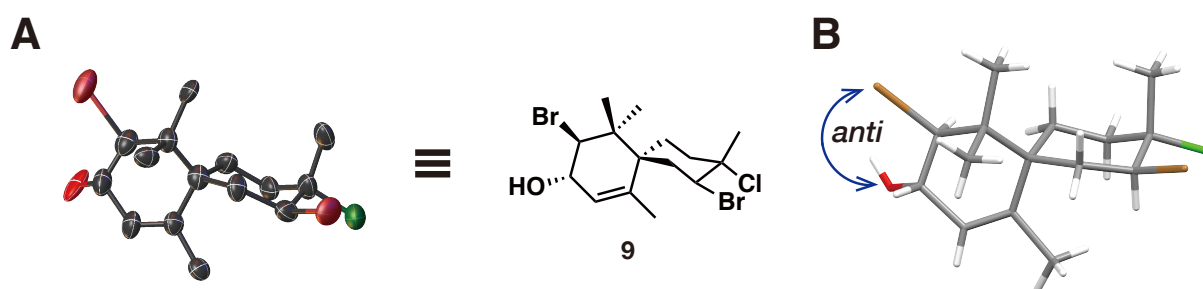


**Fig. 2–10** (A) Thermal ellipsoid plot of **9** with 30% probability. Hydrogen atoms are not shown for clarity. (B) The *anti* configuration of bromine and hydroxy substituents in **9**, that is elucidated including the absolute configurations in this study for the first time.

Structural analysis of **c** with the crystalline sponge method revealed the absolute structure of pacifenol (**5**) as shown in Fig. 2–11 [ $x = 0.054(12)$ ]. As explained in chapter 2.1, Sims *et al.* implied that **5** could be an artifact of **7** generated during silica-gel column chromatography. Since no acidic condition that may cause the isomerization is applied in sample preparation step in this study, **5** would be a NP indigenous to *L. pacifica*.

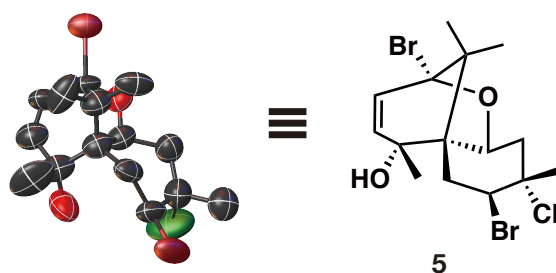


**Fig. 2–11** Thermal ellipsoid plot of **5** with 30% probability. Hydrogen atoms are not shown for clarity.

Finally, the crystalline sponge method could also provide the absolute structure of **i**, deoxyprecipacifenol (**8**) [ $\chi = 0.099(5)$ ] as shown in Fig. 2–12A. As in the case of **6** and **7** that structurally resemble **8**, there is an intermolecular interaction between **21** and **8** via bromine atoms and pyridine hydrogens in the crystal structure (Fig. 2–12B).

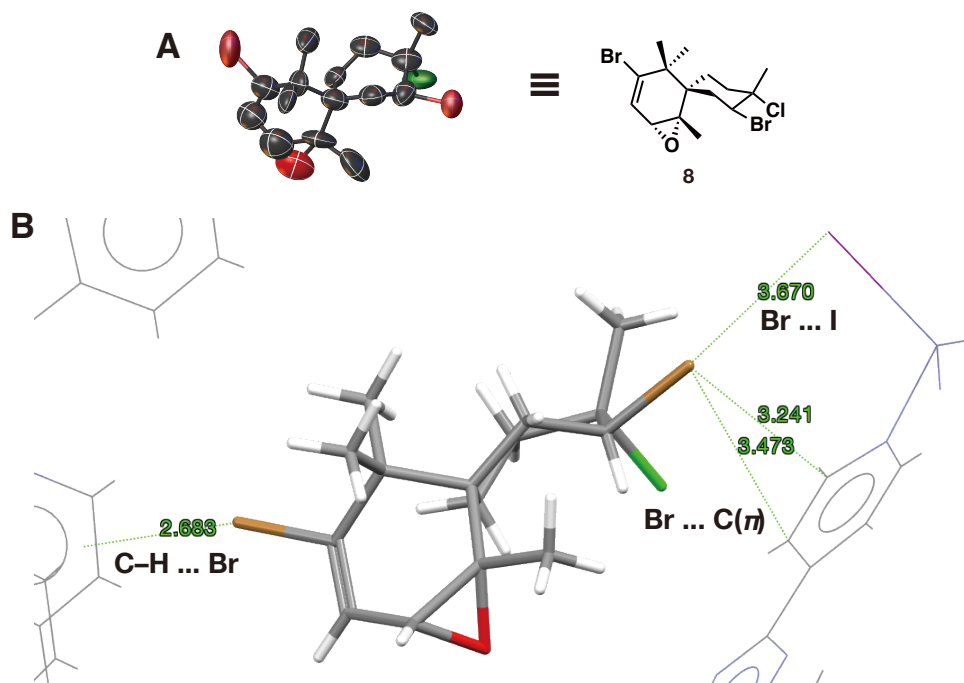


**Fig. 2–12** (A) Thermal ellipsoid plot of **8** with 30% probability. Hydrogen atoms are not shown for clarity. (B) An example of intermolecular interactions between **8** and **21**. The captions

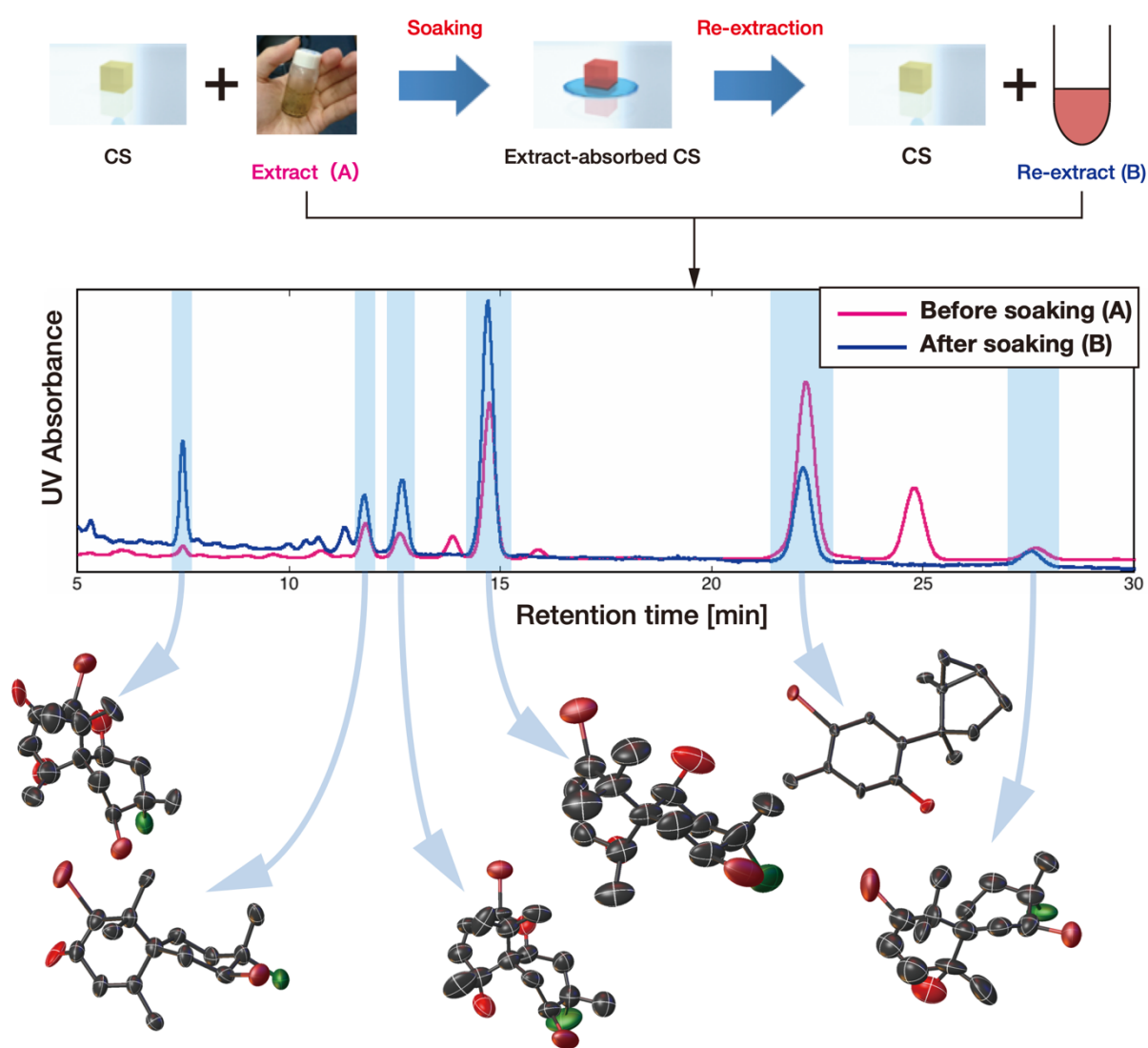
indicate the atoms involving in the interactions. The values indicate atom distances highlighted with dashed lines and in angstroms (Å).

In summary, I succeeded in determining the absolute configurations of all six components from about 10 mg of *L. pacifica* crude extract and supporting previous conclusions on the stereochemical assignments.

## 2.4 Summary

In this study, I established a new workflow for NP structural determination that maximizes the outputs from limited quantity of biological samples, by starting the confirmation of the affinity between the crystalline sponges and NPs prior to compound purification and structural analysis. The absolute configurations of six NPs were determined only from about 10 mg of the extract from the red alga *L. pacifica*, and the time required for the extraction, isolation, and structural determination of NPs, that conventionally consumes several years of research periods, was successfully reduced to several months (Fig. 2–13). CSAS can be also regarded as the prescreening tool for the guest soaking conditions, that was well demonstrated in a study by medicinal scientists.<sup>[24]</sup> The novel workflow for NP structural determination proposed in this study is expected to lead to the development of new drugs when combined with bioactivity assays, as well as to have a scale-down effect in the field of genome-based NP chemistry, where functions of various biosynthetic enzymes are investigated in recent years, and further accelerate structural determination of trace amounts of metabolites obtained in enzymatic reactions.





## Complete NP structural determination

Research Period decreased from years to months

Required amounts of extract decreased from grams to dozens of milligrams

**Fig. 2–13** Schematic representation of this study. I established a novel workflow that provides maximum outputs from limited quantity of the biological sample derived from a red alga, *L. pacifica*.

## 2.5 Experimental Section

### Materials and instruments

Solvents and chemicals were purchased from TCI Co., Ltd., FUJIFILM Wako Pure Chemical Corporation, Sigma-Aldrich Co. LLC. or Kanto Chemical Co., Inc. The crystalline sponge (CS)  $[(\text{ZnI}_2)_3(\text{tpt})_2 \cdot x(\text{cyclohexane})]_n$  (**21**; tpt = 2,4,6-tris(4-pyridyl)-1,3,5-triazine)<sup>[22]</sup> was prepared according to the reported procedure.<sup>[25]</sup> A screw-top microvial (Osaka Chemical, cat. no. 11090620), a screw cap with a septum seal (Osaka Chemical, cat. no. 53951-09FB), and a syringe needle (TERUMO, cat. no. NN-2116R) were used for guest inclusion into the porous crystals. Electrospray-ionization time-of-flight high-resolution mass spectrometry (ESI-TOF-HRMS) analysis was performed with a Bruker maXis. HPLC analyses and purification were performed with a Shimadzu LC-20AD system equipped with a CBM-20A communication bus module, a SIL-20AC auto sampler, a CTO-20AC column oven, a SPD-M20A diode array detector and a FRC-10A fraction collector, using either a Develosil ODS-5 column (4.6 mm i.d.  $\times$  150 mm, Nomura Chemical Co., Ltd., cat. no. ODS0546150W) or an Inertsil Peptides C18 column (10 mm i.d.  $\times$  250 mm, GL Sciences Inc., cat. no. 5020-08084). NMR spectra were obtained at 500 MHz ( $^1\text{H}$ ) and 125 MHz ( $^{13}\text{C}$ ) with either a JEOL ECZ-500R spectrometer or a Bruker AV-500 equipped with TCI gradient CryoProbe. All NMR spectra data were collected at 300 K and chemical shifts are reported in parts per million (ppm) relative to an internal standard tetramethylsilane ( $\delta = 0.00$  ppm for  $^1\text{H}$  and  $^{13}\text{C}$  NMR) for chloroform-*d*. Data are reported as follows: chemical shifts, integration int, multiplicity m (s=singlet, d=doublet, dd=double doublet, t=triplet, q=quartet, m=multiplet, br=broad), coupling constants *J* in Hertz (Hz). Single crystal X-ray diffraction data were collected on a Synergy-S (Rigaku Oxford Diffraction) diffractometer equipped with a micro-focus Cu K $\alpha$  radiation source ( $\lambda = 1.5418$  Å), a hybrid pixel array detector (HPAD), and a low temperature system using cold nitrogen

stream (100 K) (**21·7**, **21·8**), on a XtaLAB Pro P200 (Rigaku Oxford Diffraction) diffractometer equipped with a fine-focus Mo K $\alpha$  radiation source ( $\lambda = 0.71073$  Å), a HPAD, and a low temperature system using cold nitrogen stream (93 K) (**21·3**), and a SuperNova (Rigaku Oxford Diffraction) diffractometer equipped with a micro-focus Cu K $\alpha$  radiation source ( $\lambda = 1.5418$  Å), a high-sensitive CCD detector, and a low temperature system using cold nitrogen stream (100 K) (**21·5**, **21·6**, **21·9**). Collected data were integrated, corrected, and scaled by the program CrysAlis<sup>Pro</sup>. Empirical and numerical absorption corrections were applied in this process.

#### **Crystalline Sponge Affinity Screening (CSAS) - inclusion and extraction of the crude extracts from the crystalline sponge**

To assess the affinity of each compound present in crude extracts for CS crystals, a fine crystal of porous complex **21** was immersed in 45  $\mu$ L cyclohexane and 5  $\mu$ L 1,2-dichloroethane (DCE) containing 5  $\mu$ g of the crude extract. The solvent evaporation was conducted at 50 °C for 1 day with a needle, 3 days without a needle, and finally 2 days with a needle. Five sets were prepared for crude guest inclusion. After 6 days of crude guest inclusion, each crystal was collected and combined in a new vial. Subsequently, 100  $\mu$ L cyclohexane were added into the vial and the guests were extracted for 4 days at 25 °C. After removing the crystals and evaporating the solvent, *ca.* 50  $\mu$ L methanol were added to the vial, and 10  $\mu$ L of the solution were subjected to HPLC analysis as follows: solvent A – water, solvent B – acetonitrile, 0–30 min 60% B, 1 mL/min with a Develosil ODS-5 column. The chromatogram was monitored at 210 nm.

#### **HPLC purification of components in the crude extract from *L. pacifica***

10 mg of the crude extract was processed with solid phase extraction by methanol using a Waters Sep-Pak® Plus C18 cartridge (Waters, cat. no. WAT020515). The observed components were separated by HPLC purification as follows: solvent A – water, solvent B – acetonitrile, 0–55 min 60% B, 5 mL/min with an Inertsil Peptides C18 column. The chromatogram was monitored at 210 nm. Each HPLC fraction was dried *in vacuo*, dissolved in chloroform-*d* and subjected to NMR analysis. The yield of each compound is as follows: **3**; 0.3 mg, **5**; 0.08 mg, **6**; 0.04 mg, **7**; 0.7 mg, **8**, 0.09 mg, **9**; 0.07 mg. HRMS analysis of each HPLC fraction gave following molecular ions.

**3**;  $m/z$ : 293.0534, calculated for  $[C_{15}H_{19}O^{79}Br-H]^-$ : 293.0541, 2.4 ppm error

**5**;  $m/z$ : 462.9288, calculated for  $[C_{15}H_{21}O_2^{79}Br^{81}Br^{35}Cl+^{35}Cl]^-$ : 462.9265, 5.0 ppm error

**6**;  $m/z$ : 478.9225, calculated for  $[C_{15}H_{21}O_3^{79}Br^{81}Br^{35}Cl+^{35}Cl]^-$ : 478.9214, 2.3 ppm error

**7**;  $m/z$ : 450.9472, calculated for  $[C_{15}H_{21}O_2^{79}Br^{81}Br^{35}Cl+Na]^+$ : 450.9474, 0.4 ppm error

**9**;  $m/z$ : 448.9459, calculated for  $[C_{15}H_{23}O^{79}Br^{81}Br^{35}Cl+^{35}Cl]^-$ : 448.9472, 2.9 ppm error

### **Preparation of guest-absorbed crystalline sponges**

(prepacifenol) The guest-absorbed crystals **21·7** were prepared by immersing a single crystal of **21** in 45  $\mu$ L cyclohexane and 5  $\mu$ L DCE containing 5  $\mu$ g of **7**. The solvent evaporation was conducted at 50 °C for 9 h with a needle, 2 days without a needle, and finally 1 day with a needle. Three sets were prepared.

(laurinterol) The guest-absorbed crystals **21·3** were prepared by immersing a single crystal of **21** in 45  $\mu$ L cyclohexane and 5  $\mu$ L DCE containing 5  $\mu$ g of **3**. The solvent evaporation was conducted for 2 days with a needle at 50 °C. Five sets were prepared.

(johnstonol) The guest-absorbed crystals **21·6** were prepared by immersing a single crystal of **21** in 45  $\mu$ L cyclohexane and 2  $\mu$ L DCE containing 4  $\mu$ g of **6**. The solvent evaporation

was conducted at 50 °C for 8 h with a needle, 3 days without a needle, and finally 1 day with a needle. Three sets were prepared.

(pacifenol) The guest-absorbed crystals **21·5** were prepared by immersing a single crystal of **21** in 45 µL cyclohexane and 2.5 µL DCE containing 2.5 µg of **5**. The solvent evaporation was conducted for 2 days with a needle at 50 °C. Nine sets were prepared.

(2,10-dibromo-3-chlorochamigran-7-en-9-ol) The guest-absorbed crystals **21·9** were prepared by immersing a single crystal of **21** in 45 µL cyclohexane and 5 µL DCE containing 3.5 µg of **9**. The solvent evaporation was conducted at 50 °C for 6 h with a needle, 3 days without a needle, and finally 2 days with a needle. Five sets were prepared.

(deoxyrepacifenol) The guest-absorbed crystals **21·8** were prepared by immersing a single crystal of **21** in 45 µL cyclohexane and 1 µL DCE containing 5 µg of **8**. The solvent evaporation was conducted at 50 °C for 8 h with a needle, 3 days without a needle, and finally 1 day with a needle. Three sets were prepared.

### **Crystal structure analysis**

All crystal structures were solved using SHELXT ver. 2014/5<sup>[26]</sup> and refined using SHELXL ver. 2014/7<sup>[27]</sup> programs. All the non-hydrogen atoms were refined anisotropically. All the hydrogen atoms were grown using the proper HFIX commands and refined isotropically using the riding model. Several zinc and iodine atoms in the framework were refined with EADP commands. Guest molecules were refined with restraints on atomic displacement parameters (SIMU). Populations of the guests in the crystal were estimated from the least-square refinement of a guest/solvent disorder model under the constraint that the sum of them should be equal to 100%. Minimum numbers of restraints were applied for the guest molecules. Solvent molecules in the pores were found in the difference electron density map and refined

using the restraints (DFIX, DANG, SIMU, and ISOR). These molecules were expected to be severely disordered as a consequence of their high thermal motion and have an averaged structure of various geometry and orientation. This is a reason why some cyclohexane molecules are distorted to energetically-unfavorable (boat-shaped or twisted) structure, and the DFIX commands should be used for the refinement of the solvent molecules to avoid their close contact.

For crystal structures of **21·5**, **21·6**, **21·7**, **21·8**, and **21·9**, considerably large void remained in the crystal structure, and we assumed that the void is filled with disordered solvents or guest molecules. Therefore, the least square refinement at the last stage was performed using the reflection data modified by the *PLATON*<sup>[28]</sup>/*SQUEEZE*<sup>[29]</sup> program.

Several “Alert A” notifications were found in the validation program CheckCIF. The comments for the alerts are described in the validation response form (vrf) in each cif file.

### Crystallographic data of **21·3**

Refined formula: C<sub>307.12</sub>H<sub>308.13</sub>Br<sub>10.37</sub>I<sub>24</sub>N<sub>48</sub>O<sub>10.37</sub>Zn<sub>12</sub>, formula weight ( $M_r$ ): 9496.70, crystal system: monoclinic, space group:  $P2_1$ ,  $Z = 2$ ,  $R_{\text{int}} = 0.0489$ , Lattice parameters,  $R$ -factor on  $F^2 > 2\sigma(F^2)$ , and weighted  $R$ -factor are as follows:  $a = 33.6997(7)$  Å,  $b = 14.6833(2)$  Å,  $c = 36.7774(8)$  Å,  $\beta = 109.072(2)^\circ$ ,  $V = 17199.4(6)$  Å<sup>3</sup>, GoF = 1.043,  $R_1 = 0.0629$ ,  $wR_2 = 0.1624$ , Flack parameter calculated by Parsons’ method<sup>[23]</sup>; 0.055(7). CCDC deposit number 1812554.

The ORTEP diagram of the asymmetric unit of **21·3** is shown in Fig. 2–13. Twelve guest molecules (**A–L**) were found in the asymmetric unit. Nine of the molecules (**A–I**) are ordered at general position and have occupancies of 100%. Two guest molecules (**J** and **K**) are disordered with one guest molecule (**L**) and two solvent (cyclohexane) molecules, and their

occupancies were estimated to be 37.4(5)%, 37.4(5)% and 62.6(5)%, respectively, by least square refinement.

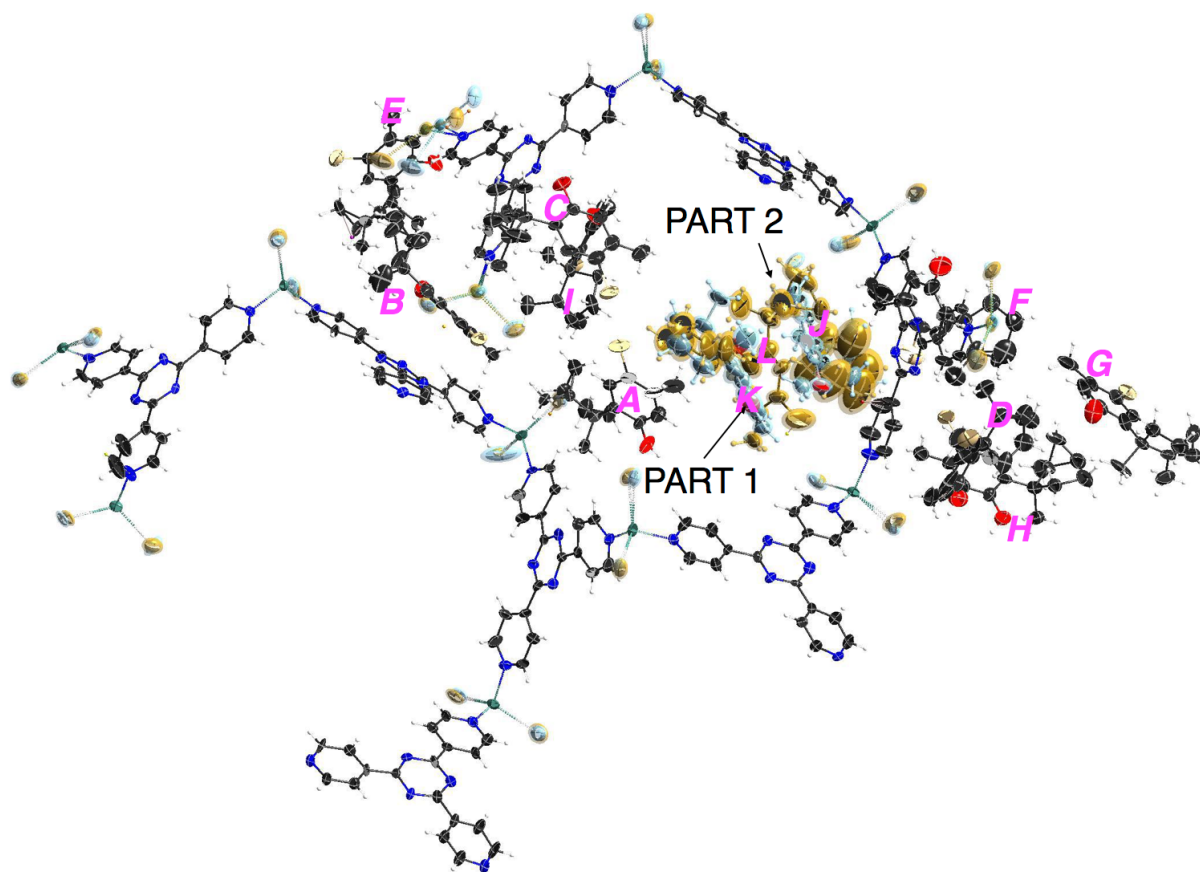


**Fig. 2–13** Thermal ellipsoid plot of **21·3** with 50% probability.

Some restraints should be applied in refinement of a disordered model. Four guest molecules (**B**, **J–L**) were refined with applying SIMU (for the whole molecules). The geometry of **A** was related with applying SAME for **B**, **D–F** and **J–L** (for the whole molecule). DELU was applied to the methyl group of **E**. In addition, RIGU was applied for the methyl group of **F**, and ISOR was applied to one carbon of **E**. The restraints used for the refinement are summarized in Fig. 2–14.

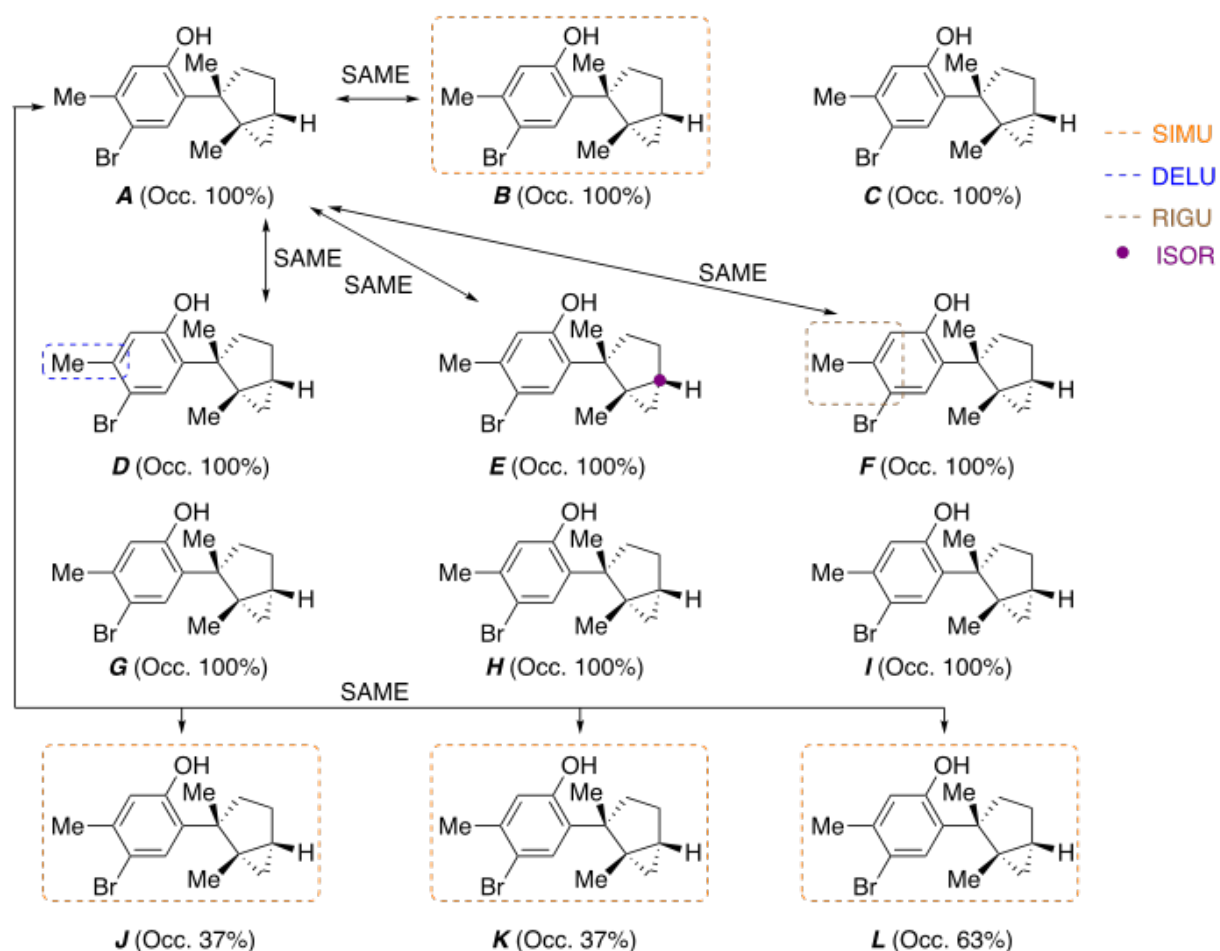


**Fig. 2–14** Restraints applied in the refinement of **21·3**.

### Crystallographic data of **21·5**

Refined formula:  $\text{C}_{106.50}\text{H}_{103.50}\text{Br}_3\text{Cl}_{1.50}\text{I}_{12}\text{N}_{24}\text{O}_3\text{Zn}_6$ , formula weight ( $M_r$ ): 3975.65, crystal system: monoclinic, space group:  $C2$ ,  $Z = 4$ ,  $R_{\text{int}} = 0.0697$ , Lattice parameters,  $R$ -factor on  $F^2 > 2\sigma(F^2)$ , and weighted  $R$ -factor are as follows:  $a = 35.5423(10) \text{ \AA}$ ,  $b = 14.9231(3) \text{ \AA}$ ,  $c = 30.4124(9) \text{ \AA}$ ,  $\beta = 101.756(3)^\circ$ ,  $V = 15792.4(7) \text{ \AA}^3$ ,  $\text{GoF} = 1.088$ ,  $R_1 = 0.0970$ ,  $wR_2 = 0.2907$ , Flack parameter calculated by Parsons' method<sup>[23]</sup>; 0.054(12). CCDC deposit number 1812570.



The ORTEP diagram of the asymmetric unit of **21·5** is shown in Fig. 2–15. Two guest molecules (**A** and **B**) were found in the asymmetric unit. One of the molecules (**A**) is ordered at general position and has an occupancy of 100%. Another guest molecule (**B**) with an occupancy of 50% is overlapped on the symmetrically generated one by the 2-fold rotation operation.

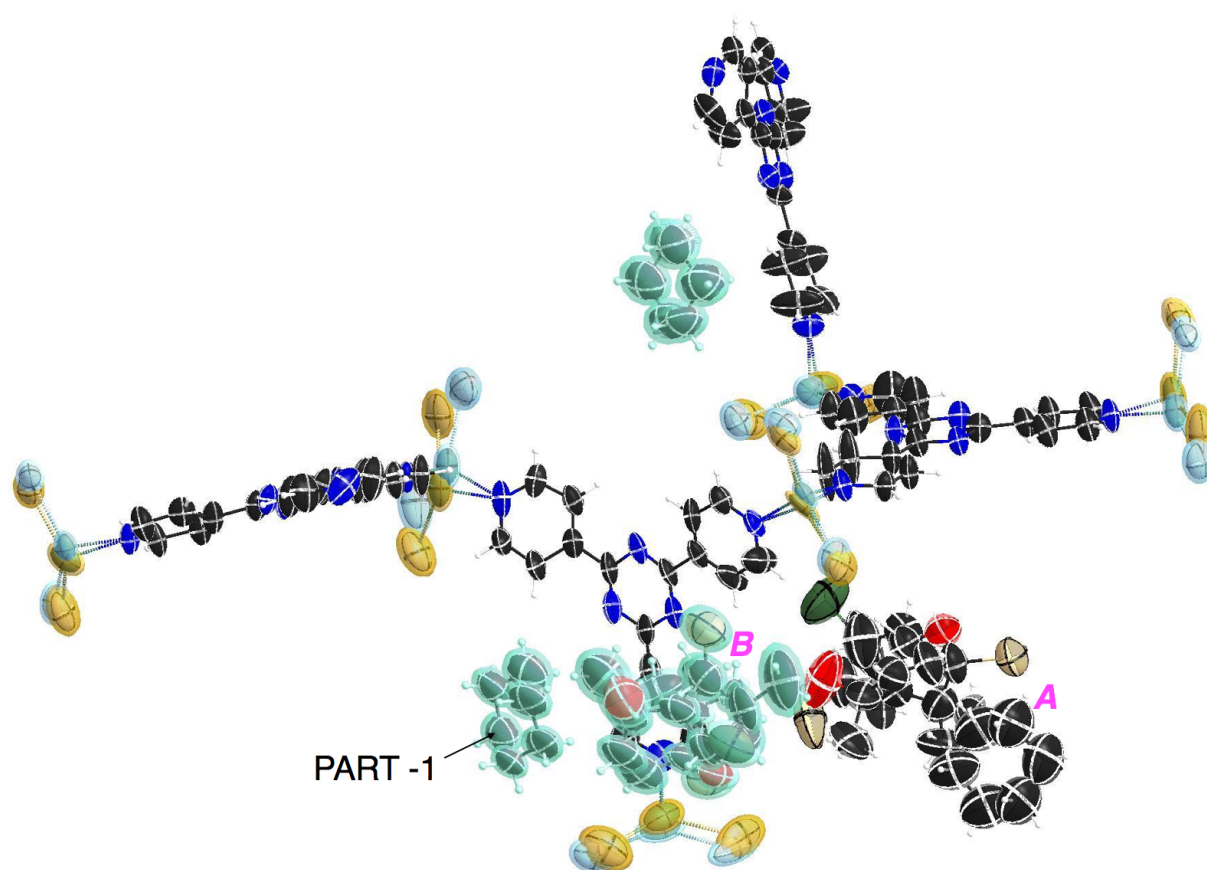


**Fig. 2–15** Thermal ellipsoid plot of **21·5** with 50% probability.

Some restraints should be applied in refinement of a disordered model. All the two guest molecules were refined by applying SIMU (for the whole molecules). DFIX was used for ten bonds. The geometry of **A** was related by applying SAME for **B** (for the whole molecule). The restraints used for the refinement are summarized in Fig. 2–16.

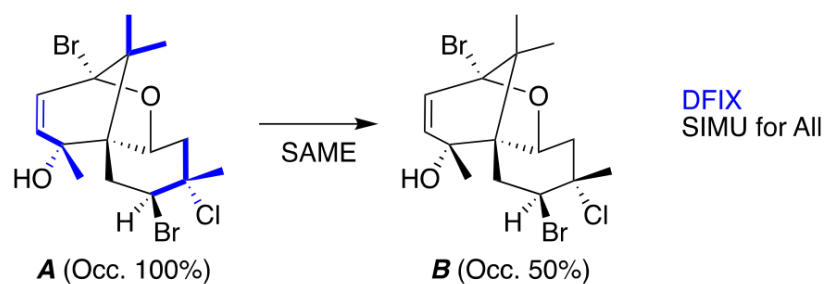


**Fig. 2–16** Restraints applied in the refinement of **21·5**.

### Crystallographic data of **21·6**

Refined formula:  $\text{C}_{98.50}\text{H}_{90.50}\text{Br}_{2.33}\text{Cl}_{1.17}\text{I}_{12}\text{N}_{24}\text{O}_{3.50}\text{Zn}_6$ , formula weight ( $M_r$ ): 3809.39, crystal system: monoclinic, space group:  $C2$ ,  $Z = 4$ ,  $R_{\text{int}} = 0.0790$ , Lattice parameters,  $R$ -factor on  $F^2 > 2\sigma(F^2)$ , and weighted  $R$ -factor are as follows:  $a = 34.6843(11) \text{ \AA}$ ,  $b = 14.8777(2) \text{ \AA}$ ,  $c = 31.2080(9) \text{ \AA}$ ,  $\beta = 101.340(3)^\circ$ ,  $V = 15789.6(7) \text{ \AA}^3$ ,  $\text{GoF} = 1.044$ ,  $R_1 = 0.0764$ ,  $wR_2 = 0.2407$ , Flack parameter calculated by Parsons' method<sup>[23]</sup>; 0.126(7). CCDC deposit number 1812553.

The ORTEP diagram of the asymmetric unit of **21·6** is shown in Fig. 2–17. Two guest molecules (**A** and **B**) were found in the asymmetric unit. One of the molecules (**A**) is disordered with a solvent (cyclohexane) molecule, and its occupancy was estimated to be 40.2(7)% by least square refinement. Another guest molecule (**B**) is disordered with a solvent (cyclohexane) molecule, and its occupancy was estimated to be 60.5(9)% by least square refinement.

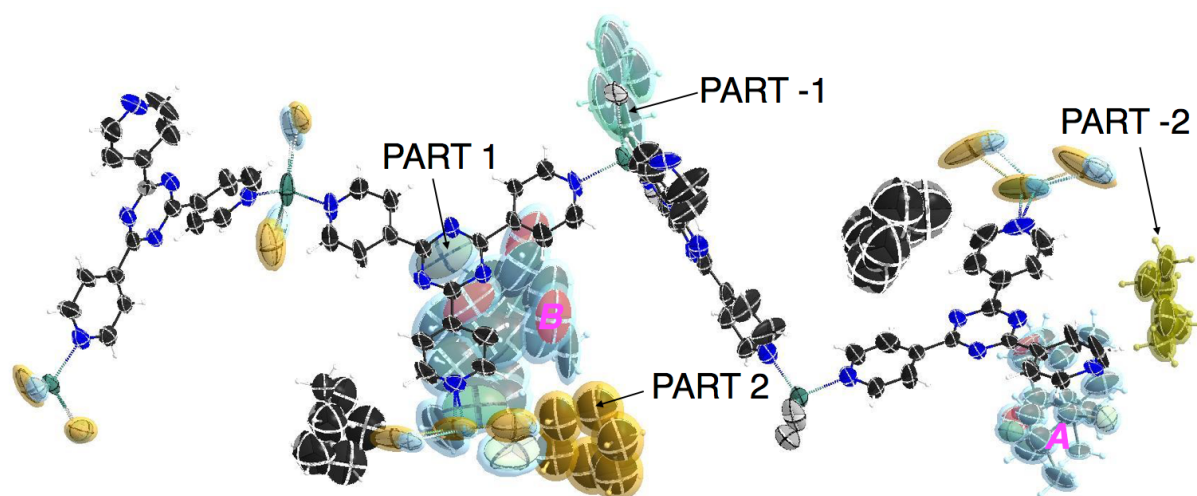


**Fig. 2–17** Thermal ellipsoid plot of **21·6** with 50% probability.

Some restraints should be applied in refinement of a disordered model. The two guest molecules were refined by applying SIMU (for the whole molecules). DFIX was used for ten bonds. The geometry of **A** was related by applying SAME for **B** (for the whole molecule). The restraints used for the refinement are summarized in Fig. 2–18.

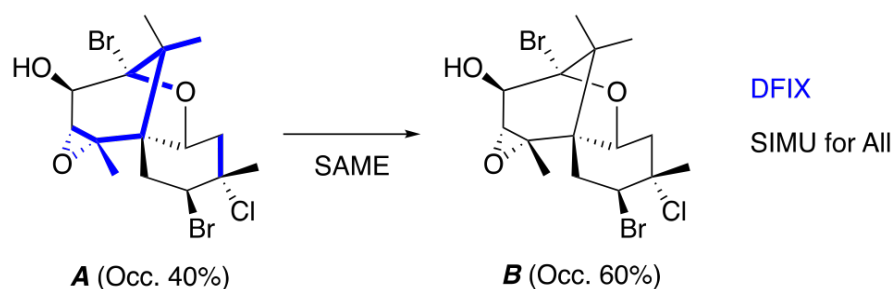


**Fig. 2–18** Restraints applied in the refinement of **21·6**.

### Crystallographic data of **21·7**

Refined formula:  $\text{C}_{95.23}\text{H}_{81.50}\text{Br}_{2.88}\text{Cl}_{3.06}\text{I}_{12}\text{N}_{24}\text{O}_{2.88}\text{Zn}_6$ , formula weight ( $M_r$ ): 3862.11, crystal system: monoclinic, space group:  $C2$ ,  $Z = 4$ ,  $R_{\text{int}} = 0.0450$ , Lattice parameters,  $R$ -factor on  $F^2 >$

$2\sigma(F^2)$ , and weighted  $R$ -factor are as follows:  $a = 35.7306(3) \text{ \AA}$ ,  $b = 14.78070(10) \text{ \AA}$ ,  $c = 30.9919(2) \text{ \AA}$ ,  $\beta = 101.7390(10)^\circ$ ,  $V = 16025.2(2) \text{ \AA}^3$ ,  $\text{GoF} = 1.073$ ,  $R_1 = 0.0538$ ,  $wR_2 = 0.1775$ , Flack parameter calculated by Parsons' method<sup>[23]</sup>;  $0.046(3)$ . CCDC deposit number 1812550.

The ORTEP diagram of the asymmetric unit of **21·7** is shown in Fig. 2–19. Two guest molecules (**A** and **B**) were found in the asymmetric unit. One of the molecules (**A**) is ordered at general position and has an occupancy of 100%. Another guest molecule (**B**) is disordered with a solvent (DCE) molecule, and its occupancy was estimated to be 44.1(5)% by least square refinement.

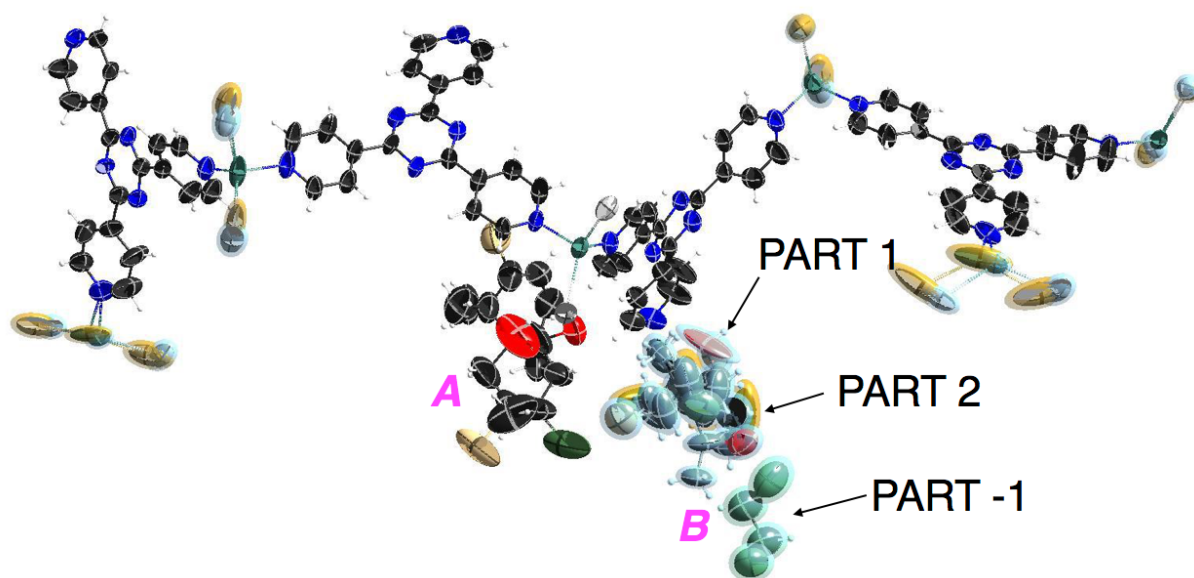


**Fig. 2–19** Thermal ellipsoid plot of **21·7** with 50% probability.

Some restraints should be applied in refinement of a disordered model. All of the two guest molecules were refined with applying SIMU (for the whole molecules). DFIX was used for eleven bonds. The geometry of **A** was related with applying SAME for **B** (for the whole

molecule). In addition, RIGU was applied for the three methyl groups of **A**. The restraints used for the refinement are summarized in Fig. 2–20.

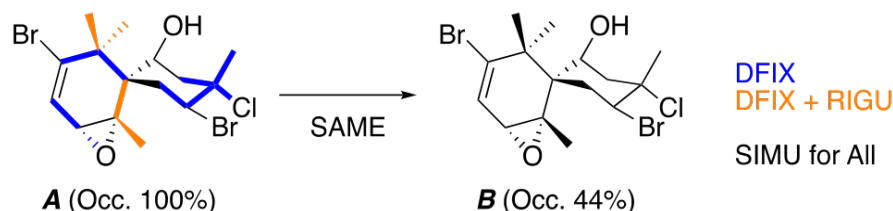


**Fig. 2–20** Restraints applied in the refinement of **21·7**.

#### Crystallographic data of **21·8**

Refined formula:  $C_{89}H_{77.70}Br_{0.95}Cl_{3.12}I_{12}N_{24}O_{0.48}Zn_6$ , formula weight ( $M_r$ ): 3592.58, crystal system: monoclinic, space group:  $C2$ ,  $Z = 4$ ,  $R_{int} = 0.0516$ , Lattice parameters,  $R$ -factor on  $F^2 > 2\sigma(F^2)$ , and weighted  $R$ -factor are as follows:  $a = 35.5810(4)$  Å,  $b = 14.84930(10)$  Å,  $c = 31.2940(3)$  Å,  $\beta = 102.0880(10)^\circ$ ,  $V = 16167.7(3)$  Å<sup>3</sup>, GoF = 1.118,  $R_1 = 0.0719$ ,  $wR_2 = 0.2463$ , Flack parameter calculated by Parsons' method<sup>[23]</sup>; 0.099(5). CCDC deposit number 1812605.

The ORTEP diagram of the asymmetric unit of **21·8** is shown in Fig. 2–21. One guest molecule (**A**) was found in the asymmetric unit. The molecule (**A**) is disordered with one solvent (cyclohexane) molecule, and its occupancy was estimated to be 46.2(7)% by least square refinement.

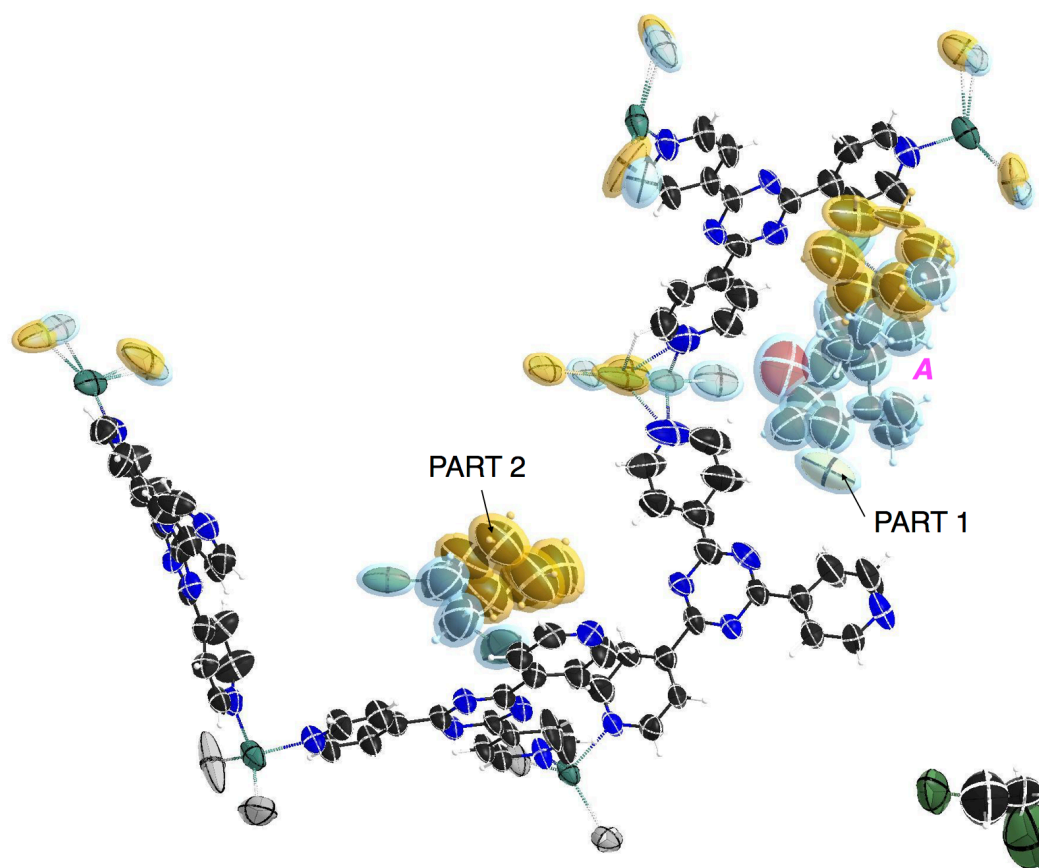


**Fig. 2–21** Thermal ellipsoid plot of **21·8** with 50% probability.

Some restraints should be applied in refinement of a disordered model. All the two guest molecules were refined by applying SIMU (for the whole molecules). DFIX was used for twenty bonds. DANG was used for ten sites. The restraints used for the refinement are summarized in Fig. 2–22.

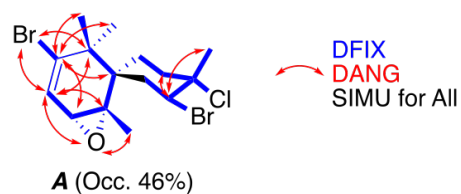


**Fig. 2–22** Restraints applied in the refinement of **21·8**.

### Crystallographic data of **21·9**

Refined formula:  $C_{106.98}H_{113.34}Br_{1.32}Cl_{0.66}I_{12}N_{24}O_{0.66}Zn_6$ , formula weight ( $M_r$ ): 3790.13, crystal system: monoclinic, space group:  $C2$ ,  $Z = 4$ ,  $R_{int} = 0.0441$ , Lattice parameters,  $R$ -factor on  $F^2 > 2\sigma(F^2)$ , and weighted  $R$ -factor are as follows:  $a = 35.7703(6)$  Å,  $b = 14.8570(2)$  Å,  $c = 30.8861(5)$  Å,  $\beta = 102.132(2)^\circ$ ,  $V = 16047.5(4)$  Å<sup>3</sup>, GoF = 1.022,  $R_1 = 0.0484$ ,  $wR_2 = 0.1573$ , Flack parameter calculated by Parsons' method<sup>[23]</sup>; 0.053(4). CCDC deposit number 1812552.

The ORTEP diagram of the asymmetric unit of **21·9** is shown in Fig. 2–23. Two guest molecules (**A** and **B**) were found in the asymmetric unit. One of the molecules (**A**) is disordered with two solvent (cyclohexane) molecules, and its occupancy was estimated to be 29.4(5)% by least square refinement. Another guest molecule (**B**) is disordered with two solvent (cyclohexane) molecules, and its occupancy was estimated to be 36.7(6)% by least square refinement.

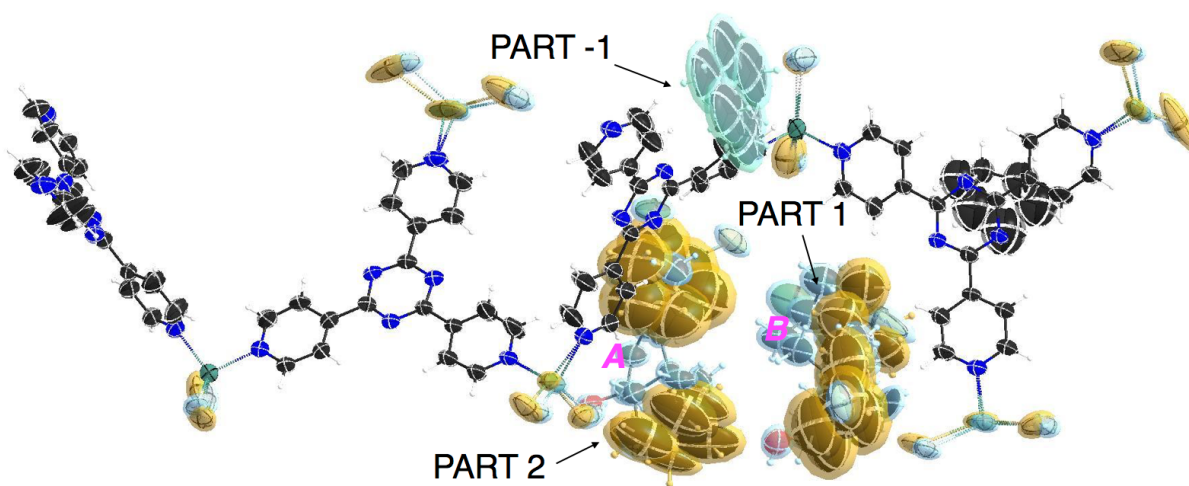


**Fig. 2–23** Restraints applied in the refinement of **21·9**.

Some restraints should be applied in refinement of a disordered model. All the two guest molecules were refined by applying SIMU (for the whole molecules). The geometry of **A** was related by applying SAME for **B** (for the whole molecule). In addition, RIGU was applied for the hydroxyl group of **A** and the methyl group and chlorine of **B**. The restraints used for the refinement are summarized in Fig. 2–24.

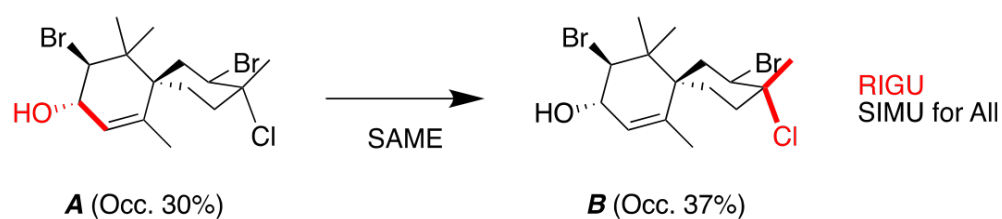
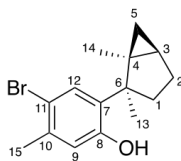


**Fig. 2–24** Restraints applied in the refinement of **21·9**.



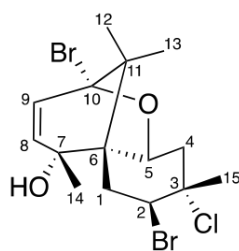
**Table 2–1** NMR data of **3** (laurinterol)



Position	$\delta(^{13}\text{C})$ [ppm] [a]	$\delta(^{13}\text{C})$ [ppm] [b]	$\delta(^1\text{H})$ [ppm] (int, m, J) [c]	$\delta(^1\text{H})$ [ppm] (int, m, J) [d]	HMBC Correlation	COSY correlation	NOESY correlation
1	36.0 (CH <sub>2</sub> )	35.9	H <sub>a</sub> : 2.08 (1H, dd, 12.9, 8.3)  H <sub>β</sub> : 1.29 (1H, m)	H <sub>a</sub> : 2.06 (1H, dd, 13.1, 8.1)  H <sub>β</sub> : 1.25 (1H, m)	2, 3, 4, 6, 13	H1 <sub>β</sub> , H2 <sub>α</sub>  H1 <sub>α</sub> , H2 <sub>β</sub>	H2 <sub>β</sub> , H13, H12, H14, 8-OH  H2 <sub>α</sub> , H2 <sub>β</sub>
2	25.3 (CH <sub>2</sub> )	25.3	H <sub>a</sub> : 1.94 (1H, m)  H <sub>β</sub> : 1.66 (1H, dd, 11.7, 8.3)	H <sub>a</sub> : 1.93 (1H, dddd, 12.2, 12.0, 8.1, 4.3) H <sub>β</sub> : 1.64 (1H, dd, 12.2, 8.0)	1, 3, 4, 5, 6	H1 <sub>α</sub> , H2 <sub>β</sub> , H3  H1 <sub>β</sub> , H2 <sub>α</sub>	H1 <sub>β</sub> , H2 <sub>β</sub> , H3, H13  H1 <sub>α</sub> , H1 <sub>β</sub> , H2 <sub>α</sub> , H3, H5
3	24.5 (CH)	24.4	1.14 (1H, m)	1.12 (1H, ddd, 7.8, 4.3, 3.9)	-	H2 <sub>α</sub> , H5	H2 <sub>α</sub> , H2 <sub>β</sub> , H5
4	29.6 (C)	29.6	-	-	-	-	-
5	16.3 (CH <sub>2</sub> )	16.2	0.55 (2H, m)	H <sub>a</sub> : 0.52 (1H, dd, 7.8, 4.7) H <sub>β</sub> : 0.56 (1H, dd, 4.7, 3.9)	2, 4, 6, 14	H3	H2 <sub>β</sub> , H3, H12, H14, 8-OH
6	48.1 (C)	48.0	-	-	-	-	-
7	134.0 (C)	134.1	-	-	-	-	-
8	153.3 (C)	153.3	-	-	-	-	-
9	118.9 (CH)	118.8	6.61 (1H, s)	6.59 (1H, s)	7, 8, 11, 15	-	H15, 8-OH
10	136.0 (C)	135.9	-	-	-	-	-
11	115.0 (C)	114.9	-	-	-	-	-
12	132.4 (CH)	132.3	7.60 (1H, s)	7.59 (1H, s)	6, 8, 10, 11	-	H1 <sub>α</sub> , H5, H13, H14
13	23.6 (CH <sub>3</sub> )	23.5	1.40 (3H, s)	1.39 (3H, s)	1, 4, 6, 7	-	H1 <sub>α</sub> , H2 <sub>α</sub> , H12, 8-OH
14	18.6 (CH <sub>3</sub> )	18.6	1.31 (3H, s)	1.31 (3H, s)	3, 4, 5, 6	-	H1 <sub>α</sub> , H5, H12
15	22.2 (CH <sub>3</sub> )	22.2	2.29 (3H, s)	2.27 (3H, s)	9, 10, 11	-	H9
8-OH	-	-	5.09 (1H, s)	N.D.	7, 8, 9	-	H1 <sub>α</sub> , H5, H9, H13

[a] <sup>13</sup>C NMR data of isolated laurinterol. Assignment of carbons by <sup>13</sup>C-DEPT 135 spectroscopy. [b] <sup>13</sup>C NMR data of laurinterol in chloroform-*d* from reference.<sup>[30]</sup> [c] <sup>1</sup>H NMR data of isolated laurinterol. [d] <sup>1</sup>H NMR data of laurinterol in chloroform-*d* from reference.<sup>[30]</sup> N.D.=not detected.

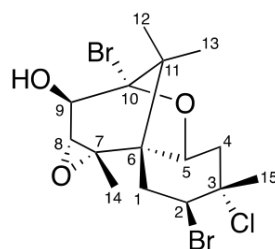
**Table 2–2** NMR data of **5** (pacifenol).



Position	$\delta(^1\text{H})$ [ppm] (int, m, $J$ ) <sup>[a]</sup>	$\delta(^1\text{H})$ [ppm] (int, m, $J$ ) <sup>[b]</sup>
1	H <sub>a</sub> : 2.19 (1H, m) H <sub>β</sub> : 2.35 (1H, m)	H <sub>a</sub> : 2.18 (1H, dd, 14.5, 13.5) H <sub>β</sub> : 2.35 (1H, dd, 14.5, 2.0)
2	5.44 (1H, dd, 13.2, 3.4)	5.45 (1H, dd, 13.5, 3.8)
3	-	-
4	H <sub>a</sub> : 2.35 (1H, m) H <sub>β</sub> : 2.69 (1H, dd, 14.9, 5.5)	H <sub>a</sub> : 2.36 (1H, dd, 15.0, 14.0) H <sub>β</sub> : 2.70 (1H, dd, 15.0, 5.3)
5	4.68 (1H, dd, 12.6, 5.2)	4.69 (1H, dd, 13.5, 5.0)
6	-	-
7	-	-
8	5.38 (1H, d, 9.7)	5.40 (1H, d, 10.0)
9	6.06 (1H, d, 9.7)	6.07 (1H, d, 10.0)
10	-	-
11	-	-
12	1.11 (3H, s)	1.12 (3H, s)
13	1.30 (3H, s)	1.31 (3H, s)
14	1.53 (3H, s)	1.52 (3H, s)
15	1.79 (3H, s)	1.78 (3H, s)
7-OH	1.86 (1H, s)	1.88 (1H, s)

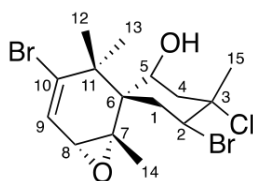
[a] <sup>1</sup>H NMR data of isolated pacifenol. N.D.=not detected. [b] <sup>1</sup>H NMR data of pacifenol in chloroform-*d* from reference.<sup>[31]</sup>

**Table 2–3** NMR data of **6** (johnstonol).



Position	$\delta(^1\text{H})$ [ppm] (int, m, $J$ ) <sup>[a]</sup>	$\delta(^1\text{H})$ [ppm] (int, m, $J$ ) <sup>[b]</sup>
1	2.15 (2H, m)	H <sub>a</sub> : 2.13 (1H, dd, 15.0 13.0) H <sub>β</sub> : 2.23 (1H, dd, 15.0, 2.0)
2	4.30 (1H, dd, 13.5, 2.0)	4.31 (1H, dd, 13.0, 2.5)
3	-	-
4	H <sub>a</sub> : 2.15 (1H, m) H <sub>β</sub> : 2.56 (1H, dd, 14.3, 4.6)	H <sub>a</sub> : 2.24 (1H, dd, 14.5, 13.5) H <sub>β</sub> : 2.57 (1H, dd, 14.5, 5.0)
5	4.66 (1H, dd, 13.2, 4.6)	4.67 (1H, dd, 14.0, 5.0)
6	-	-
7	-	-
8	3.20 (1H, s)	3.21 (1H, s)
9	4.03 (1H, d, 2.3)	4.04 (1H, d, 1.5)
10	-	-
11	-	-
12	1.16 (3H, s)	1.17 (3H, s)
13	1.28 (3H, s)	1.29 (3H, s)
14	1.45 (3H, s)	1.46 (3H, s)
15	1.74 (3H, s)	1.75 (3H, s)
7-OH	-	-
9-OH	2.59 (1H, d, 2.3)	2.60 (1H, d, 1.5)

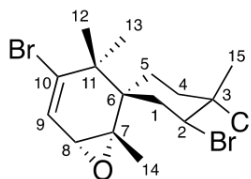
[a] <sup>1</sup>H NMR data of isolated johnstonol. [b] <sup>1</sup>H NMR data of johnstonol in chloroform-*d* from reference.<sup>[31]</sup>

**Table 2–4** NMR data of **7** (prepacifenol)

Position	$\delta(^{13}\text{C})$ [ppm] <sup>[a]</sup>	$\delta(^1\text{H})$ [ppm] (int, m, <i>J</i> ) <sup>[b]</sup>	$\delta(^1\text{H})$ [ppm] (int, m, <i>J</i> ) [c]	HMBC correlation	COSY correlation	NOESY correlation
1	36.0	H <sub>ax</sub> : 2.42 (1H, m) H <sub>eq</sub> : 2.31 (1H, ddd, 14.5, 3.6, 1.4)	2.4 (2H, m)	2, 3, 5, 6	H2	H2, H13 H2, H12
2	62.1	H <sub>ax</sub> : 4.74 (1H, dd, 13.4, 3.6)	4.72 (1H, dd)	1, 3, 6, 15	H1	H1 <sub>ax</sub> , H1 <sub>eq</sub> , H4 <sub>ax</sub> , H14
3	70.9	-	-	-	-	-
4	47.2	H <sub>ax</sub> : 2.49 (1H, dd, 15.0, 3.0) H <sub>eq</sub> : 2.42 (1H, m)	2.4 (2H, m)	2, 3, 5, 6, 15	H5	H2, H5, H15  H5, H15
5	70.2	H <sub>eq</sub> : 4.32 (1H, br)	H <sub>eq</sub> : 4.41 (1H, dd)	-	H4	H4 <sub>ax</sub> , H4 <sub>eq</sub> , H9
6	52.1	-	-	-	-	-
7	60.3	-	-	-	-	-
8	58.1	3.02 (1H, d, 2.7)	3.02 (1H, d, 3)	7, 9, 10, 14	H9	H9, H12, H14
9	123.7	6.25 (1H, d, 2.7)	6.25 (1H, d, 3)	7, 8, 10, 11	H8	H5, H8, H12
10	144.5	-	-	-	-	-
11	46.4	-	-	-	-	-
12	27.6	1.23 (3H, s)	1.24 (3H, s)	6, 10, 11, 13	-	H1 <sub>eq</sub> , H8, H9
13	26.0	1.41 (3H, s)	1.42 (3H, s)	6, 10, 11, 12	-	H1 <sub>ax</sub>
14	22.8	1.62 (3H, s)	1.63 (3H, s)	6, 7, 8	-	H2, H8
15	28.5	1.87 (3H, s)	1.88 (3H, s)	2, 3, 4	-	H4 <sub>eq</sub>
5-OH	-	N.D.	1.50 (1H, d, 5)	-	-	-

[a] Carbon assignments of isolated prepacifenol based on HSQC and HMBC NMR experiments. [b]  $^1\text{H}$  NMR data of isolated prepacifenol. Assignment of axial (H<sub>ax</sub>) and equatorial (H<sub>eq</sub>) hydrogens based on a NOESY NMR experiment. N.D.=not detected. [c]  $^1\text{H}$  NMR data of prepacifenol in chloroform-*d* from reference.<sup>[11]</sup>

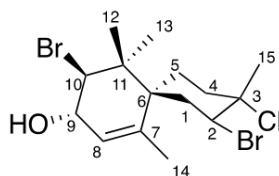
**Table 2–5** NMR data of deoxyprepacifenol (**8**).



Position	$\delta(^1\text{H})$ [ppm] (int, m, $J$ ) <sup>[a]</sup>	$\delta(^1\text{H})$ [ppm] (int, m, $J$ ) <sup>[b]</sup>
1	H <sub>a</sub> : 2.15 (1H, br) H <sub>β</sub> : 2.43 (1H, dt, 14.5, 4.0)	H <sub>a</sub> : 2.16 (1H, dd, 14.5, 13.0) H <sub>β</sub> : 2.43 (1H, ddd, 14.5, 4.4, 3.3)
2	4.69 (1H, dd, 13.2, 4.6)	4.69 (1H, dd, 13.0, 4.4)
3	-	-
4	H <sub>a</sub> : 2.22 (1H, dt, 14.1, 3.6) H <sub>β</sub> : 2.29 (1H, dd, 15.0, 3.5)	H <sub>a</sub> : 2.21 (1H, ddd, 13.8, 4.0, 3.6) H <sub>β</sub> : 2.30 (1H, ddd, 13.8, 13.8, 3.3)
5	H <sub>a</sub> : 1.36 (1H, br) H <sub>β</sub> : 1.78 (1H, qd, 6.8, 3.3)	H <sub>a</sub> : 1.33 (1H, ddd, 13.9, 13.8, 4.0) H <sub>β</sub> : 1.77 (1H, dddd, 13.9, 3.6, 3.3, 3.3)
6	-	-
7	-	-
8	2.94 (1H, d, 2.9)	2.94 (1H, d, 2.8)
9	6.25 (1H, d, 2.9)	6.24 (1H, d, 2.8)
10	-	-
11	-	-
12	1.19 (3H, s)	1.17 (3H, s)
13	1.21 (3H, s)	1.20 (3H, s)
14	1.63 (3H, s)	1.63 (3H, s)
15	1.70 (3H, s)	1.69 (3H, s)

[a] <sup>1</sup>H NMR data of isolated deoxyprepacifenol. [b] <sup>1</sup>H NMR data of deoxyprepacifenol in chloroform-*d* from reference.<sup>[32]</sup>

**Table 2–6** NMR data of 2,10-dibromo-3-chlorochamigran-7-en-9-ol (**9**).



Position	$\delta(^1\text{H})$ [ppm] (int, m, <i>J</i> ) <sup>[a]</sup>	$\delta(^1\text{H})$ [ppm] (int, m, <i>J</i> ) <sup>[b]</sup>
1	2.26 (2H, m)	2.24 (2H, m)
2	4.90 (1H, dd, 12.0, 7.0)	4.91 (1H, dd, 12.0, 6.5)
3	-	-
4	2.33 (2H, m)	2.33 (2H, m)
5	1.74 (1H, m) 2.10 (1H, m)	1.73 (1H, m) 2.10 (1H, ddd, 14.0, 13.5, 5.5)
6	-	-
7	-	-
8	5.45 (1H, d, 2.0)	5.45 (1H, dd, 3.0, 1.5)
9	4.28 (1H, m)	4.27 (1H, ddd, 9.0, 3.0, 2.0)
10	4.36 (1H, d, 9.0)	4.37 (1H, d, 9.0)
11	-	-
12	0.99 (3H, s)	0.99 (3H, s)
13	1.23 (3H, s)	1.23 (3H, s)
14	2.06 (3H, s)	2.06 (3H, t, 1.8)
15	1.71 (3H, s)	1.71 (3H, s)
9-OH	N.D.	N.D.

[a]  $^1\text{H}$  NMR data of isolated 2,10-dibromo-3-chlorochamigran-7-en-9-ol. N.D.=not detected. [b]  $^1\text{H}$  NMR data of 2,10-dibromo-3-chlorochamigran-7-en-9-ol in chloroform-*d* from reference.<sup>[31]</sup>

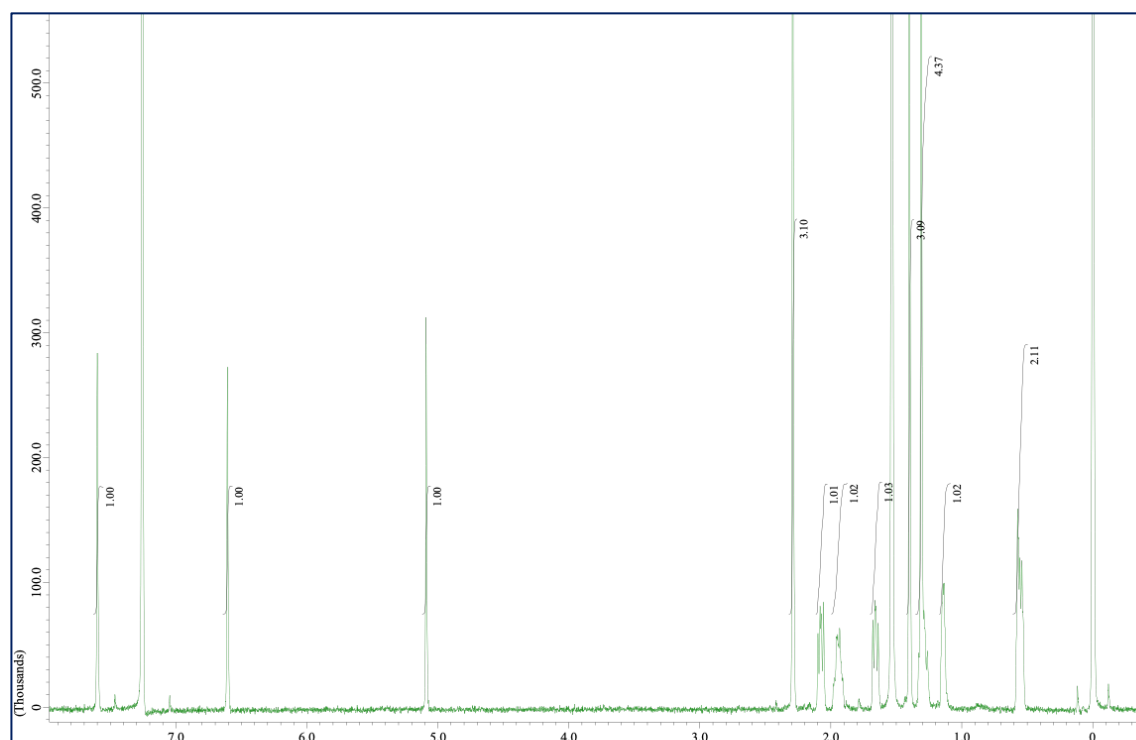


**Fig. 2–25**  $^1\text{H}$  NMR spectrum of **3**.

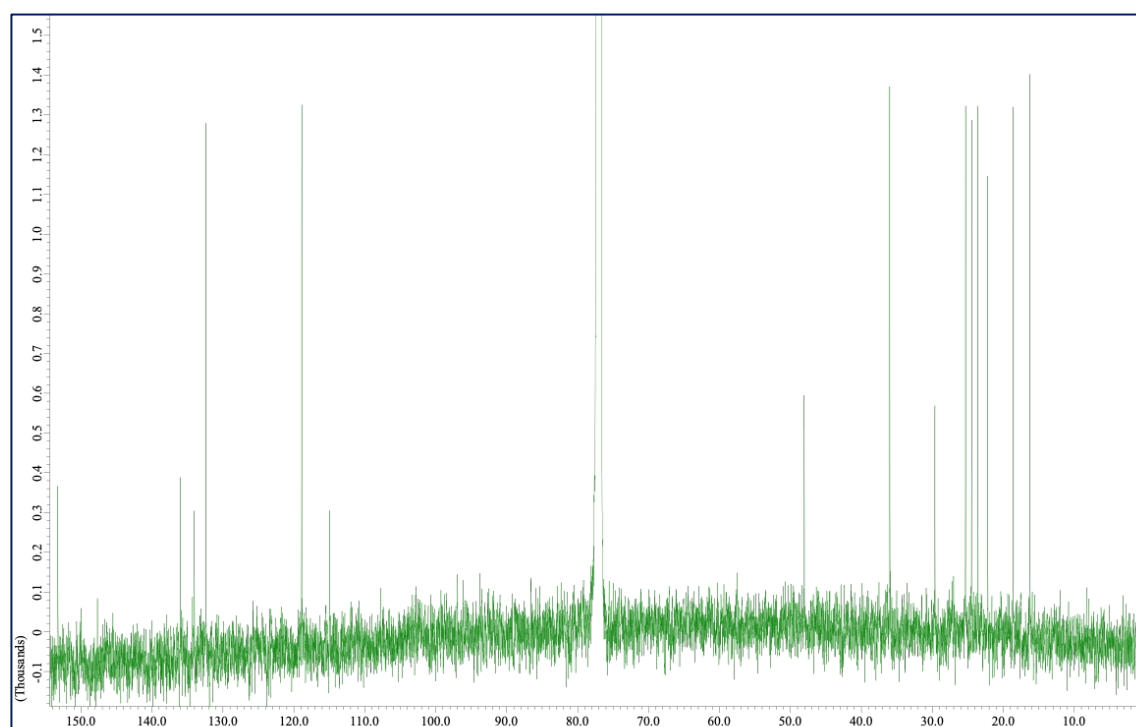


**Fig. 2–26**  $^{13}\text{C}$  NMR spectrum of **3**.

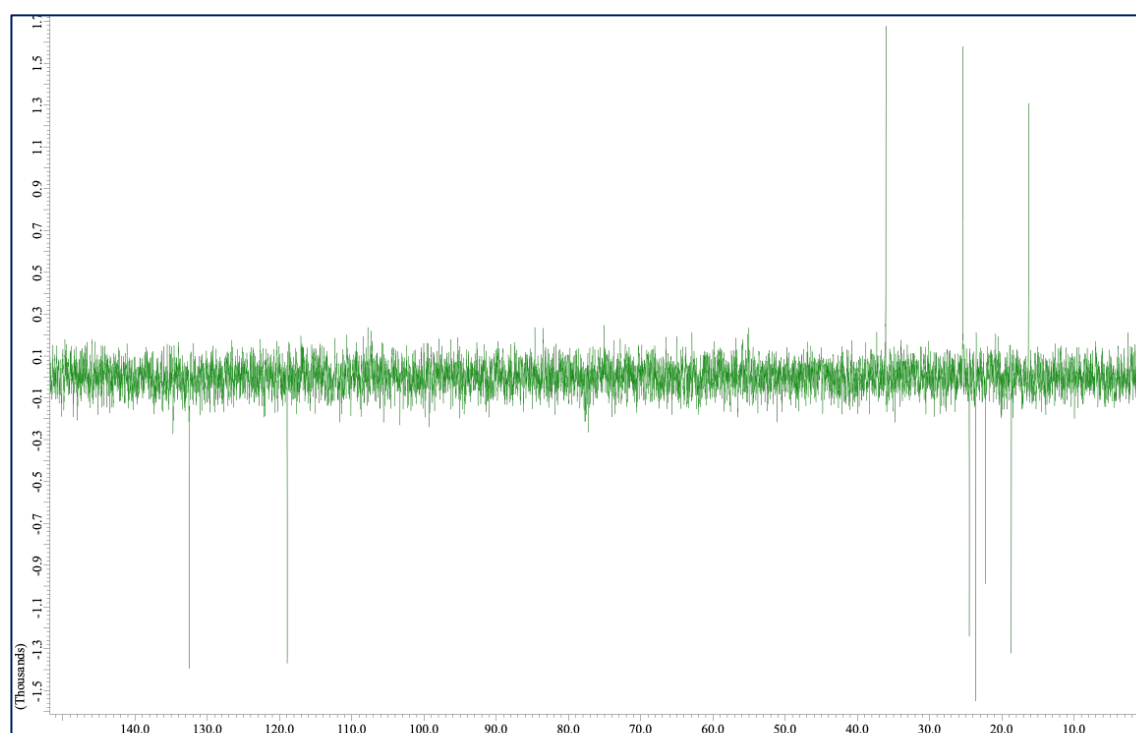


**Fig. 2–27**  $^{13}\text{C}$ -DEPT135 NMR spectrum of **3**.

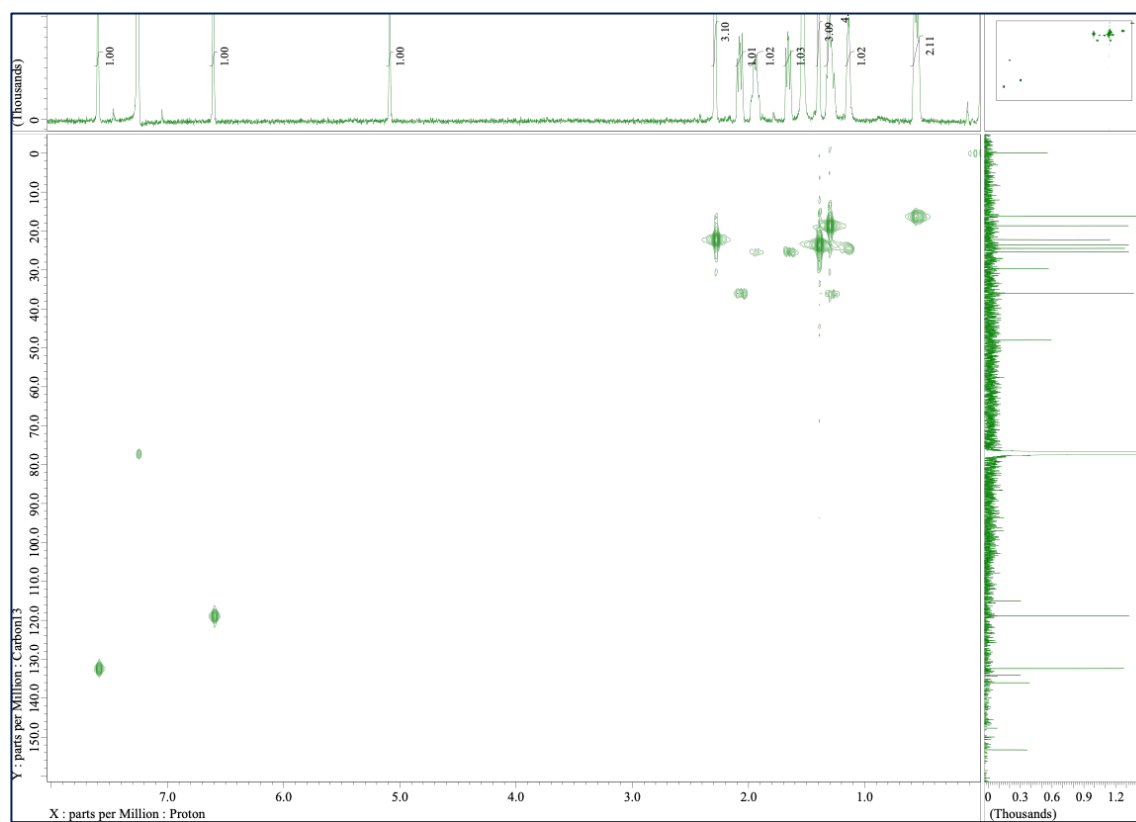


**Fig. 2–28** HMQC NMR spectrum of **3**.



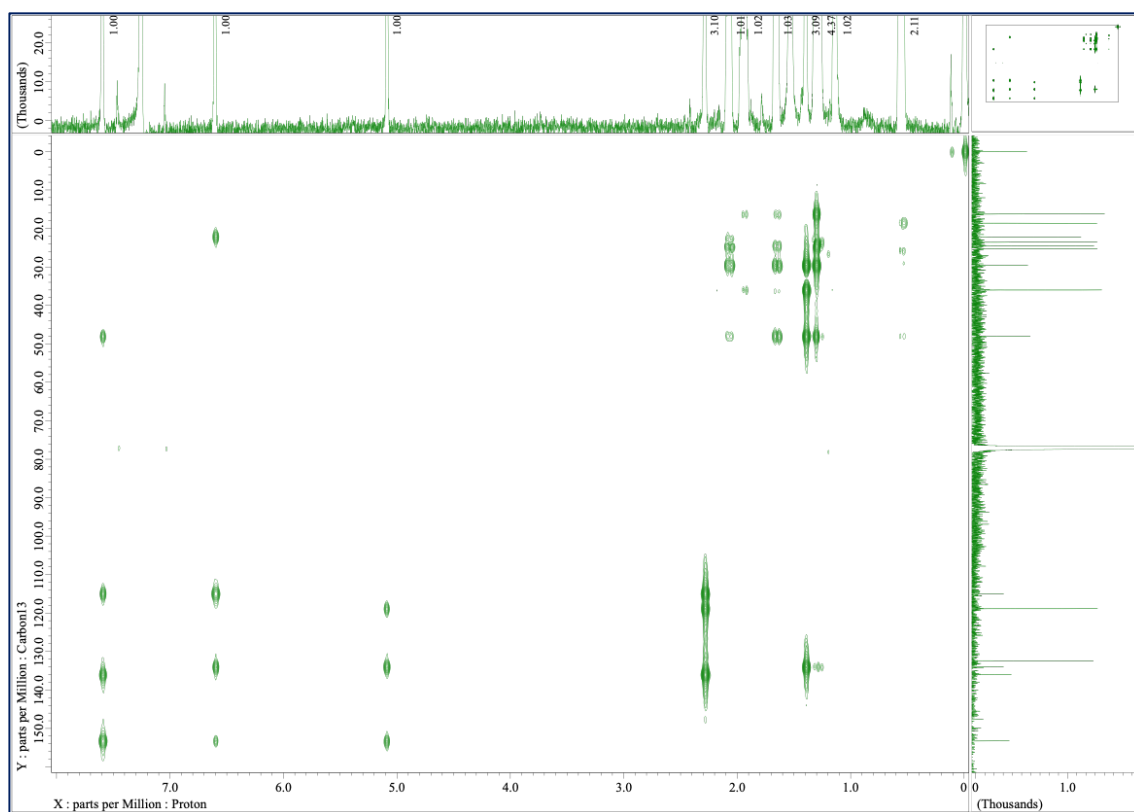


**Fig. 2–29** HMBC NMR spectrum of **3**.

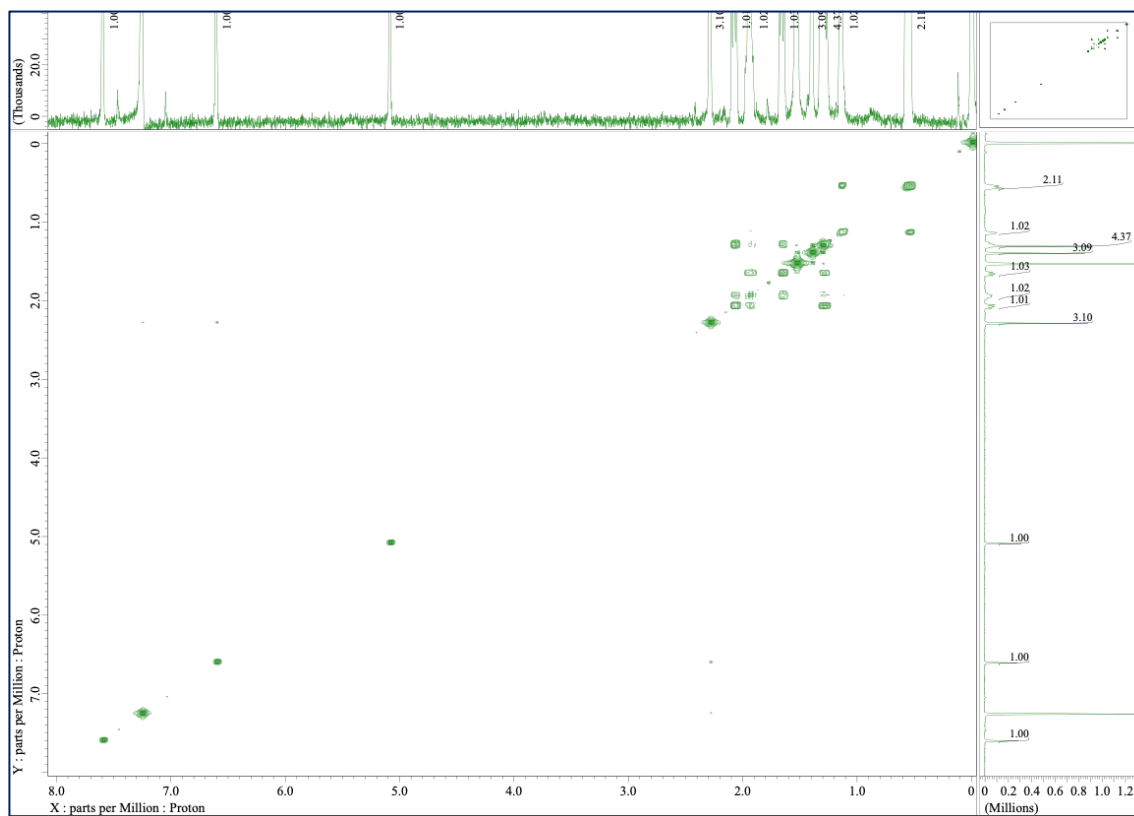


**Fig. 2–30**  $^1\text{H}$ - $^1\text{H}$  COSY NMR spectrum of **3**.

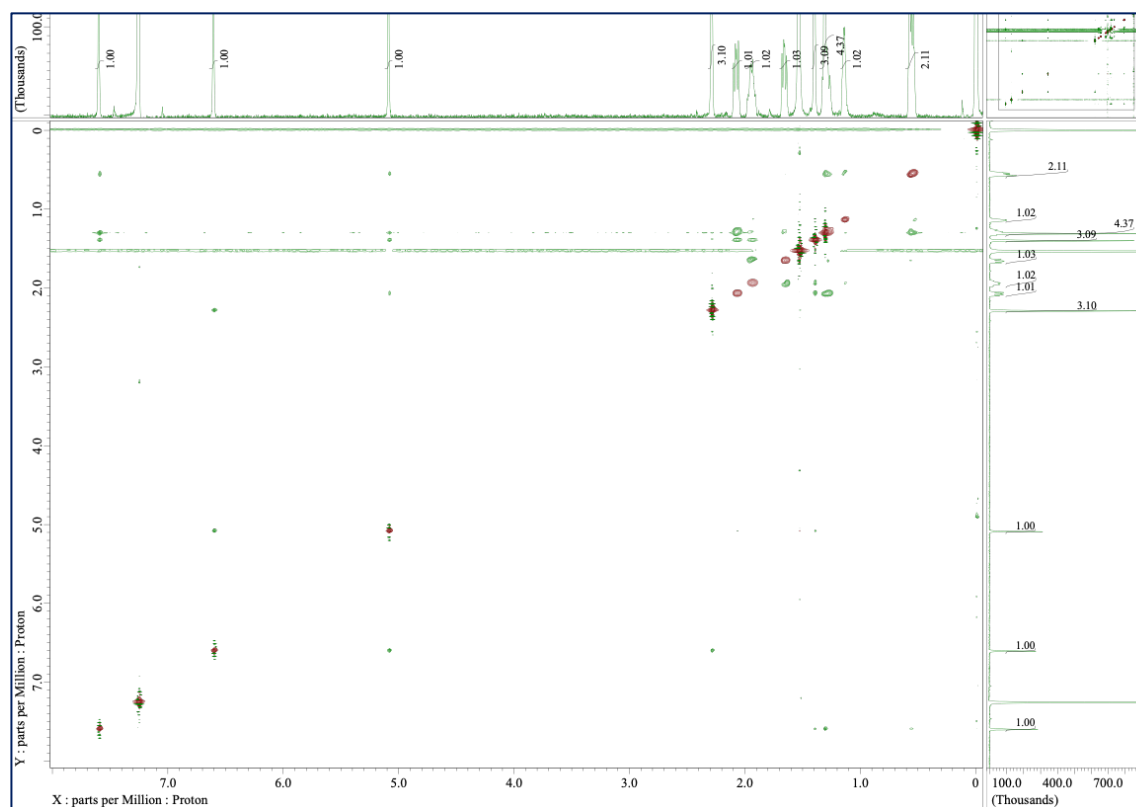


**Fig. 2–31** NOESY NMR spectrum of **3**.

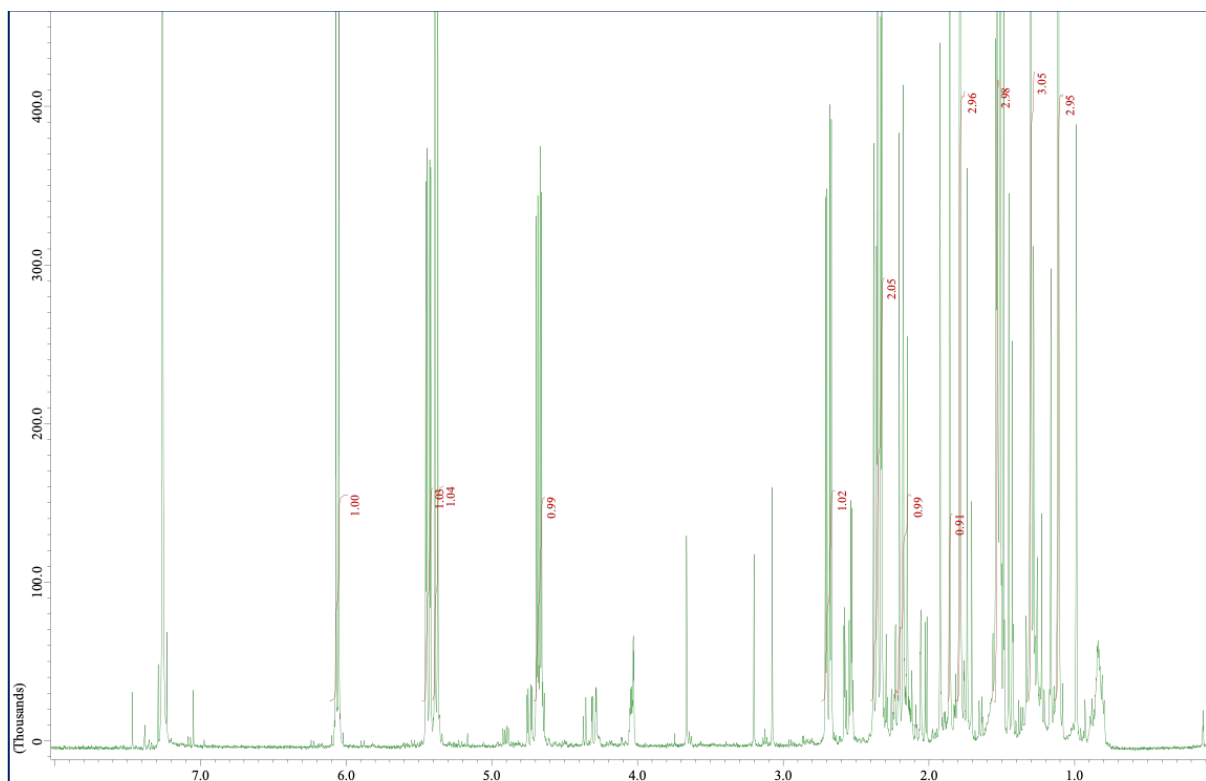


**Fig. 2–32**  $^1\text{H}$  NMR spectrum of **5**.

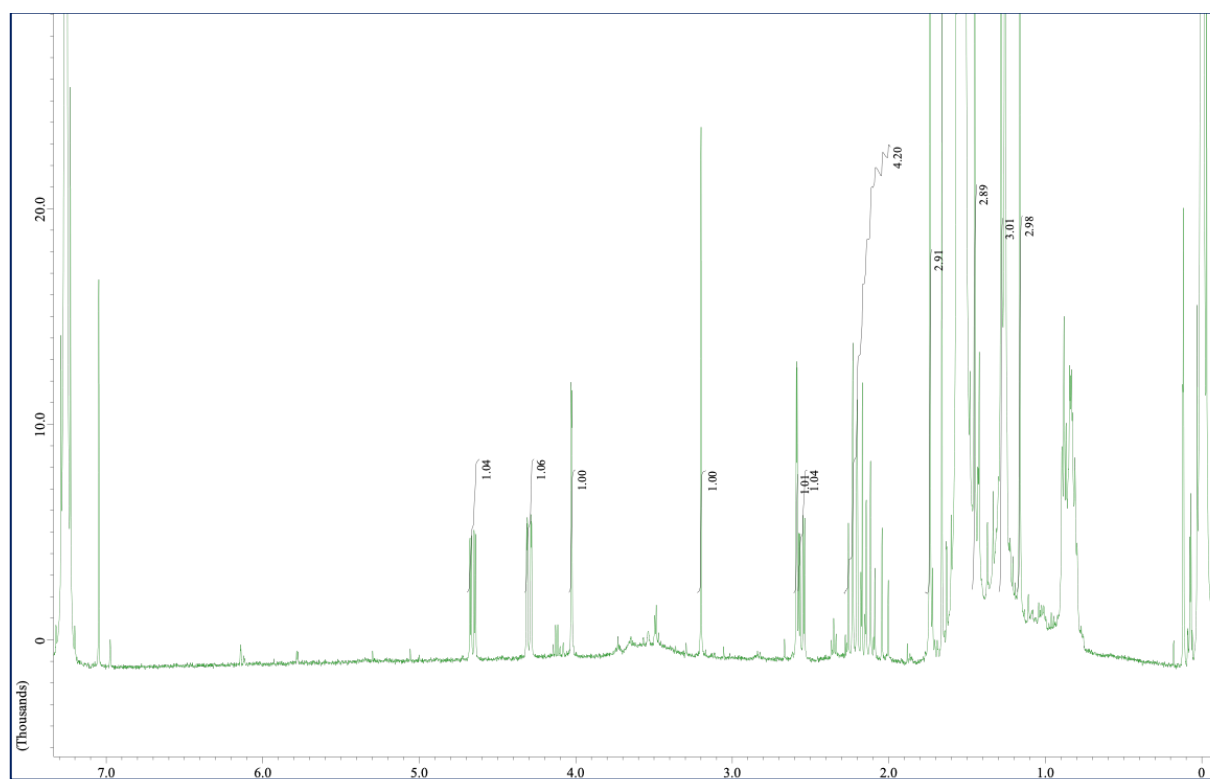


Fig. 2–33  $^1\text{H}$  NMR spectrum of **6**.

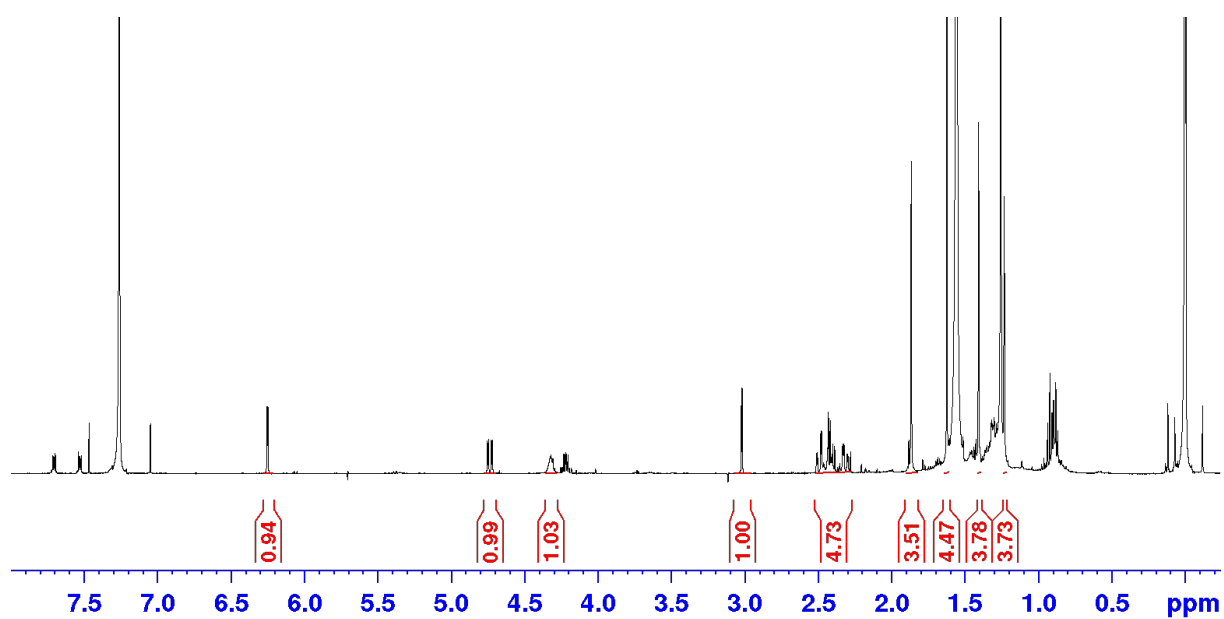


Fig. 2–34  $^1\text{H}$  NMR spectrum of **7**.

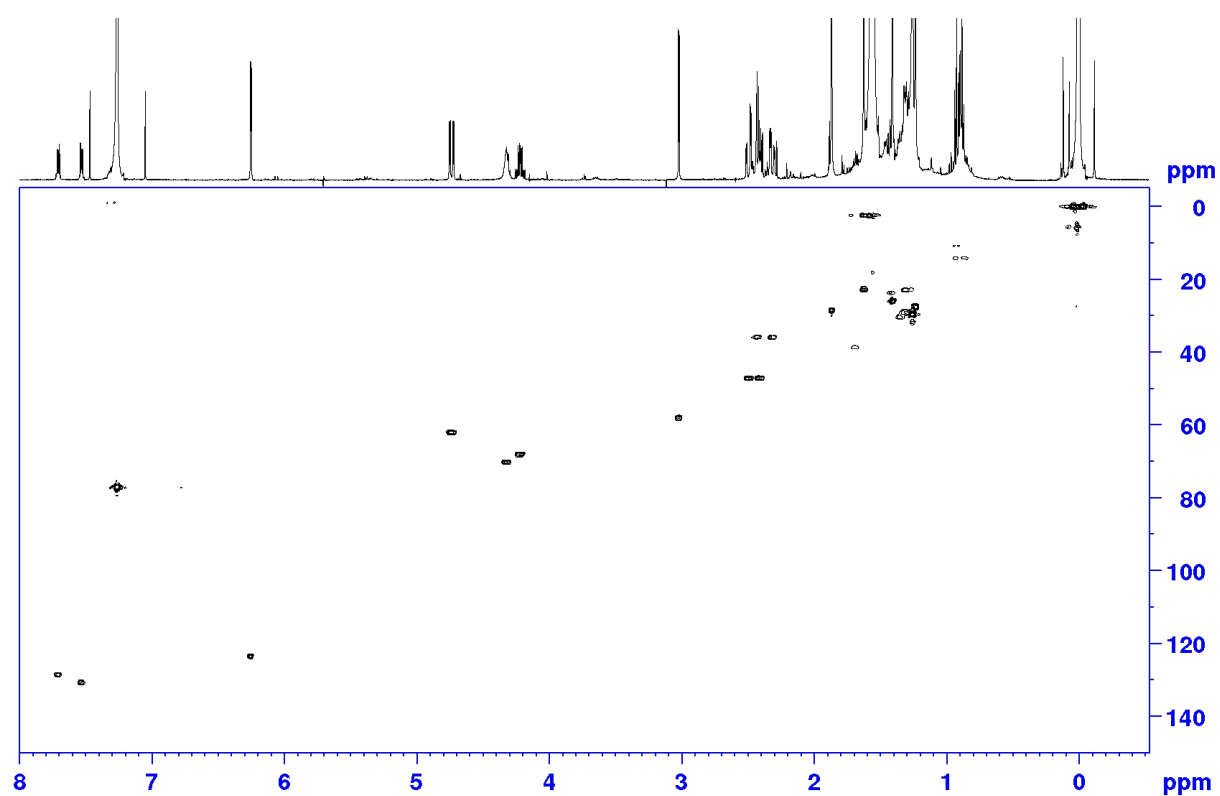


Fig. 2–35 HSQC NMR spectrum of 7.

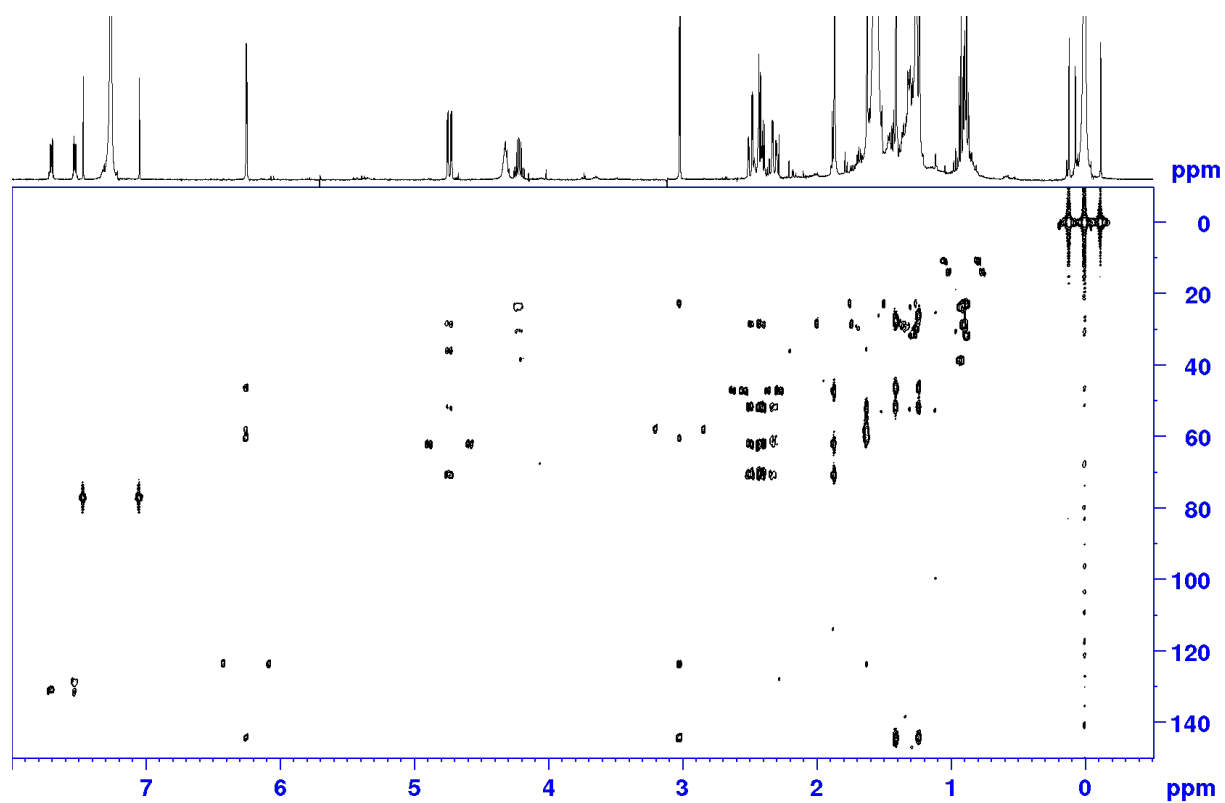
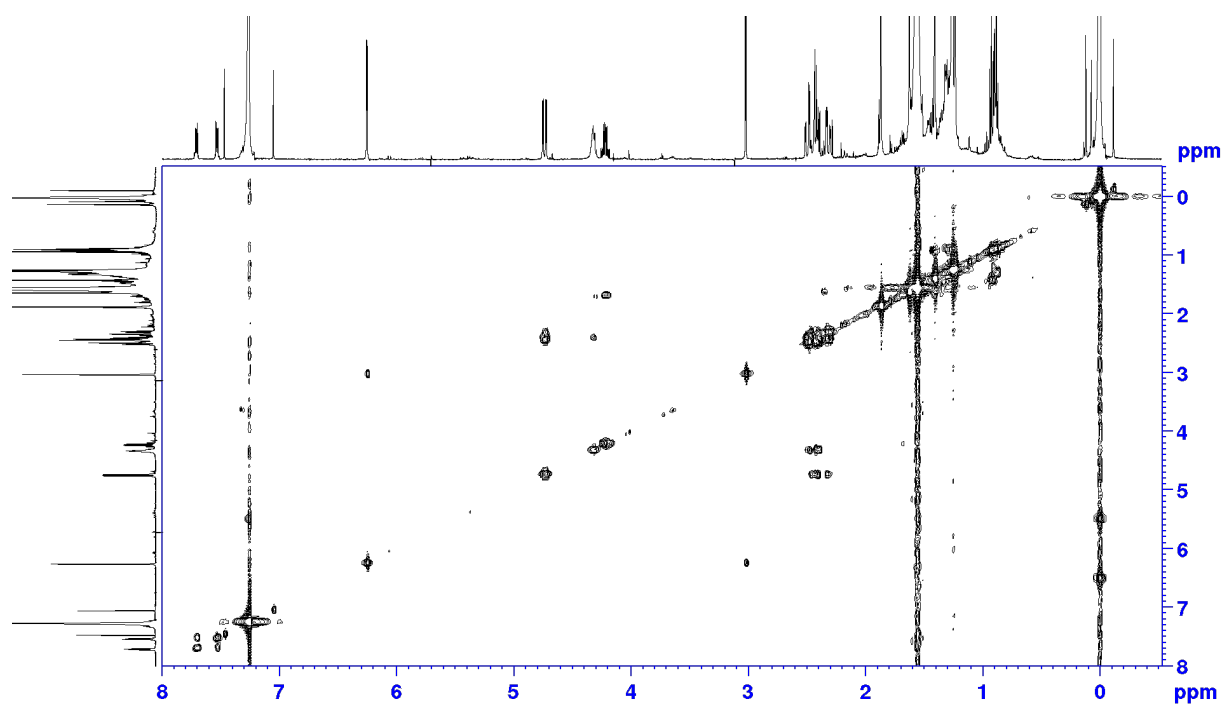
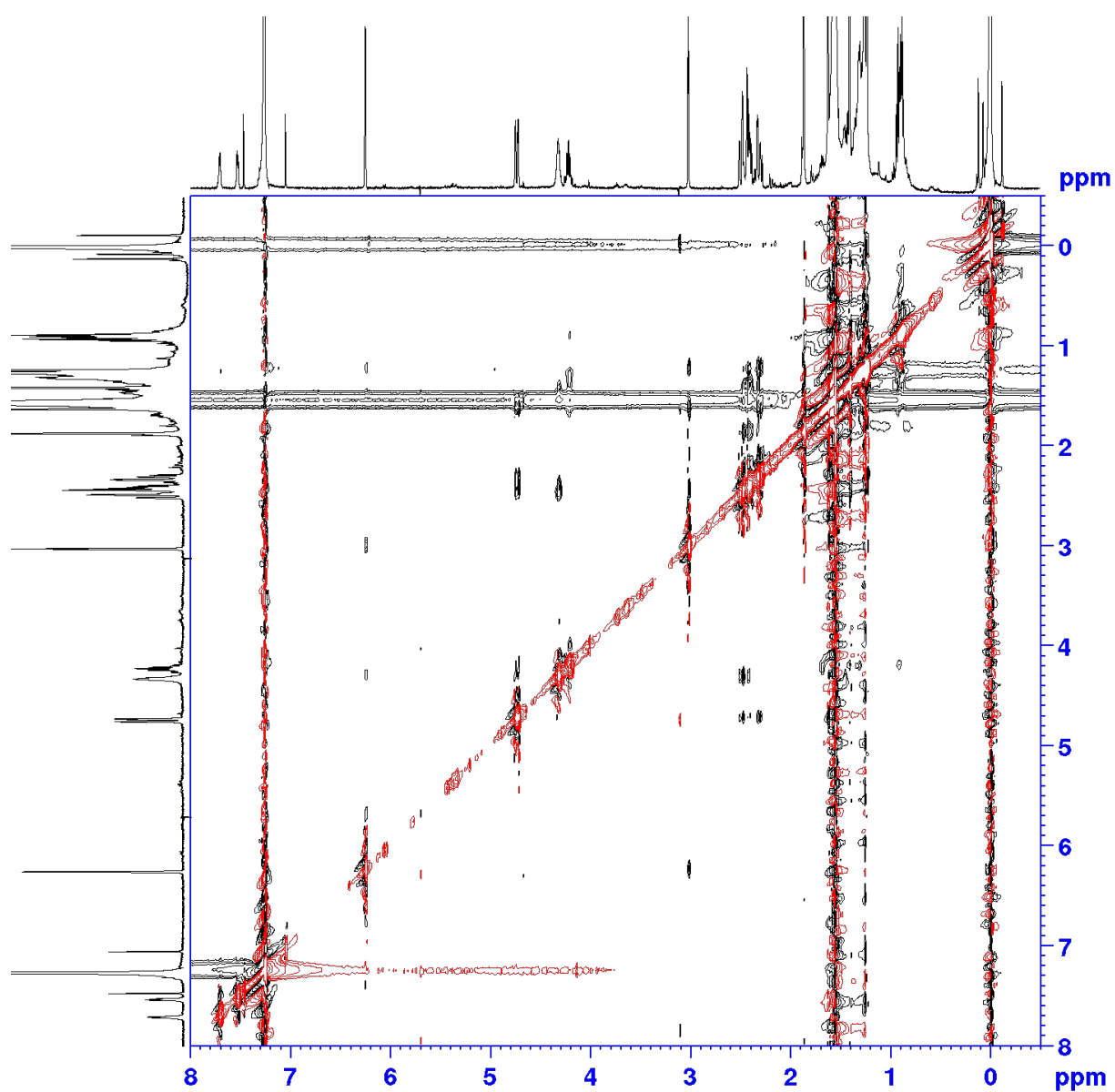


Fig. 2–36 HMBC NMR spectrum of 7.



**Fig. 2–37**  $^1\text{H}$ - $^1\text{H}$ -COSY NMR spectrum of **7**.



**Fig. 2–38** NOESY NMR spectrum of **7**.

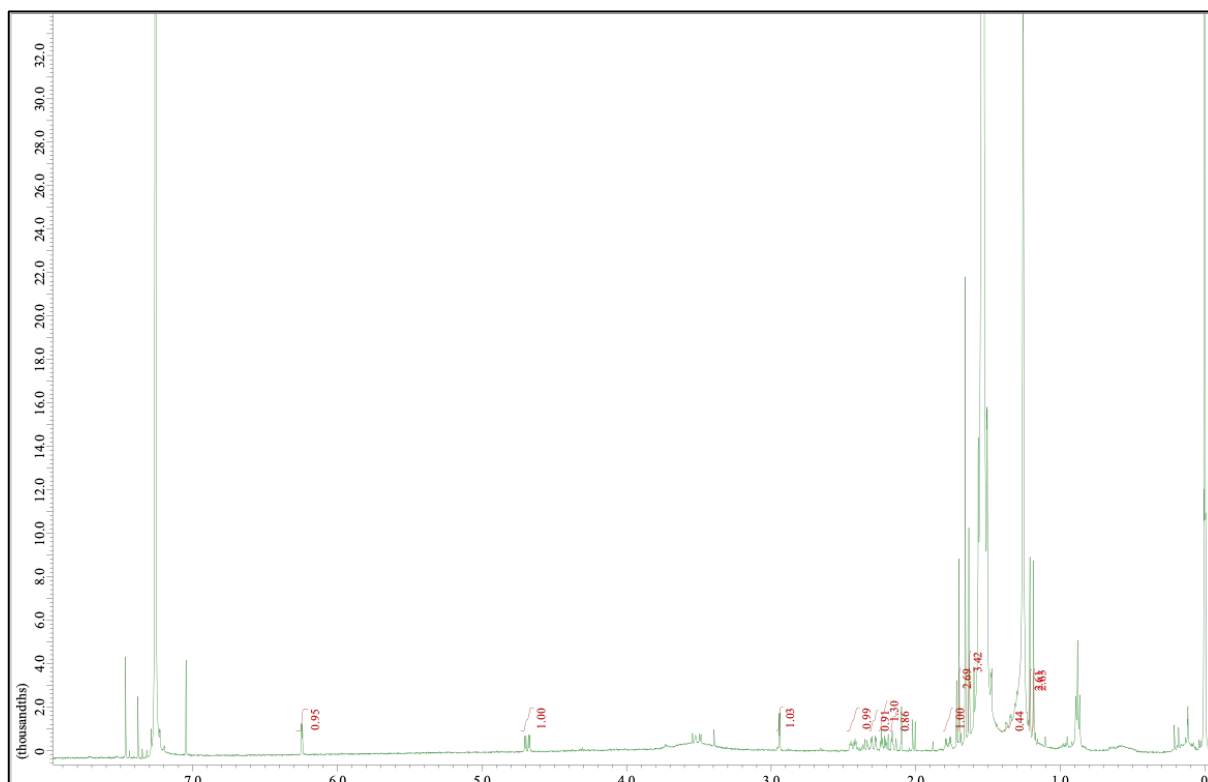


**Fig. 2–39**  $^1\text{H}$  NMR spectrum of **8**.

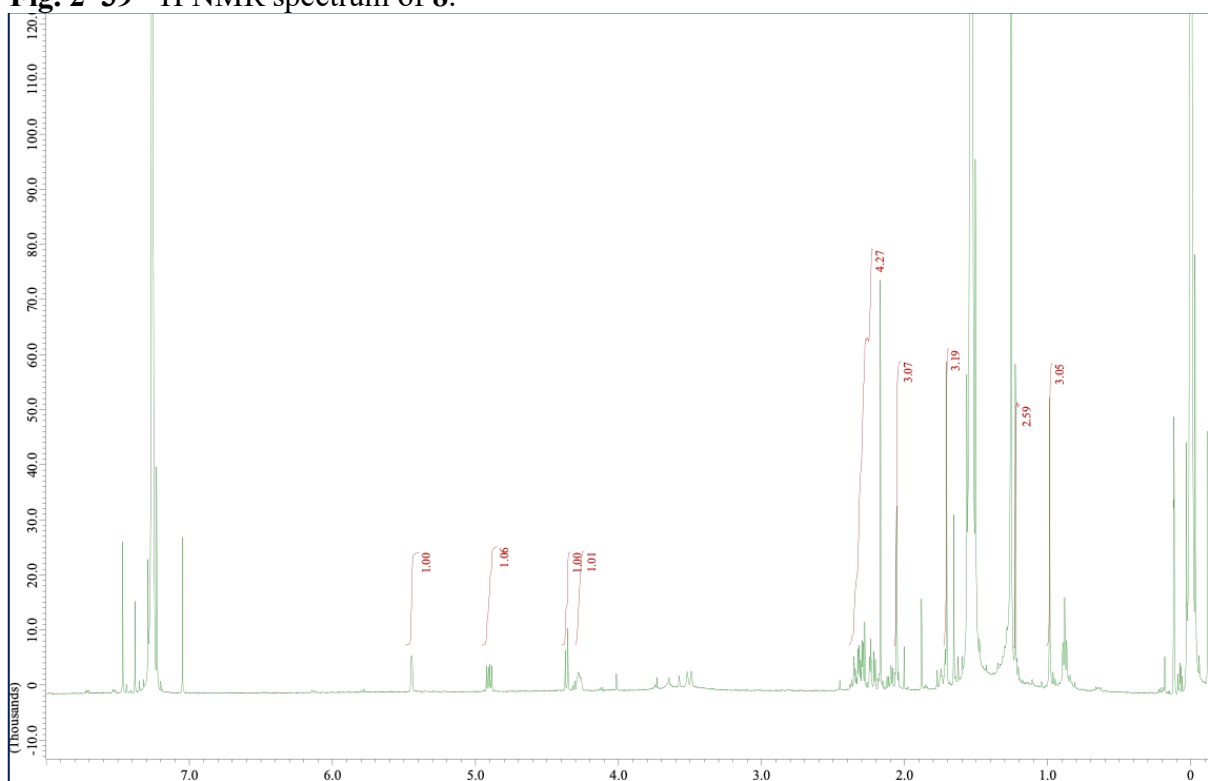


**Fig. 2–40**  $^1\text{H}$  NMR spectrum of **9**.

## 2.6 References

- [1] D. J. Newman and G. M. Cragg, *J. Nat. Prod.* **2020**, *83*, 770-803.
- [2] O. Keiichi, *Kagaku To Seibutsu* **1975**, *13*, 252-259.
- [3] E. Kurosawa and M. Suzuki, *Kagaku To Seibutsu* **1983**, *21*, 23-32.
- [4] T. Tanaka and Y. Toyama, *Nippon kagaku zasshi* **1959**, *80*, 1329-1332.
- [5] S. Yamamura and Y. Hirata, *Tetrahedron* **1963**, *19*, 1485-1496.
- [6] T. Irie, M. Suzuki, E. Kurosawa and T. Masamune, *Tetrahedron Lett.* **1966**, *7*, 1837-1840.
- [7] a) A. F. Cameron, G. Ferguson and J. M. Robertson, *Chem. Comm. (London)* **1967**, 271-272; b) A. F. Cameron, G. Ferguson and J. M. Robertson, *J. Chem. Soc. (B)* **1969**, 692-697.
- [8] J. J. Sims, W. Fenical, R. M. Wing and P. Radlick, *J. Am. Chem. Soc.* **1971**, *93*, 3774-3775.
- [9] F. R. Fronczek and S. Caccamese, *Acta Cryst. C* **1986**, *42*, 1649-1651.
- [10] J. J. Sims, W. Fenical, R. M. Wing and P. Radlick, *Tetrahedron Lett.* **1972**, *13*, 195-198.
- [11] J. J. Sims, W. Fenical, R. M. Wing and P. Radlick, *J. Am. Chem. Soc.* **1973**, *95*, 972-972.
- [12] C. Ireland, M. O. Stallard, D. J. Faulkner, J. Finer and J. Clardy, *J. Org. Chem.* **1976**, *41*, 2461-2465.
- [13] W. Fenical, *Phytochemistry* **1976**, *15*, 511-512.
- [14] M. Suzuki, E. Kurosawa and A. Furusaki, *Bull. Chem. Soc. Jpn.* **1988**, *61*, 3371-3373.
- [15] S. Lee, M. Hoshino, M. Fujita and S. Urban, *Chem. Sci.* **2017**, *8*, 1547-1550.
- [16] a) L. R. de Carvalho, M. T. Fujii, N. d. F. Roque, M. J. Kato and J. H. G. Lago, *Tetrahedron Lett.* **2003**, *44*, 2637-2640; b) L. R. de Carvalho, M. T. Fujii, N. F. Roque and J. H. Lago, *Phytochemistry* **2006**, *67*, 1331-1335.
- [17] a) S. Takahashi, M. Yasuda, T. Nakamura, K. Hatano, K. Matsuoka and H. Koshino, *J. Org. Chem.* **2014**, *79*, 9373-9380; b) O. A. Mukhina, H. Koshino, M. T. Crimmins and A. G. Kutateladze, *Tetrahedron Lett.* **2015**, *56*, 4900-4903.



- [18] A. G. Kutateladze and D. S. Reddy, *J. Org. Chem.* **2017**, *82*, 3368-3381.
- [19] a) D. E. White, I. C. Stewart, R. H. Grubbs and B. M. Stoltz, *J. Am. Chem. Soc.* **2008**, *130*, 810-811; b) B. S. Matsuura, P. Kolle, D. Trauner, R. de Vivie-Riedle and R. Meier, *ACS Cent. Sci.* **2017**, *3*, 39-46; c) A. J. Burckle, V. H. Vasilev and N. Z. Burns, *Angew. Chem. Int. Ed.* **2016**, *55*, 11476-11479.
- [20] a) T. Ohshiro and Y. Izumi, *Kagaku To Seibutsu* **1994**, *32*, 35-43; b) A. Butler and J. N. Carter-Franklin, *Nat. Prod. Rep.* **2004**, *21*, 180-188; c) J. N. Carter-Franklin and A. Butler, *J. Am. Chem. Soc.* **2004**, *126*, 15060-15066; d) R. D. Kersten, S. Lee, D. Fujita, T. Pluskal, S. Kram, J. E. Smith, T. Iwai, J. P. Noel, M. Fujita and J. K. Weng, *J. Am. Chem. Soc.* **2017**, *139*, 16838-16844; e) G. Wei, Q. Jia, X. Chen, T. G. Kollner, D. Bhattacharya, G. K. Wong, J. Gershenzon and F. Chen, *Plant Physiol.* **2019**, *179*, 382-390.
- [21] S. Sairenji, S. Lee and M. Fujita, *J. Synth. Org. Chem. Jpn.* **2017**, *75*, 538-547.
- [22] a) K. Biradha and M. Fujita, *Angew. Chem. Int. Ed.* **2002**, *41*, 3392-3395; b) K. Biradha, Y. Hongo and M. Fujita, *Angew. Chem. Int. Ed.* **2002**, *41*, 3395-3398.
- [23] S. Parsons, H. D. Flack and T. Wagner, *Acta Cryst. B* **2013**, *69*, 249-259.
- [24] L. Rosenberger, C. von Essen, A. Khutia, C. Kuhn, K. Georgi, A. K. H. Hirsch, R. W. Hartmann and L. Badolo, *Eur. J. Pharm. Sci.* **2021**, *164*, 105884.
- [25] Y. Inokuma, S. Yoshioka, J. Ariyoshi, T. Arai and M. Fujita, *Nat. Protoc.* **2014**, *9*, 246-252.
- [26] G. M. Sheldrick, *Acta Cryst. A* **2015**, *71*, 3-8.
- [27] G. M. Sheldrick, *Acta Cryst. C* **2015**, *71*, 3-8.
- [28] A. L. Spek, *J. Appl. Crystallogr.* **2003**, *36*, 7-13.
- [29] A. L. Spek, *Acta Cryst. C* **2015**, *71*, 9-18.

- [30] Y. Okamoto, N. Nitanda, M. Ojika and Y. Sakagami, *Biosci. Biotechnol. Biochem.* **2001**, *65*, 474-476.
- [31] W. Wang, J. Hong, C.-O. Lee, H. Y. Cho, S. Shin and J. H. Jung, *Nat. Prod. Sci.* **2004**, *10*, 253-261.
- [32] R. Denys, J. C. Coll and B. F. Bowden, *Aust. J. Chem.* **1993**, *46*, 933-937.

## Chapter 3

### Stereochemical Analysis of Steroids

#### Using Polar Solvents

##### 3.1 Introduction

The crystalline sponge method has been applied to structural analysis of various compounds, especially natural products (NPs) derived from living materials, and successfully revealed the chemical structures including absolute configurations. The flourishing applications of the crystalline sponge method have been accompanied with multiple approaches to increase the practicability and accuracy of the method.<sup>[1]</sup> Ramadhar *et al.* examined the terminal ligand effect in the crystalline sponge complex,  $[(\text{ZnI}_2)_3(\text{tpt})_2 \cdot x(\text{solvent})]_n$  (**1a**; tpt = 2,4,6-tris(4-pyridyl)-1,3,5-triazine) through reporting synthetic methods of congeners with zinc bromine

and zinc chlorine ligands (**1b** and **1c**) and performing the guest soaking with (1*R*)-(-)-menthyl acetate (**2**) (Fig. 3–1A and Fig. 3–1B).<sup>[2]</sup> Sakurai *et al.* further demonstrated that the use of **1c**, that is less prone to nucleophilic attacks by the guests than **1a**, or the guest soaking under mild conditions (lower temperatures or lower guest amounts) yielded higher success rates in structural analysis of nitrogen-containing nucleophilic derivatives.<sup>[3]</sup> The use of synchrotron radiation allows minimization of collection time (typically less than 1 h per crystal) of diffraction images, which usually takes from hours to days with in-house X-ray diffractometers.<sup>[4]</sup> The formation of ion-pair between the amine guests and acid additives was effective for clear observation of the guests by preventing deterioration of the crystallinity of complex **1c** (Fig. 3–1C).<sup>[5]</sup> As illustrated above, the current approaches mostly focus on the modification and optimization of ligands types, temperature, concentration, time, or additives in the guest soaking step.

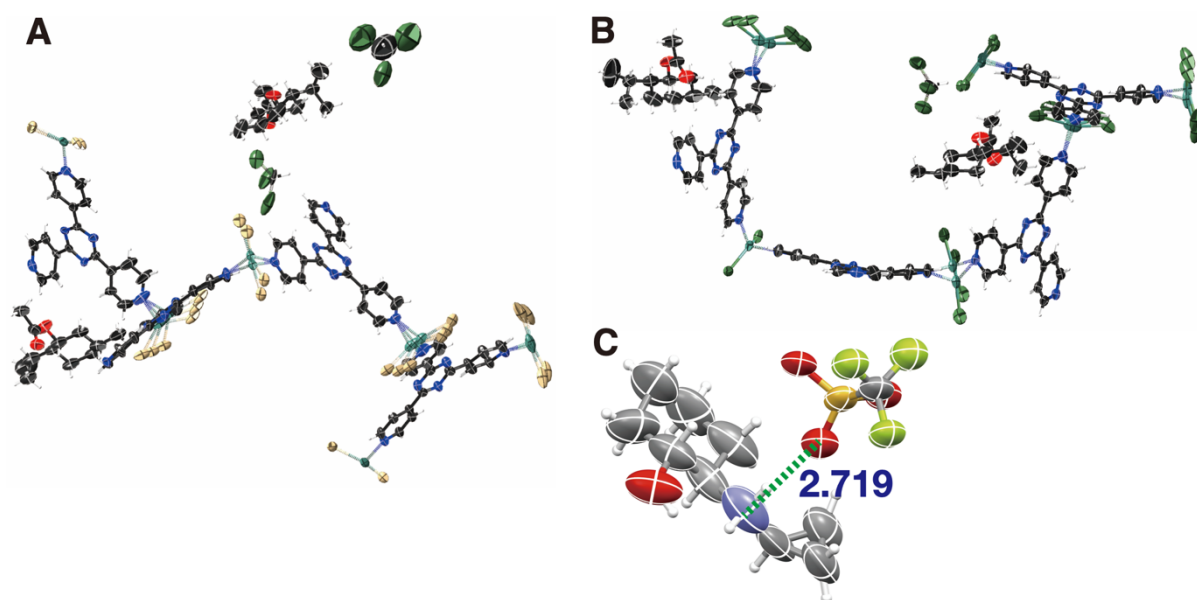


**Fig. 3–1** Thermal ellipsoid plot of asymmetric units of (A)  $[(\text{ZnBr}_2)_3(\text{tpt})_2 \cdot x(\text{solvent})]_n$  (**1b**) and (B)  $[(\text{ZnCl}_2)_3(\text{tpt})_2 \cdot x(\text{solvent})]_n$  (**1c**) complexes encapsulating **2** as guests with 50%

probability (CCDC 1063685 and 1063686).<sup>[2]</sup> (C) Thermal ellipsoid plot of an ion-pair of an amine guest and an acid additive formed in **1c** with 50% probability (CCDC 1999698).<sup>[5]</sup> The values indicate atom distances highlighted with dashed lines and in angstroms (Å).

Although it is common that solvents used in the guest soaking are observed in the crystal structures with the target guests, few reports have mentioned or investigated how solvents affect the data quality in the crystallographic analysis.<sup>[6]</sup> On the contrary, the forementioned guidelines on the preparation of the crystalline sponges rather suggested the use of non-coordinating hydrocarbon solvents such as *n*-hexane and cyclohexane,<sup>[7]</sup> because coordinating polar solvents could interact too strongly with the host complex and disturb smooth diffusion of the guest (Fig. 3–2). Indeed, the crystallinity of the less robust host **1a** easily deteriorates upon the contact with the polar solvent, that may lead scientists reluctant to use polar solvents in the crystalline sponge method. In this study, I chose a series of steroid derivatives as guest analytes because of their importance to the pharmaceutical field and found that the choice of solvent used in the soaking step is an important parameter for ordering the absorbed guest molecules in the pores of the crystal. As opposed to the assumption that polar solvents disturb the guest ordering, I demonstrated that optimization of the solvent condition is an important parameter to increase the occupancy, promote ordering of guests, and expand the application scope of the crystalline sponge method. The expansion of the scope will eventually lead to the broad use of the method and can streamline the research workflow where structural analysis of compounds is a bottleneck.

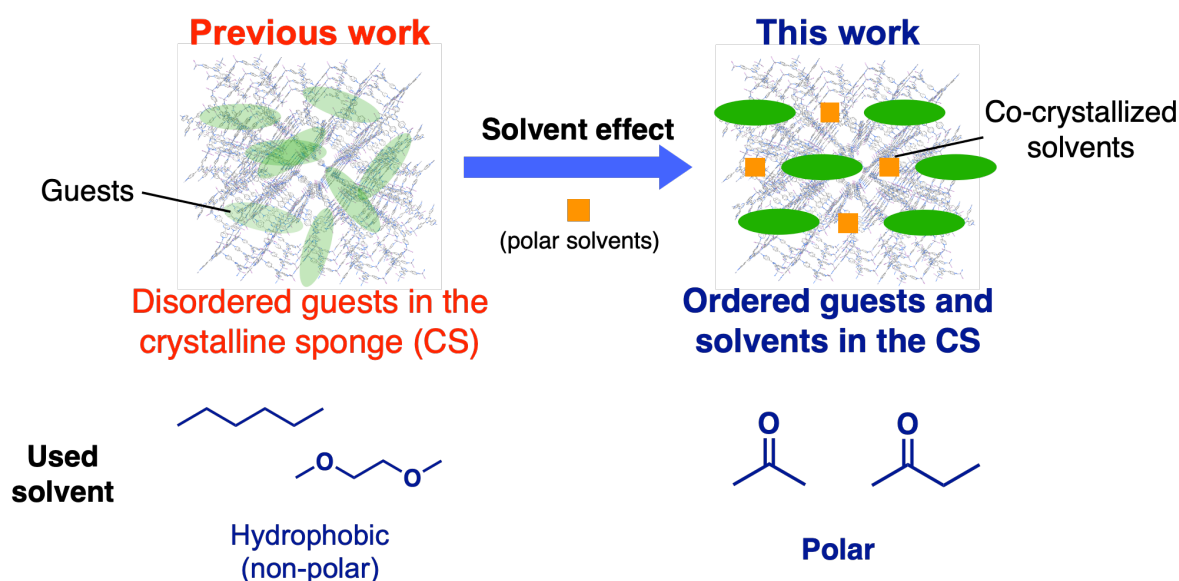


**Fig. 3–2** The schematic illustration of this study. In the previous works where the crystalline sponge method is applied to structural analysis, hydrophobic (non-polar) solvents were preferentially used in the guest-soaking step. However, this might lead to undesirable disorders of the guest soaking in the pores. In this work, I aimed to promote the guest ordering by forming co-crystallizing structures of the analytes and polar solvents within the pores.

### 3.2 Structural Analysis of Cholesterol with the Conventional Soaking Procedures

In this chapter, I selected cholesterol (**2**) as a model steroid to investigate the solvent effect in the crystalline sponge method. **2** and its derivatives are an important group of compounds involved in various biological phenomena, and many of them exhibit characteristic biological activities *in vivo*. The structural diversity is generated by various metabolic enzymes that introduce or eliminate functional groups, including cytochrome P450 (CYP), which is a ubiquitous enzyme in organisms and mostly responsible for the oxidation of C-H bonds. I firstly analyzed **2** by the crystalline sponge method with a standard condition. 0.09  $\mu\text{g } \mu\text{L}^{-1}$  of **2** in 55  $\mu\text{L}$  of a mixture of *n*-hexane and dimethoxyethane (DME) was contacted with a single crystal

of **1c** in a glass vial, and solvents were gradually evaporated at 50 °C for 1 day. After the guest soaking, diffraction images were collected with an in-house diffractometer. Crystallographic analysis revealed two crystallographically-independent molecules, **2A** and **2B** in an asymmetric unit (Fig. 3–3A). However, the obtained geometry of the guest was chemically unacceptable. The sp<sup>3</sup> hybridization angles at C–20 deviated considerably from normal values, and I could not convincingly assign the stereochemistry in the alkyl chain moiety. As shown in Fig. 3–3B, the electron density of **2** was blurred on the alkyl chain. Subsequently, as performed in the usual optimization in the guest soaking step, different temperatures (4–60 °C), concentrations (0.09–0.9 µg µL<sup>-1</sup>), and soaking times (1–5 days) were applied to improve the guest geometry. In all attempts, the guests could not be modelled in crystallographic analyses or consistently showed unnatural chemical structures (See Table 3–1 in Chapter 3.6 for details).

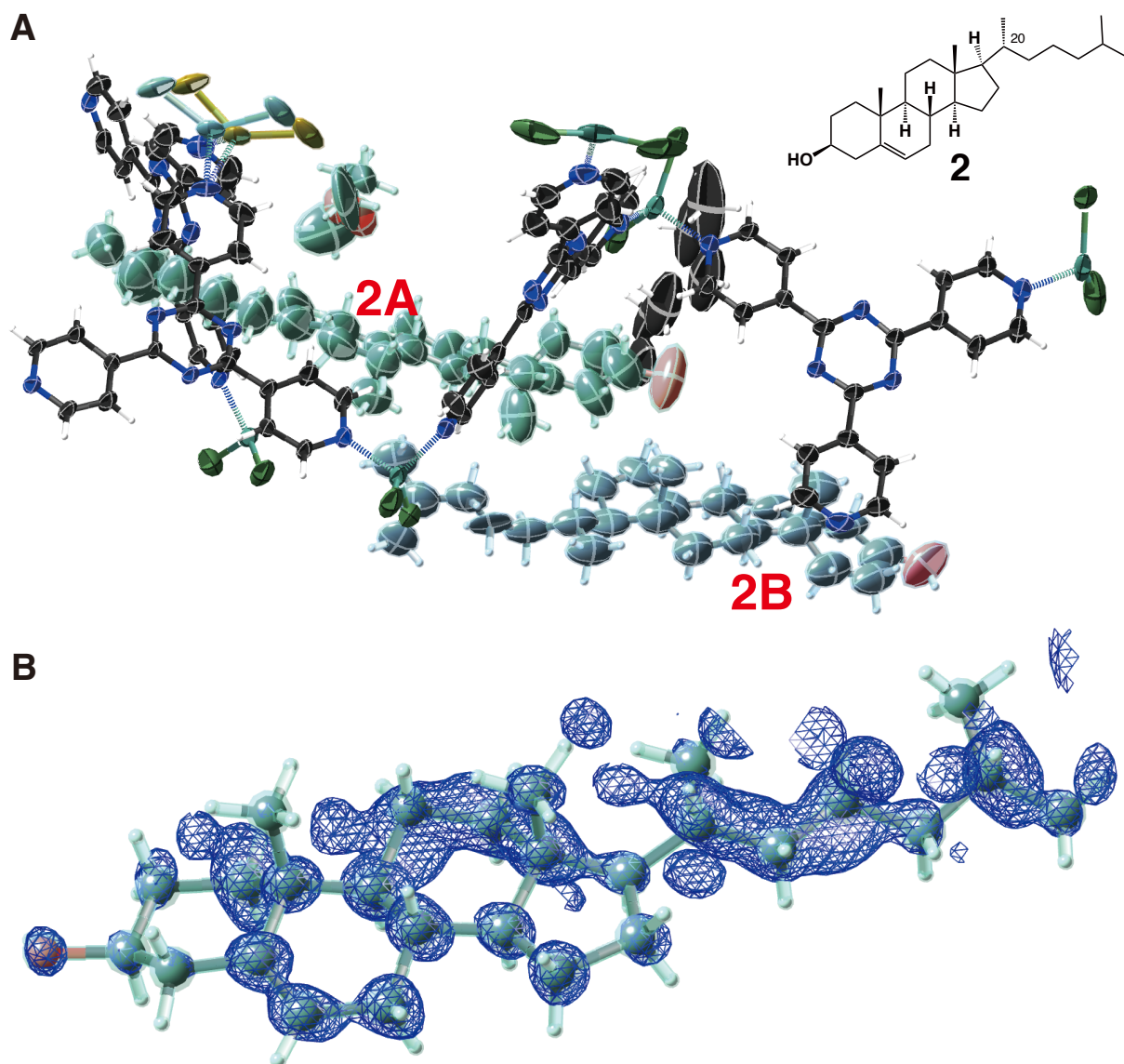


**Fig. 3–3** (A) Thermal ellipsoid plot of an asymmetric unit of **1c·2** with 50% probability. (B) Electron density ( $F_o$ ) map around **2A** drawn at a contour level of  $1.0\sigma$  ( $1.1 \text{ e}\text{\AA}^{-3}$ ).

### 3.3 Establishment of New Solvent Conditions Available in the Crystalline Sponge

#### Method

The blurred electron density observed in the alkyl chain moiety would result from the disorder with the solvent (*n*-hexane), that tends to remain in the hydrophobic pore of **1c** but do not have specific intermolecular interaction with the host. Moreover, it is suspected that



steroidal guests are less soluble during the guest soaking process in hydrophobic solvents. To discover solvents that do not inhibit the guest ordering and solvate steroidal guests well, various polar solvents (chloroform, *tert*-butyl methyl ether, acetone, dimethyl sulfoxide, methanol, ethanol, isopropanol, hexafluoro isopropanol, diacetyl, 2-butanone) with potential sites for intermolecular interaction were applied in the soaking steps in lieu of *n*-hexane.

When the guest soaking was performed with acetone as a solvent, the guest geometry significantly improved (Fig. 3–4A). The guests **2C** and **2D** observed in an asymmetric unit showed unblurred electron density in alkyl chain moiety, and the sum of the three  $sp^3$  hybridization angle at C–20 was  $327.7399(11)^\circ$ , within a  $2\sigma$  deviation range from the average values that are based on protein crystal structures reported in CCDC database.<sup>[8]</sup> Therefore, the configuration at a chiral center at C–20 was unambiguously determined to be *R*. As shown in Fig. 3–4B, **2C** was in van der Waals contact with an acetone molecule. The carbonyl group of acetone was electrostatically trapped in the host framework. The positively charged carbon was forming  $ZnCl \cdots C=O$  interactions, and the negatively charged oxygen was forming  $PyH \cdots O=C$  (or  $CH \cdots O=C$ ) interactions. This phenomenon can be also described as co-crystallization, where acetone solvents interact efficiently with both the framework **1c** and guest **2** in the crystal structure. The Flack parameter calculated by the Parsons' method also decreased from 0.121(8) in the *n*-hexane/DME condition to 0.033(12) in the acetone condition, that supports that chirality transfer from a chiral guest **2** to achiral host **1c** is more enhanced in the acetone condition.

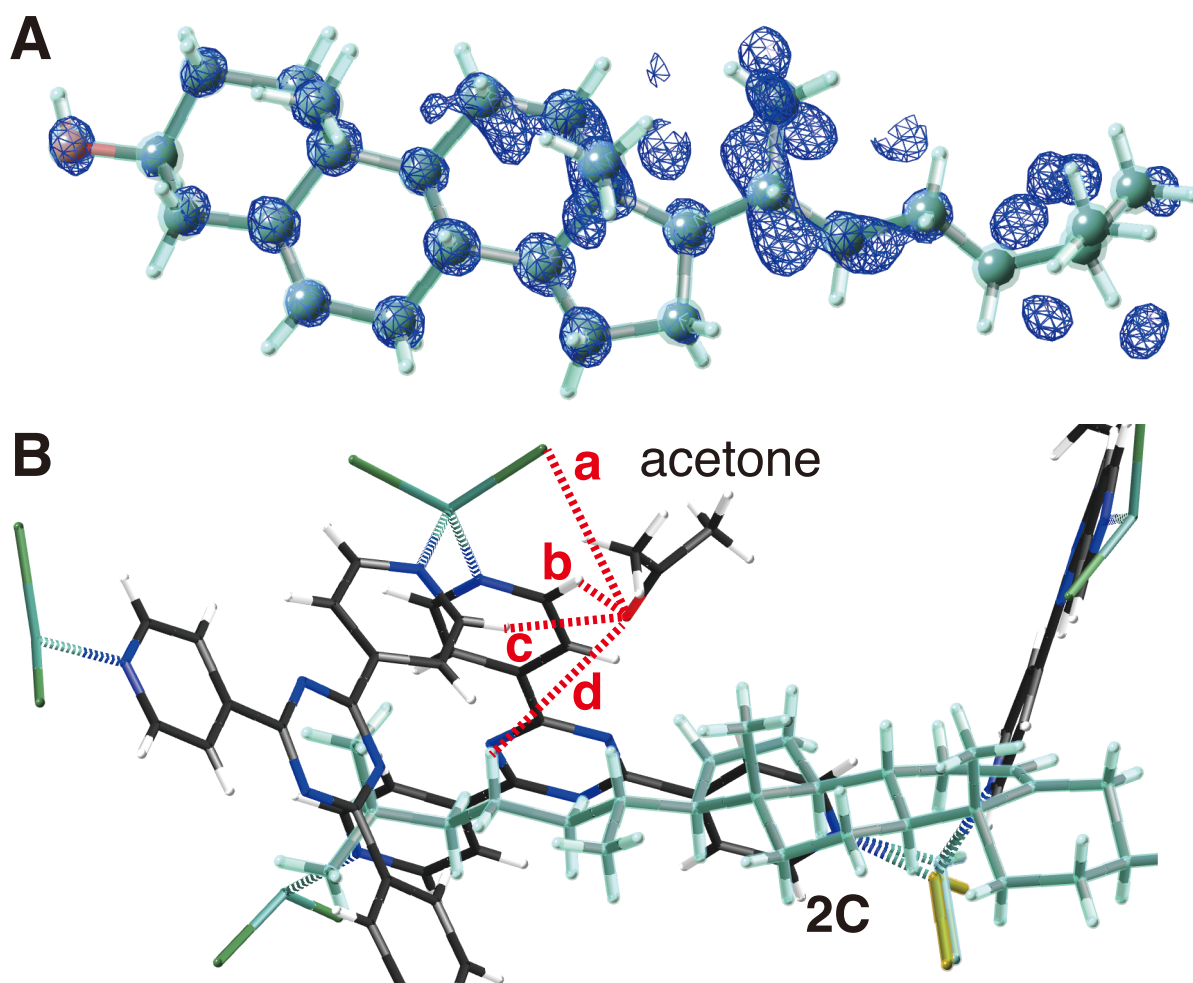


**Fig. 3–4** (A) Electron density ( $F_o$ ) map around **2C** drawn at a contour level of  $1.3\sigma$  ( $1.5 \text{ e}\text{\AA}^{-3}$ ). (B) Proximity of an acetone molecule to host framework **1c** and guest **2C**. Distances are a (Cl...C=O):  $3.46559(3) \text{ \AA}$ ; b and c (Py-H...O=C):  $2.47397(2) \text{ \AA}$  and  $2.386208(19) \text{ \AA}$ , respectively; d CH...O=C:  $2.618195(16) \text{ \AA}$ . van der Waals contacts of the acetone methyl groups are observed with guest **2C** and the host framework. Similar interactions are observed around another acetone molecule with host **1c** and guest **2D**.

The similar co-crystallization effect was observed in the guest soaking conducted with 2-butanone, and the Flack parameter  $x$  was also low enough ( $0.062(22)$ ).

There are several advantages of using ketone solvents in the soaking step: (i) A variety of organic compounds are highly soluble in ketones, thus the guests can be more concentrated during gradual solvent evaporation in ketones than in non-polar solvents. (ii) Ketone solvents can interact with guests in a variety of modes such as van der Waals interactions, hydrogen bonding and electrostatic interactions. (iii) Ketones can co-crystallize with the guests and enables the tight packing. The functionalization of ketones (eg. introducing chiral centers or heavy atoms) is also worthwhile to be considered. Moreover, I confirmed that an ester solvent, ethyl acetate, can co-crystallize with a steroid, epiandrosterone (**3**) (Fig. 3–5).

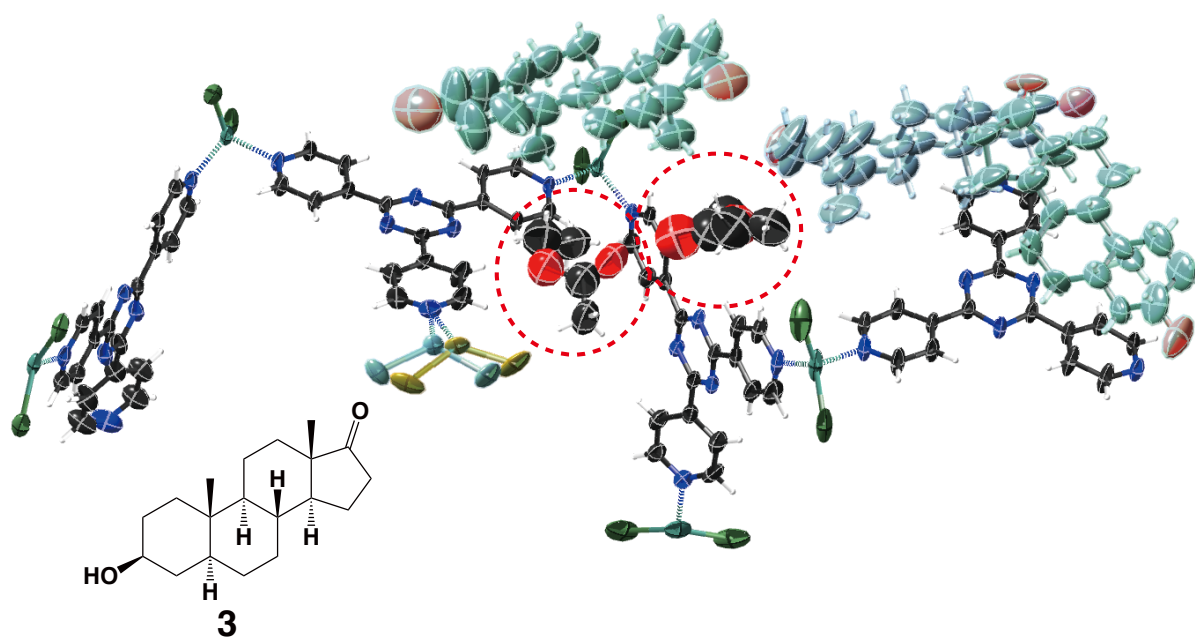


**Fig. 3–5** Thermal ellipsoid plot of an asymmetric unit of **1c·3** co-crystallized with ethyl acetate with 50% probability. Solvents (ethyl acetate) are highlighted by red circles.

### 3.4 Stereochemical Analysis of Hydroxy Steroids

Encouraged by the successful structural analyses of **2** and **3**, I examined various steroids using polar solvents with the crystalline sponge method. The chemical structures of three derivatives of **3**, 20*S*-hydroxycholesterol (**4**) and epimer pair, 22*R*-hydroxycholesterol (**5**) and 22*S*-hydroxycholesterol (**6**), were all elucidated from 5  $\mu\text{g}$  of the samples by the crystalline sponge method (Fig. 3–6). For all cases, the optimal soaking solvent was 2-butanone, and the guest soaking with acetone solvent did not give crystal structures of the target compounds. One benefit of using 2-butanone was that the guest soaking can be performed at an elevated temperature (70 °C) than those with *n*-hexane and acetone, of which boiling points were both less than 70 °C. As observed in conventional optimization of the guest soaking conditions, guest diffusions into the cavity of the host **1c** can be promoted at elevated temperatures.

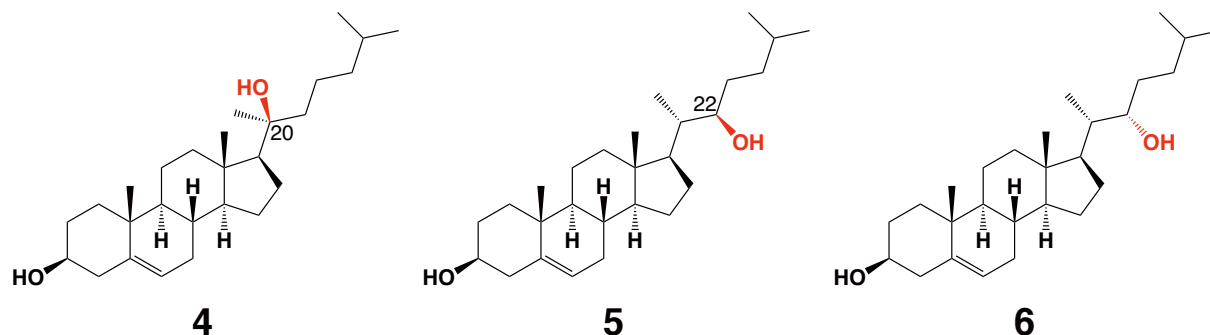


**Fig. 3–6** Chemical structures of **4–6**.

Special care should be taken in stereochemical determination of the quaternary carbon (C-20) of **4**, because hydroxy and methyl groups can be misassigned in crystallographic analysis of ambiguous data. Although the Mosher's NMR method is a primary way to determine absolute configurations of alcohols, it cannot be applied to determine configurations of sterically-hindered tertiary alcohols like **4**. Thus, for **4**, X-ray crystallography would be the

most appropriate method to determine the stereochemistry. In the crystal structure of **1c**·**4** by the crystalline sponge method, the electron density derived from the hydroxy oxygen was more intense than that from the methyl carbon. In addition, the hydroxy group formed hydrogen bonding with a chlorine atom and a tpt ligand of the framework **1c**, as evidenced by the atomic distances, 2.93261(2) and 3.15680(4) Å, respectively (Fig. 3–7). These observations were convincing enough to assign the *S* configuration at C–20.

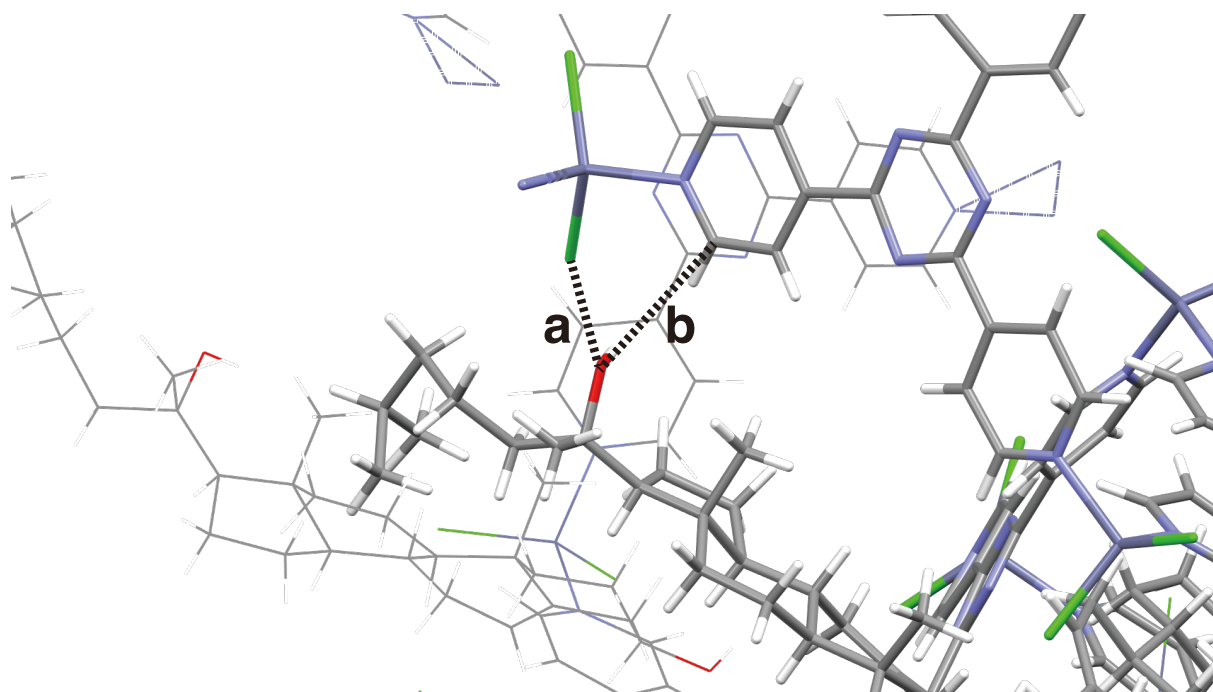


**Fig. 3–7** Proximity of **4** to host framework **1c**. Captions indicate hydrogen bonding featured in the main text; a (Cl•••O–H) and b (Py–H•••O–H).

The discrimination of an epimer pair **5** and **6** is challenging for several spectroscopic methods. For instance, mass spectrometry cannot provide information of stereochemical configurations. Nevertheless, with the crystalline sponge method, the electron density derived from a hydroxy group at C–22 of **5** was clearly observed. This formed hydrogen bonding with

two pyridine hydrogen atoms (3.42(3) and 3.03(3) Å) and is close to a chlorine atom of the zinc chloride of **1c** (3.58(3) Å) (Fig. 3–8). These observations indicate *R* stereochemistry at C–22. On the other hand, a hydroxy group at C–22 of **6** did not show close contact with a chlorine atom of the framework (4.180465(19) Å). It is noteworthy that each epimer is recognized by the framework **1c** differently, that again supports the robustness of the crystalline sponge method in stereochemical analysis.

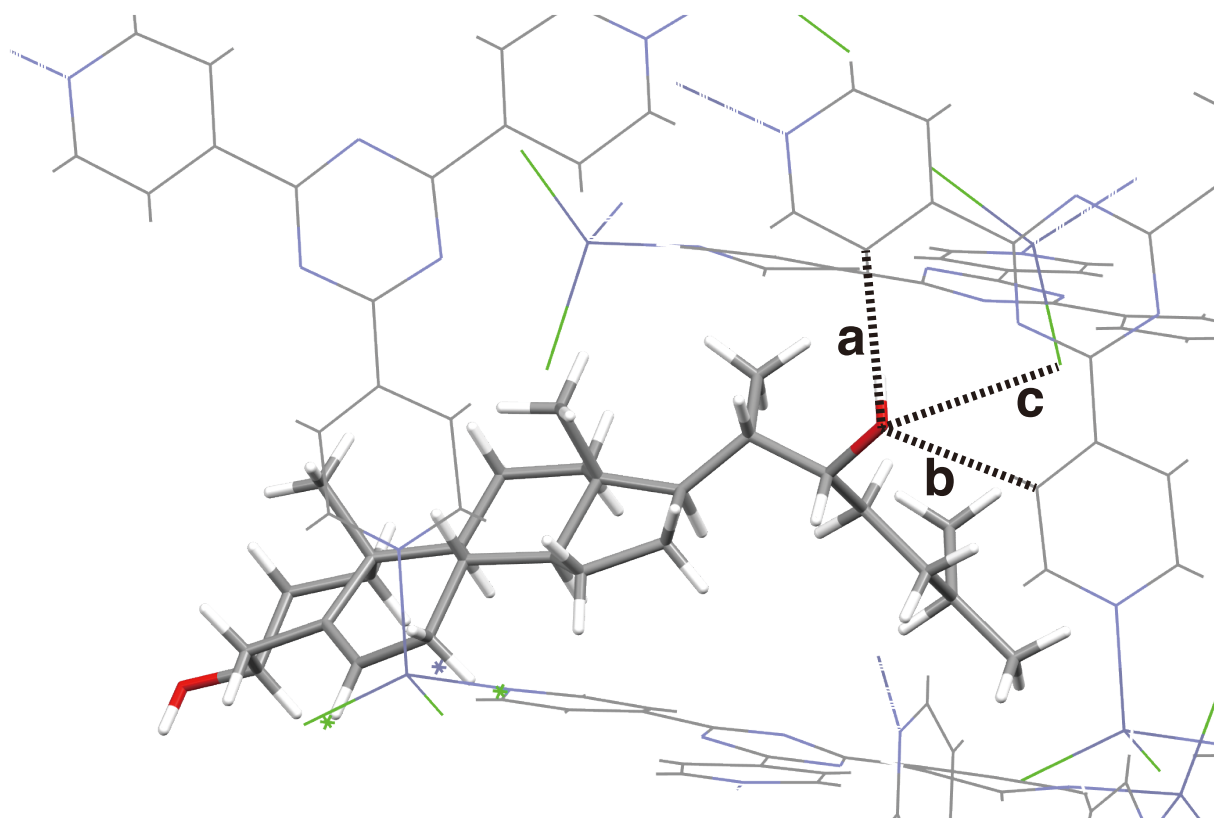


**Fig. 3–8** Proximity of **5** to host framework **1c**. Captions indicate hydrogen bonding featured in the main text; a, b (Py-H...O–H) and c (Cl...H–O).

Finally, I aimed to apply this updated protocol using polar solvents in structural analysis of an unknown sample obtained in a biosynthetic study to demonstrate that it is effective for

the workflow innovation in that field. The collaborators at the Jing-Ke Weng Group (Whitehead Institute for Biomedical Research, the United States) purified an unknown steroid **7** by heterologous expression of a CYP enzyme in a yeast strain. Their tandem mass spectrometry (MS/MS) analysis indicated the molecular formula of  $C_{27}H_{46}O_3$ , and **7** harbors three hydroxy groups at C-3, C-16, and C-22.<sup>[9]</sup> Since MS/MS analysis does not give any information of relative configurations, the stereochemistry should be elucidated by other methods such as NOESY NMR spectroscopy and single crystal X-ray diffraction (SCXRD) analysis. However, due to the conformational changes in the alkyl chain moiety, NOESY NMR would not provide reliable information of the relative configuration at C-22. Thus, SCXRD seemed the only way to elucidate the structure of **7**. It should be mentioned Watanabe *et al.* recently synthesized all the four 16,22-stereoisomers and determined the absolute structures by SCXRD.<sup>[10]</sup> However, crystallization conditions to grow suitable crystals for SCXRD are different for all isomers prepared in hundred-milligram scales, implying that the optimization step needed samples in at least milligram scales. In the experiment at Weng group, 1.5 mg of **7** was obtained from bacterial cultivation in large scales (12 L medium). Obtaining single crystals from the purified sample or further scaling-up of the cultivation were not realistic.

**7** was analyzed by the crystalline sponge method. The guest-including complex **1c**·**7** was obtained from only 5  $\mu$ g of the sample when acetone solvent was used. Crystallographic analysis revealed three crystallographically-independent molecules of **7** with six acetone solvents in an asymmetric unit. The resolved structures all correspond to (16*S*,22*S*)-dihydroxycholesterol (Fig. 3-9A). The electron density derived from **7** was strongly observed (Fig. 3-9B) with the reasonable Flack parameter  $x$  (0.120(5)) for determination of absolute structures. Interestingly, water molecules were also observed in the crystal structure and formed

hydrogen bonding networks with **7** and acetone. The water could be residual impurity in the acetone solvent or be from water vapors in the atmosphere. The observation of water in the crystalline sponge is a rare situation when hydrophobic solvents (eg. *n*-hexane and cyclohexane) are used. Considering the hydrophilicity of ketone solvents, addition of trace amounts of water during the soaking step may rather promote ordering of solvent and guest molecules. It is also noteworthy that this study became the first example of directly determining the absolute stereochemistry of **7**. In the previous studies, **7** was beyond the scope of the modified Mosher's method<sup>[11]</sup> at the C-16 hydroxyl group, thus the C-16 stereochemistry needed to be indirectly inferred from experimental rules in <sup>1</sup>H NMR chemical shift values at C-18.<sup>[12]</sup>

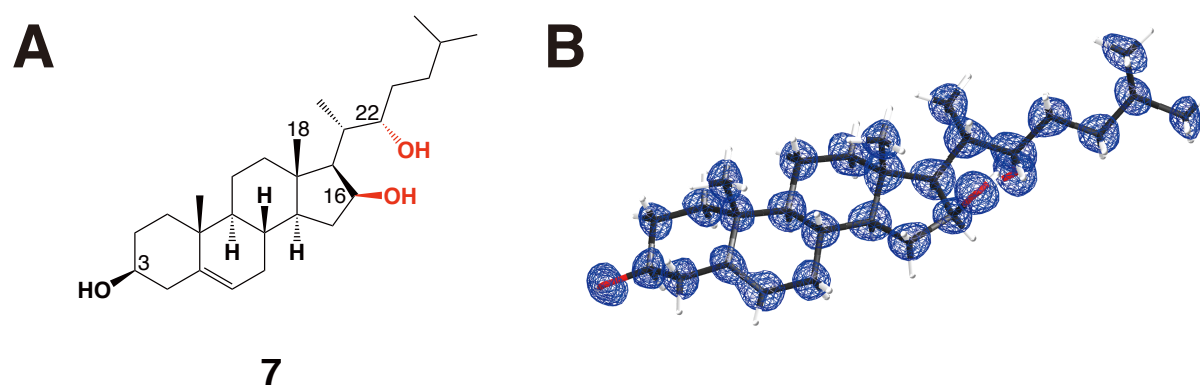


**Fig. 3-9** (A) Chemical structure of **7**. (B) Electron density ( $F_o$ ) map around **7** drawn at a contour level of  $1.3\sigma$  ( $1.6 \text{ e}\text{\AA}^{-3}$ ).

### 3.5 Summary

In this chapter, I firstly demonstrated that polar solvents can efficiently co-crystallize with the guests in the soaking process in the crystalline sponge method and successfully expanded the application scope of the method, in which we originally avoided the use of polar



solvents. With the novel soaking strategy, stereochemical analysis of standard steroid **2** was facilitated by the crystalline sponge method compared to the original protocol that suggested the exclusive use of non-polar solvents. Moreover, steroids **4–6** with subtle structural differences were also clearly discriminated. The chemical structure of an unknown metabolite **7** obtained by heterologous protein expression in yeast was also elucidated by the crystalline sponge method, including the absolute stereochemistry.

The modifications suggested in this chapter increases the practicability and success rates of structural determinations in the crystalline sponge method. This will further lead to streamline the workflow of research fields involving structural analysis of chemical compounds (eg. natural product chemistry, genome-based biosynthetic studies, organic synthesis, etc.) as a bottleneck, time-consuming process.

### 3.6 Experimental Section

#### **Materials and instruments**

Solvents and chemicals were purchased from TCI Co., Ltd., Wako Chemicals Ltd., Sigma-Aldrich Co. LLC., Kanto Chemical Co., Inc., or Cayman Chemical Company. The crystalline sponge  $[(\text{ZnCl}_2)_3(\text{tpt})_2 \cdot x(\text{solvent})]_n$  (**1c**, tpt = 2,4,6-tris(4-pyridyl)-1,3,5-triazine), of which solvent was chloroform, was prepared according to the reported procedure.<sup>[3]</sup> A screw-top microvial (Osaka Chemical, cat. no. 11090620), a screw cap with a septum seal (Osaka Chemical, cat. no. 53951-09FB), and a syringe needle (TERUMO, cat. no. NN-2116R) were used for guest inclusion into **1c**. HPLC analyses were performed with a JASCO MD-2018 photodiode array detector equipped with a JASCO PU-2089 pump, JASCO AS-2059 sampler and JASCO CO-2060 column thermostat, using a Develosil ODS-5 column (4.6 mm i.d.  $\times$  150 mm, Nomura Chemical Co., Ltd., cat. no. ODS0546150W).

#### **Solvent exchange of the crystalline sponge**

The solvents of the crystalline sponge complex **1c** were exchanged from chloroform to appropriate organic solvents (*n*-hexane, *tert*-butyl methyl ether, 2-butanone, or ethyl acetate). In a tube containing crystals of **1c** and 10 mL of chloroform, layer 5 mL of the appropriate solvent onto chloroform phase and store the tube at room temperature overnight. In the next day, discard almost all of the solvents by pipetting and add 5 mL of the appropriate solvent (repeated twice). The crystals of **1c** in the appropriate solvent were selected for actual use under microscope as described previously.<sup>[7]</sup>

#### **Preparation of the guest-absorbed crystals**

**(1c·2)** The guest-absorbed crystals **1c·2** were prepared by immersing a single crystal of **1c** (solvent = *n*-hexane) in 50  $\mu$ L *n*-hexane and 5  $\mu$ L dimethoxyethane (DME) containing 5  $\mu$ g of **2** in a vial. The solvent evaporation was conducted by piercing the septum with a syringe needle followed by storage of the vial at 50 °C overnight. For experiments using the acetone and 2-butanone (butanone) conditions, a crystal of **1c** (solvent = *tert*-butyl methyl ether) was collected into a vial. Subsequently, *tert*-butyl methyl ether in the vial was discarded by pipetting, and 55  $\mu$ L of acetone or butanone containing 5  $\mu$ g of **2** were quickly added. The solvent evaporation was conducted similarly as in hexane/DME conditions except the soaking temperature (50°C for acetone and 70 °C for butanone).

**(1c·4)** A crystal of **1c** (solvent = *tert*-butyl methyl ether) was collected into a vial. Subsequently, *tert*-butyl methyl ether in the vial was discarded by pipetting, and 55  $\mu$ L butanone containing 5  $\mu$ g of **4** were quickly added. The solvent evaporation was conducted by piercing the septum with a needle followed by storage of the vial at 70 °C overnight, to give the guest-absorbed crystals **1c·4**.

**(1c·5 and 1c·6)** A crystal of **1c** (solvent = *tert*-butyl methyl ether) was collected into a vial. Subsequently, *tert*-butyl methyl ether in the vial was discarded by pipetting, and 45  $\mu$ L butanone containing 5  $\mu$ g of **5** or **6** were quickly added. The solvent evaporation was conducted by piercing the septum with a needle followed by storage of the vial at 70 °C overnight, to give the guest-absorbed crystals **1c·5** or **1c·6**.

**(1c·7)** A crystal of **1c** (solvent = *tert*-butyl methyl ether) was collected into a vial. Subsequently, *tert*-butyl methyl ether in the vial was discarded by pipetting, and 55  $\mu$ L acetone containing 5  $\mu$ g of **7** were quickly added. The solvent evaporation was conducted by piercing the septum with a needle followed by storage of the vial at 50 °C for 24 hrs, to give the guest-absorbed crystals **1c·7**.

### **Crystalline sponge affinity screening (CSAS) for the yeast extract containing 7**

In order to assess the affinity of **7** present in yeast extracts for CS crystals, a fine crystal of the porous complex  $[(\text{ZnI}_2)_3(\text{tpt})_2 \cdot x(\text{cyclohexane})]_n^{[7]}$  was immersed in 45  $\mu\text{L}$  cyclohexane and 1  $\mu\text{L}$  1,2-dichloroethane containing 10  $\mu\text{g}$  of the crude extract. The guest-soaking was performed in a glass vial with a screw cap. The solvent evaporation was conducted at 50  $^\circ\text{C}$  for 24 h by piercing the septum with a needle. 5 crystals were used in total. The resulting crystals were transferred to a clean vial, and 50  $\mu\text{L}$  cyclohexane was added to wash the crystal surface for  $\sim 15$  s. The wash solution was again transferred to a clean vial, evaporated, dissolved in  $\sim 100$   $\mu\text{L}$  methanol. The crystals were soaked in 200  $\mu\text{L}$  methanol at 50  $^\circ\text{C}$  for 2 d. 5  $\mu\text{L}$  of the extract was subjected to HPLC analysis. The analytical method was as follows: solvent A – water, solvent B – acetonitrile, 0–30 min 85% B, 1 mL/min. The chromatogram was monitored at 200 nm. The obtained chromatogram is shown in Fig. 3–30.

### **Single crystal X-ray diffraction experiment**

Single crystal X-ray diffraction data were collected on XtaLAB Synergy-S (Rigaku Oxford Diffraction) diffractometer equipped with a micro-focus Cu K $\alpha$  radiation source ( $\lambda = 1.5418$  Å), a hybrid pixel array detector (HPAD), and a low temperature system using cold nitrogen stream (100 K) (**1c·2** in the hexane/DME and acetone conditions, **1c·4–1c·6**), on a SuperNova (Rigaku Oxford Diffraction) diffractometer equipped with a micro-focus Cu K $\alpha$  radiation source ( $\lambda = 1.5418$  Å), a high-sensitive CCD detector, and a low temperature system using cold nitrogen stream (100 K) (**1c·2** in the butanone condition), and on a Bruker D8 Venture Kappa DUO four-circle diffractometer equipped with an I $\mu$ S micro-focus sealed tube (Cu K $\alpha$  radiation), a Bruker Photon2 CPAD and a low temperature system using cold nitrogen

stream (100 K) (**1c·7**). Collected data were integrated, corrected, and scaled by the program CrysAlis<sup>Pro</sup> except **1c·7** processed by SAINT and SADABS programs. Empirical and numerical absorption corrections were applied in this process.

### **Crystal structure analysis**

All crystal structures were solved using SHELXT ver. 2018/2<sup>[13]</sup> and refined using SHELXL ver. 2018/3<sup>[14]</sup> programs. All the non-hydrogen atoms were refined anisotropically. All the hydrogen atoms were grown using the proper HFIX commands and refined isotropically using the riding model. Several zinc and iodine atoms in the framework were refined with EADP commands. Guest molecules are refined using DFIX, DANG, SIMU, ISOR, RIGU, FLAT and SAME (if more than one molecule are found in an asymmetric unit) commands as needed. Solvent molecules in the pores were refined using DFIX, DANG, SIMU and ISOR commands.

For the crystal structure of **1c·2** in the hexane/DME condition, we could not build a reasonable disorder model for the guest B, although it seems to be disordered with solvent molecules, because of severe disorders. Therefore, we estimated the occupancy of the guest B as 20.0% (at the 2-fold rotational axis), so that its isotropic thermal parameters would have reasonable values ( $U_{\text{iso}} = 0.080\text{--}0.25$ ) and fixed them in the refinement. For the crystal structure of **1c·5**, we estimated the occupancy of the guests as 30.0%, so that their isotropic thermal parameters would have reasonable values ( $U_{\text{iso}} = 0.080\text{--}0.25$ ) and fixed them in the refinement.

For crystal structures of **1c·2** in the acetone and butanone conditions, **1c·6**, and **1c·7**, considerably large void remained in the crystal structure, and we assumed that the void is filled with disordered solvent molecules. Therefore, the least square refinement at the last stage was performed using the reflection data modified by *PLATON*<sup>[15]</sup>/*SQUEEZE*<sup>[16]</sup> program.

For the crystal structure of **1c·5**, twin refinement was performed by using HKLF5 reflection file generated by CrysAlis<sup>Pro</sup>.

Several “Alert A” notifications were found in the validation program CheckCIF. The comments for the alerts are described in the validation response form (vrf) in each cif file.

#### Crystallographic data of **1c·2** in the hexane/DME condition

Refined formula: C<sub>95.90</sub>H<sub>92</sub>Cl<sub>12</sub>N<sub>24</sub>O<sub>1.70</sub>Zn<sub>6</sub>, formula weight ( $M_r$ ): 2425.55, crystal system: monoclinic, space group:  $C2$ ,  $Z = 4$ ,  $R_{\text{int}} = 0.0332$ , Lattice parameters,  $R$ -factor on  $F^2 > 2\sigma(F^2)$ , and weighted  $R$ -factor are as follows:  $a = 32.9343(3)$  Å,  $b = 14.43010(10)$  Å,  $c = 31.3232(2)$  Å,  $\beta = 100.6810(10)^\circ$ ,  $V = 14628.3(2)$  Å<sup>3</sup>, GoF = 1.053,  $R_1 = 0.0708$ ,  $wR_2 = 0.2421$ , Flack parameter calculated by Parsons’ method<sup>[17]</sup>; 0.121(8). CCDC deposit number 1978851.

The ORTEP diagram of the asymmetric unit of **1c·2** in the hexane/DME condition is shown in Fig. 3–10. Two (**A** and **B**) were found in the asymmetric unit. One of the molecules (**A**) with an occupancy of 50% is overlapped on the symmetrically generated one by the 2-fold rotation operation. The restraints used for the refinement are summarized in Fig. 3–11.

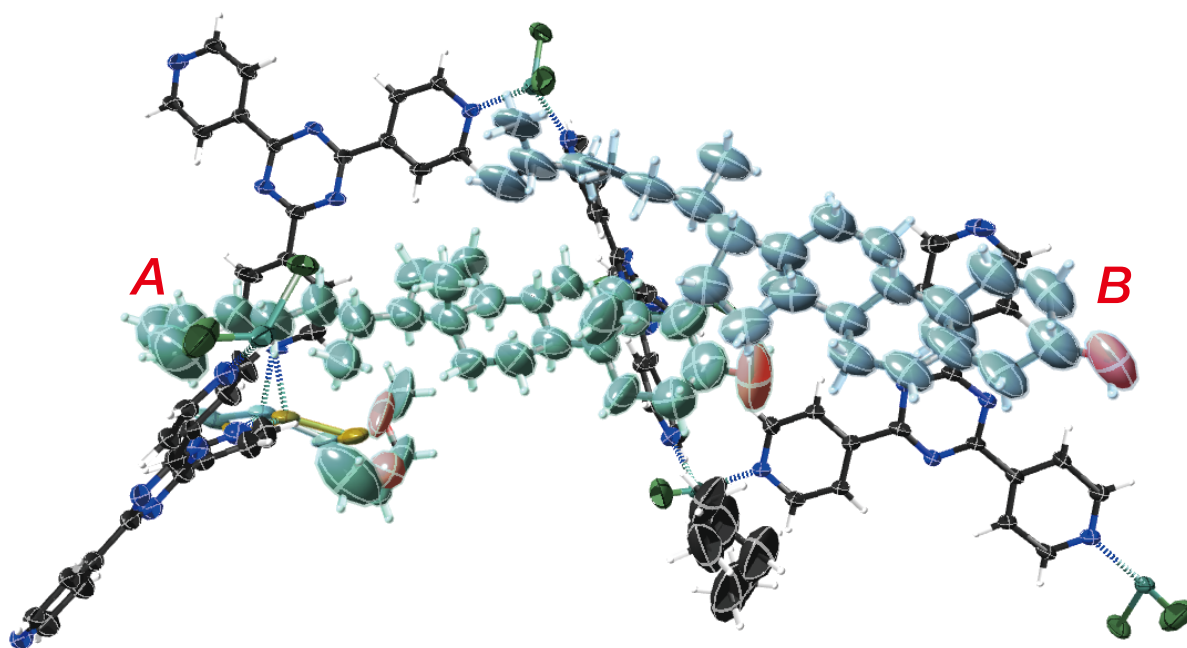


**Fig. 3–10** Thermal ellipsoid plots with 50% probability in an asymmetric unit of **1c·2** in the hexane/DME condition. Guests A and B correspond to **2A** and **2B** in the main text.

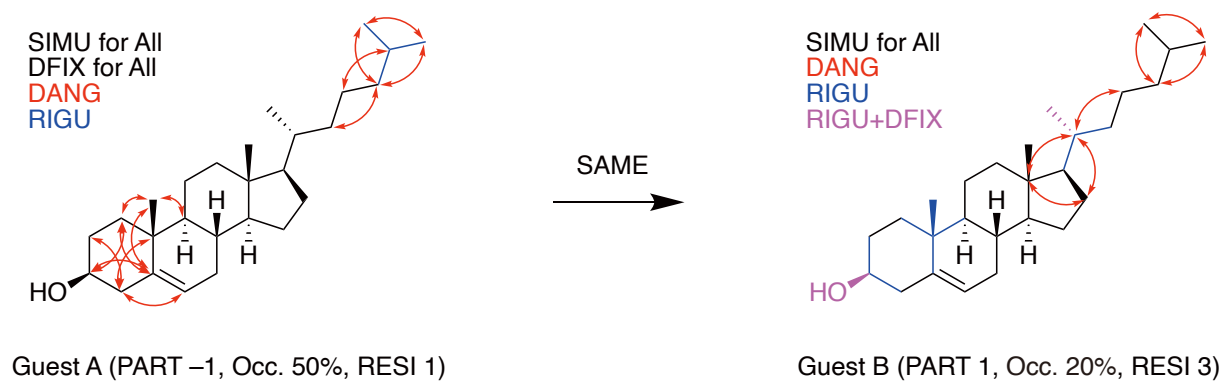


**Fig. 3–11** Restraints applied in the refinement of the guest molecules **2** in the hexane/DME condition.

#### Crystallographic data of **1c·2** in the acetone condition

Refined formula:  $C_{105}H_{106}Cl_{12}N_{24}O_3Zn_6$ , formula weight ( $M_r$ ): 2569.75, crystal system: monoclinic, space group:  $C2$ ,  $Z = 4$ ,  $R_{int} = 0.0404$ , Lattice parameters,  $R$ -factor on  $F^2 > 2\sigma(F^2)$ ,

and weighted  $R$ -factor are as follows:  $a = 32.1957(3) \text{ \AA}$ ,  $b = 14.48550(10) \text{ \AA}$ ,  $c = 31.6250(2) \text{ \AA}$ ,  $\beta = 100.1450(10)^\circ$ ,  $V = 14518.4(2) \text{ \AA}^3$ ,  $\text{GoF} = 1.056$ ,  $R_1 = 0.0484$ ,  $wR_2 = 0.1437$ , Flack parameter calculated by Parsons' method<sup>[17]</sup>; 0.033(12). CCDC deposit number 1978852.

The ORTEP diagram of the asymmetric unit of **1c·2** in the acetone condition is shown in Fig. 3–12. Two (**A** and **B**) were found in the asymmetric unit. Both molecules with occupancies of 50% are overlapped on the symmetrically generated one by the 2-fold rotation operation. The restraints used for the refinement are summarized in Fig. 3–13.

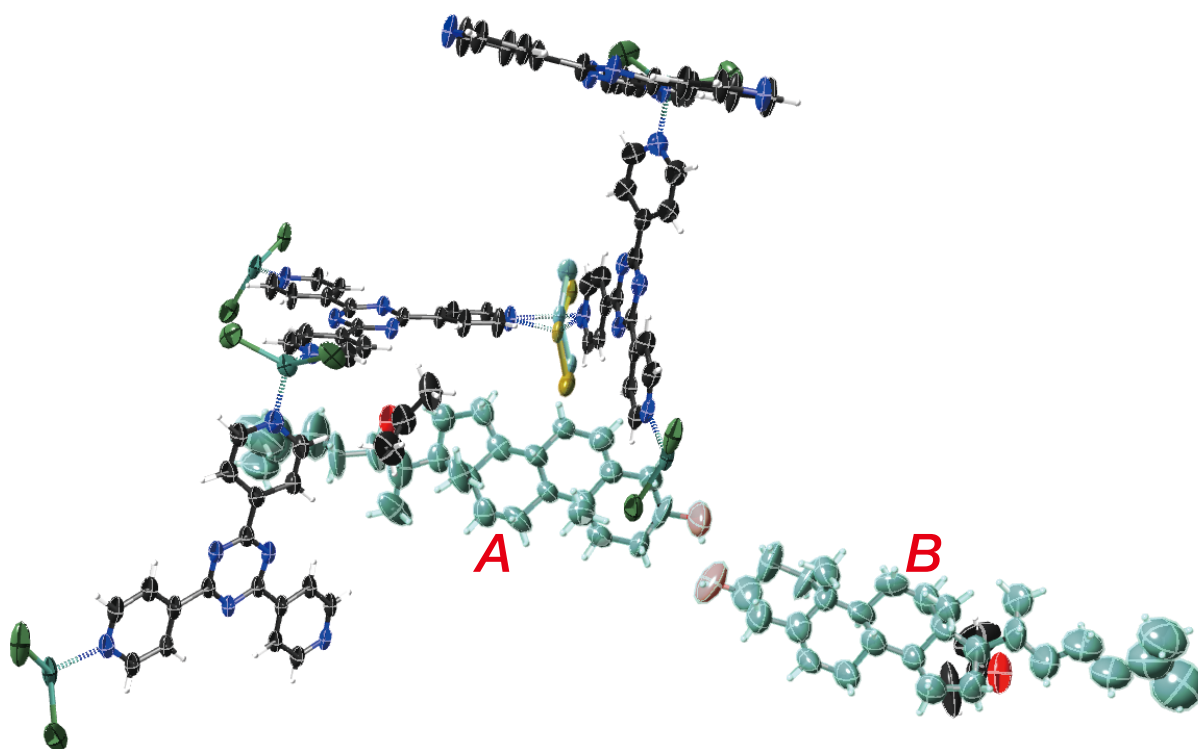


**Fig. 3–12** Thermal ellipsoid plots with 50% probability in an asymmetric unit of **1c·2** in the acetone condition. Guests **A** and **B** correspond to **2C** and **2D** in the main text.



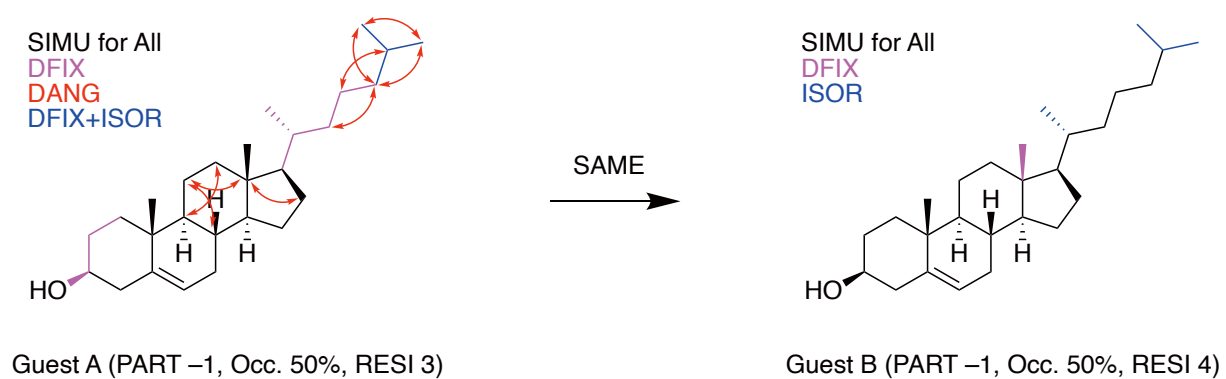


**Fig. 3–13** Restraints applied in the refinement of the guest molecules **2** in the acetone condition.

The alkyl side-chain chiral center of **2** observed in the hexane/DME and acetone conditions

As shown in Fig. 3–14 and Table 3–1, crystallographic analysis of **2** with the acetone condition offered normal  $sp^3$  C-C-C angles around C-20, whereas those obtained in the hexane/DME condition were apparently deviated from the average parameters calculated from crystal structures available in the Cambridge Structural Database.<sup>[8]</sup> In the refinement of the two crystal structures CCDC1978851 and 1978852, we did not apply the SHELXL geometrical restraint DANG to  $sp^3$  carbons around C-20.

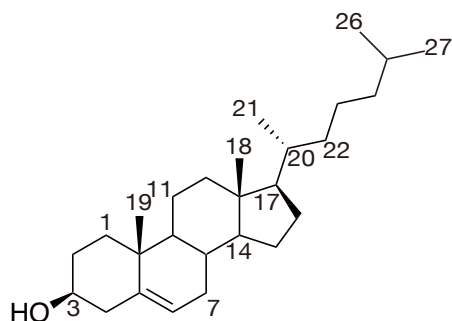


**Fig. 3–14** The numbering for **2**.

**Table 3–1** The angle parameters around C-20 of **2**.

Angle positions	Average values (°) (From reference [8])	Observed values in <b>2A</b> (°) (CCDC1978851)	Observed values in <b>2C</b> (°) (CCDC1978852)
C-17_C-20_C-21 ( $\alpha$ )	110.5(1.7)	115.8574(5)	110.0734(6)
C-21_C-20_C-22 ( $\beta$ )	110.7(3.0)	111.5655(5)	104.6003(6)
C-17_C-20_C-22 ( $\gamma$ )	110.4(1.7)	126.1342(8)	113.0662(7)
$\alpha + \beta + \gamma$	331.6(3.8) <sup>a</sup>	353.5571(11) <sup>a</sup>	327.7399(11) <sup>a</sup>

<sup>a</sup> The standard deviation value  $\sigma(\alpha + \beta + \gamma)$  is the root-sum-square of  $\sigma(\alpha)$ ,  $\sigma(\beta)$  and  $\sigma(\gamma)$ .

### The soaking experiments of 2 in the hexane/DME condition with various factors

To investigate the effect of factors other than solvent choice on the crystallographic results for cholesterol, we performed supplementary experiments. As shown in Table 3–2, we varied the temperature (Entry 1, 2 and 7), concentration (Entry 3 and 4) and soaking time (Entry 5 and 6) from the standard condition (Entry 0) in our soaking experiments. In none of the experiments, we could improve the quality of X-ray data significantly

**Table 3–2** Investigation into the effect of temperature, concentration and soaking time.

Entry	Data ID (Machine name)	Temp. (°C)	Guest amount (μg)	Soaking time	Description of the X-ray data
0	exp_2896 (Synergy-S)	50	5	overnight	2 guest molecules were observed in an asymmetric unit. The angle sum ( $\alpha + \beta + \gamma$ ) around C-20 were 353.56°.
1	exp_943 (P200)	30	5	overnight	No guest molecules were found in an asymmetric unit.
2	exp_938 (P200)	4	5	3 d	Diffraction intensities were weak. The unit cell parameter could not be calculated.
3	exp_921 (Synergy Custom)	50	10	3 d <sup>a</sup> and overnight	1 guest molecule was observed in an asymmetric unit. The angle sum ( $\alpha + \beta + \gamma$ ) around C-20 were 359.83°.
4	exp_923 (Synergy Custom)	50	50	5 d <sup>a</sup> and overnight	1 guest molecule was observed in an asymmetric unit. The angle sum ( $\alpha + \beta + \gamma$ ) around C-20 were 357.89°.
5	exp_946 (P200)	50	5	overnight	1 guest molecule was observed in an asymmetric unit. The C-21 methyl group could not be modelled properly without DANG restraints.
6	exp_929 (Synergy Custom)	50	5	overnight	No guest molecules were found in an asymmetric unit.
7	exp_945 (P200)	50	5	overnight	No guest molecules were found in an asymmetric unit.

<sup>a</sup> The septa of the vial cap were not pierced with a syringe needle (TERUMO, cat. no. NN-2116R).

#### Crystallographic data of **1c·2** in the butanone condition

Refined formula: C<sub>107</sub>H<sub>110</sub>Cl<sub>12</sub>N<sub>24</sub>O<sub>3</sub>Zn<sub>6</sub>, formula weight (*M<sub>r</sub>*): 2597.80, crystal system: monoclinic, space group: *C*2, *Z* = 4, *R*<sub>int</sub> = 0.0357, Lattice parameters, *R*-factor on *F*<sup>2</sup> > 2σ(*F*<sup>2</sup>), and weighted *R*-factor are as follows: *a* = 32.0837(4) Å, *b* = 14.45340(10) Å, *c* = 31.6753(3) Å, β = 100.1200(10)°, *V* = 14459.9(3) Å<sup>3</sup>, GoF = 1.052, *R*<sub>1</sub> = 0.0618, *wR*<sub>2</sub> = 0.1929, Flack parameter calculated by Parsons' method<sup>[17]</sup>; 0.062(22). CCDC deposit number 1978853.

The ORTEP diagram of the asymmetric unit of **1c·2** in the butanone condition is shown in Fig. 3–15. Two (**A** and **B**) were found in the asymmetric unit. Both molecules with occupancies of 50% are overlapped on the symmetrically generated one by the 2-fold rotation operation. The restraints used for the refinement are summarized in Fig. 3–16.

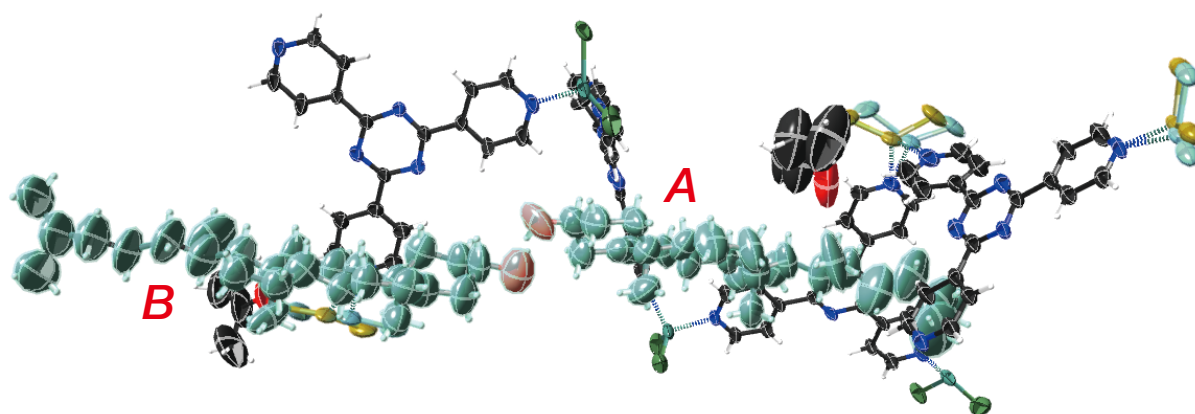


**Fig. 3–15** Thermal ellipsoid plots with 50% probability in an asymmetric unit of **1c·2** in the butanone condition.

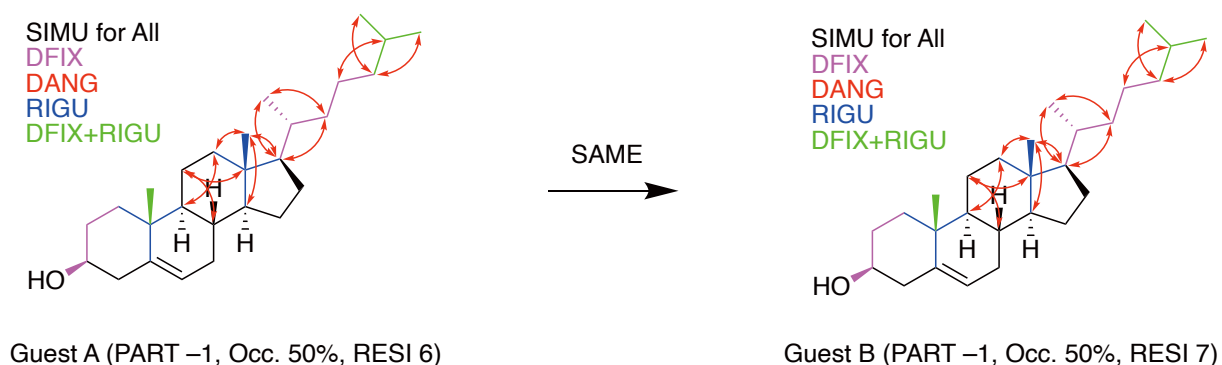


**Fig. 3–16** Restraints applied in the refinement of the guest molecules **2** in the butanone condition.

### Crystallographic data of **1c·3**

Refined formula:  $C_{408}H_{392}Cl_{48}N_{96}O_{25}Zn_{24}$ , formula weight ( $M_r$ ): 2593.76, crystal system: monoclinic, space group:  $C2$ ,  $Z = 4$ ,  $R_{int} = 0.0311$ , Lattice parameters,  $R$ -factor on  $F^2 > 2\sigma(F^2)$ , and weighted  $R$ -factor are as follows:  $a = 32.37470(10) \text{ \AA}$ ,  $b = 14.44790(10) \text{ \AA}$ ,  $c = 31.14390(10) \text{ \AA}$ ,  $\beta = 100.34^\circ$ ,  $V = 14330.87(12) \text{ \AA}^3$ , GoF = 1.037,  $R_1 = 0.0804$ ,  $wR_2 = 0.2476$ , Flack parameter calculated by Parsons' method<sup>[17]</sup>; 0.063(7). CCDC deposit number 2045102.

The ORTEP diagram of the asymmetric unit of **1c·3** is shown in Fig. 3–17. Three (**A–C**) were found in the asymmetric unit. Two of the molecules (**A** and **C**) with occupancies of 50% and 0.293(4)%, respectively, are overlapped on the symmetrically generated one by the 2-fold rotation operation. One guest molecule (**B**) in the general position is disordered with one guest molecule (**C**), and its occupancy were estimated to be 0.415(8)% by least square refinement. The restraints used for the refinement are summarized in Fig. 3–18.

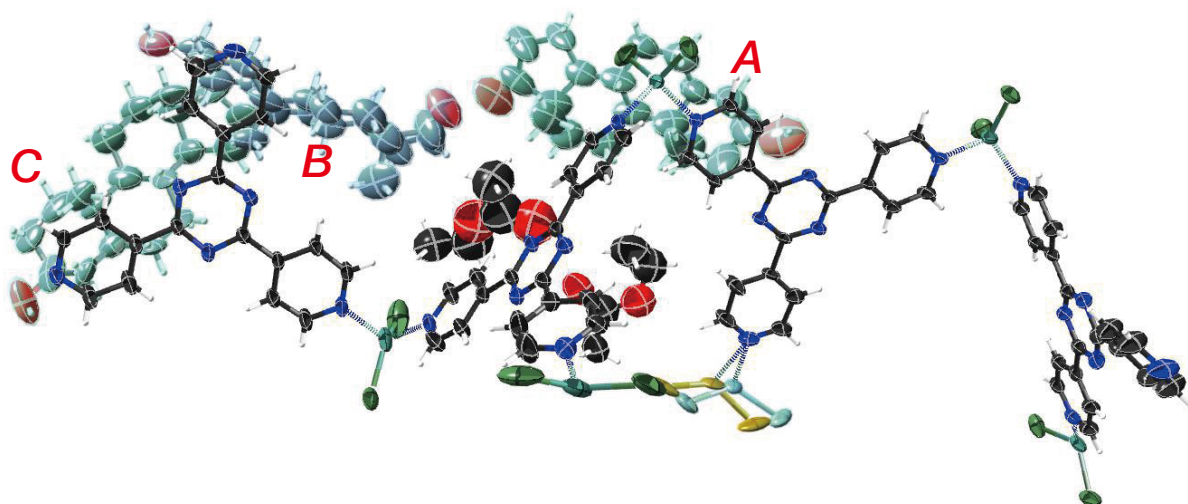


**Fig. 3–17** Thermal ellipsoid plots with 50% probability in an asymmetric unit of **1c·3**.

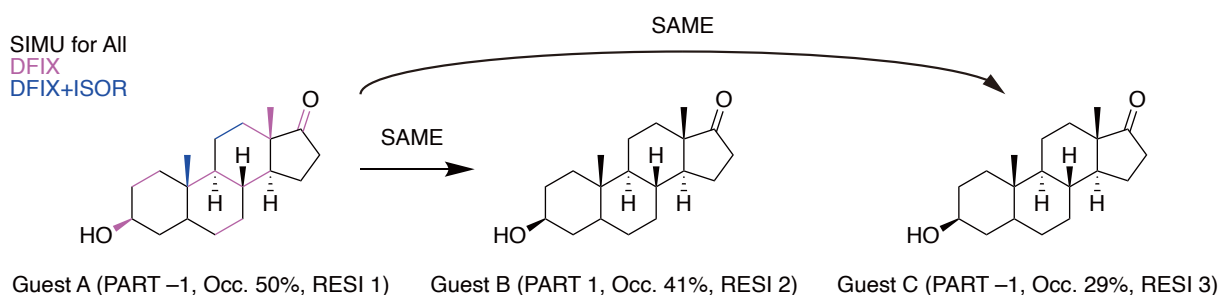


**Fig. 3–18** Restraints applied in the refinement of the guest molecules **3**.

### Crystallographic data of **1c·4**

Refined formula:  $C_{99}H_{94}Cl_{12}N_{24}O_2Zn_6$ , formula weight ( $M_r$ ): 2469.60, crystal system: monoclinic, space group:  $C2$ ,  $Z = 4$ ,  $R_{int} = 0.0414$ , Lattice parameters,  $R$ -factor on  $F^2 > 2\sigma(F^2)$ , and weighted  $R$ -factor are as follows:  $a = 32.3740(4)$  Å,  $b = 14.42050(10)$  Å,  $c = 30.9985(3)$  Å,  $\beta = 99.6730(10)^\circ$ ,  $V = 14265.9(2)$  Å<sup>3</sup>, GoF = 1.317,  $R_1 = 0.0936$ ,  $wR_2 = 0.3188$ , Flack parameter calculated by Parsons' method<sup>[17]</sup>; 0.170(8). CCDC deposit number 1978855.

The ORTEP diagram of the asymmetric unit of **1c·4** is shown in Fig. 3–19. Two (**A** and **B**) were found in the asymmetric unit. Both molecules with occupancies of 50% are overlapped on the symmetrically generated one by the 2-fold rotation operation. The restraints used for the refinement are summarized in Fig. 3–20. Electron density observed around **A** is shown in Fig. 3–20.

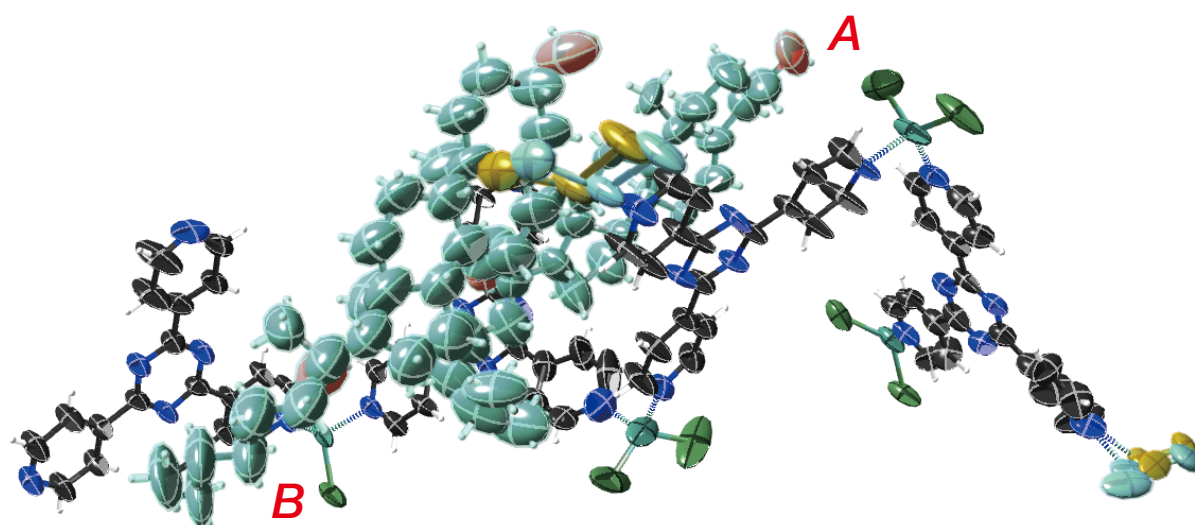


**Fig. 3–19** Thermal ellipsoid plots with 50% probability in an asymmetric unit of **1c·4**.

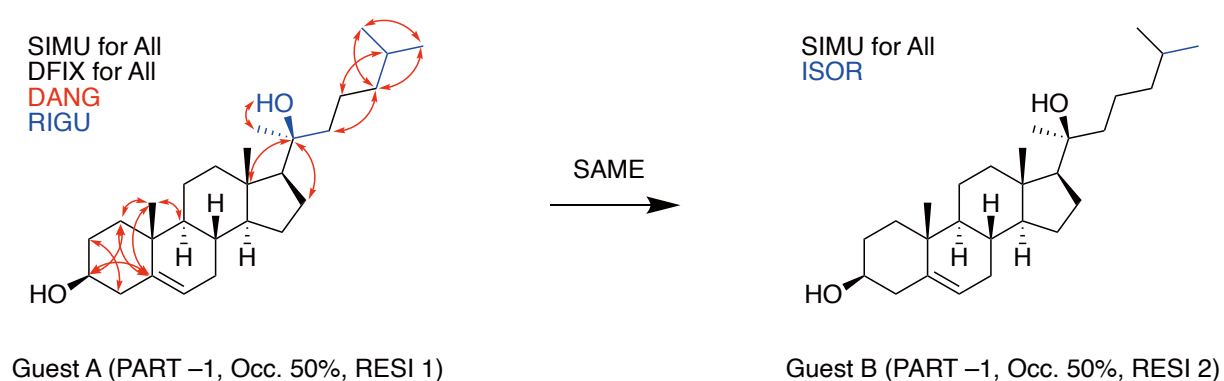


**Fig. 3–20** Restraints applied in the refinement of the guest molecules **4**.

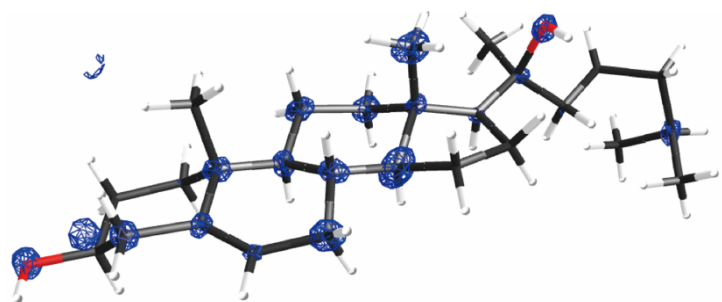


**Fig. 3–21** Electron density ( $F_o$ ) map around **4** drawn at a contour level of  $1.6\sigma$  ( $1.5 \text{ e}\text{\AA}^{-3}$ ).

### Crystallographic data of **1c·5**

Refined formula:  $\text{C}_{80.10}\text{H}_{61.80}\text{Cl}_{12}\text{N}_{24}\text{O}_{0.60}\text{Zn}_6$ , formula weight ( $M_r$ ): 2187.75, crystal system: monoclinic, space group:  $C2$ ,  $Z = 4$ ,  $R_{\text{int}} = 0.077$ , Lattice parameters,  $R$ -factor on  $F^2 > 2\sigma(F^2)$ , and weighted  $R$ -factor are as follows:  $a = 32.9189(3) \text{ \AA}$ ,  $b = 14.45780(10) \text{ \AA}$ ,  $c = 31.3394(3) \text{ \AA}$ ,  $\beta = 100.8830(10)^\circ$ ,  $V = 14647.3(2) \text{ \AA}^3$ ,  $\text{GoF} = 1.147$ ,  $R_1 = 0.0919$ ,  $wR_2 = 0.2956$ , Flack parameter calculated by Parsons' method<sup>[17]</sup>; 0.191(38). CCDC deposit number 1978856.

The ORTEP diagram of the asymmetric unit of **1c·5** is shown in Fig. 3–22. One (**4**) was found in the asymmetric unit. The restraints used for the refinement are summarized in Fig. 3–23. Electron density observed around **4** is shown in Fig. 3–24.



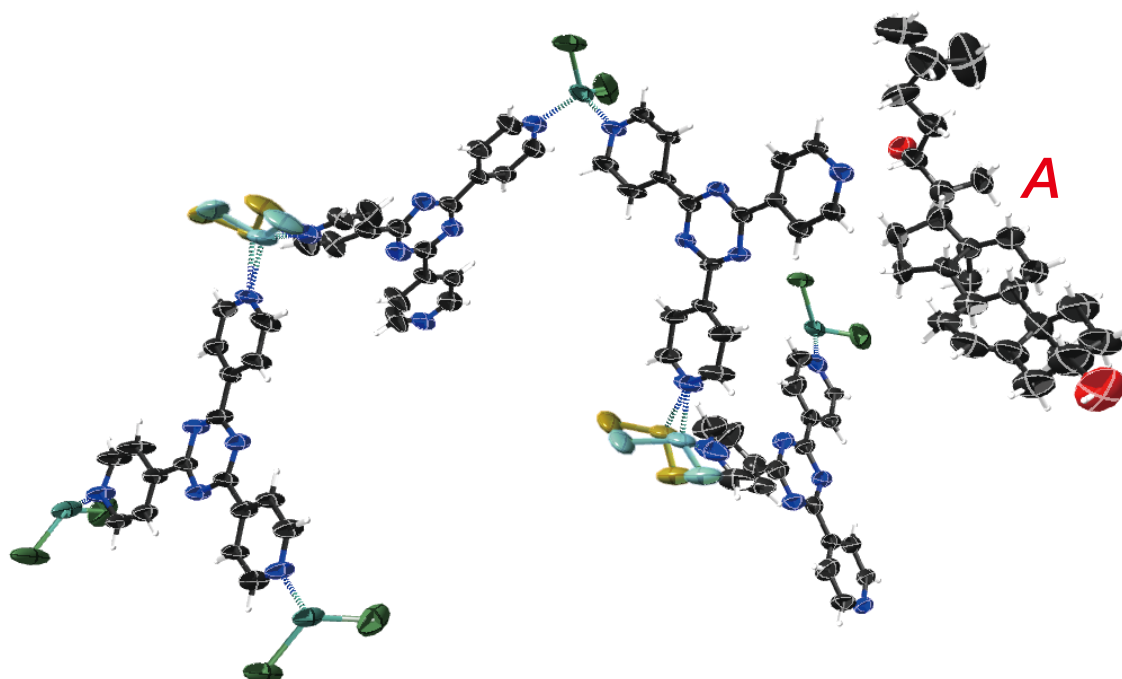
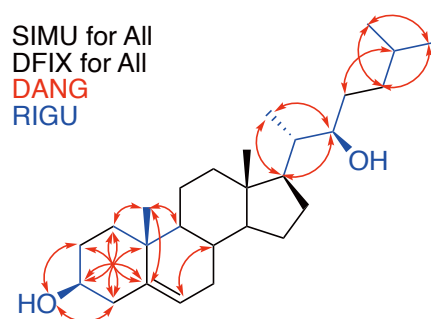


**Fig. 3–22** Thermal ellipsoid plots with 50% probability in an asymmetric unit of **1c·5**.



Guest A (PART 0, Occ. 30%, RESI 1)

**Fig. 3–23** Restraints applied in the refinement of the guest molecule **5**.

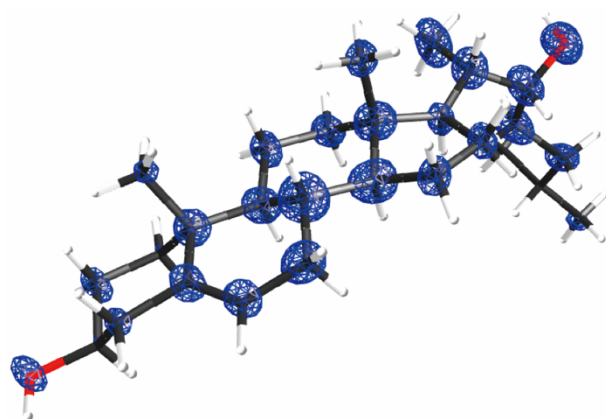


**Fig. 3–24** Electron density ( $F_o$ ) map around **5** drawn at a contour level of  $1.0\sigma$  ( $1.0 \text{ e}\text{\AA}^{-3}$ ).

#### Crystallographic data of **1c·6**

Refined formula:  $\text{C}_{85.50}\text{H}_{71}\text{I}_{12}\text{N}_{24}\text{OZn}_6$ , formula weight ( $M_r$ ): 2268.28, crystal system: monoclinic, space group:  $C2$ ,  $Z = 4$ ,  $R_{\text{int}} = 0.0254$ , Lattice parameters,  $R$ -factor on  $F^2 > 2\sigma(F^2)$ , and weighted  $R$ -factor are as follows:  $a = 32.1475(3) \text{ \AA}$ ,  $b = 14.40660(10) \text{ \AA}$ ,  $c = 31.2342(2) \text{ \AA}$ ,  $\beta = 99.3160(10)^\circ$ ,  $V = 14274.89(19) \text{ \AA}^3$ ,  $\text{GoF} = 0.872$ ,  $R_1 = 0.0490$ ,  $wR_2 = 0.2132$ , Flack parameter calculated by Parsons' method<sup>[17]</sup>;  $0.317(8)$ . CCDC deposit number 1978857.

The ORTEP diagram of the asymmetric unit of **1c·6** is shown in Fig. 3–25. One (**A**) was found in the asymmetric unit. **A** with occupancies of 50% is overlapped on the symmetrically generated one by the 2-fold rotation operation. The restraints used for the refinement are summarized in Fig. 3–26. Electron density observed around **A** is shown in Fig. 3–27.

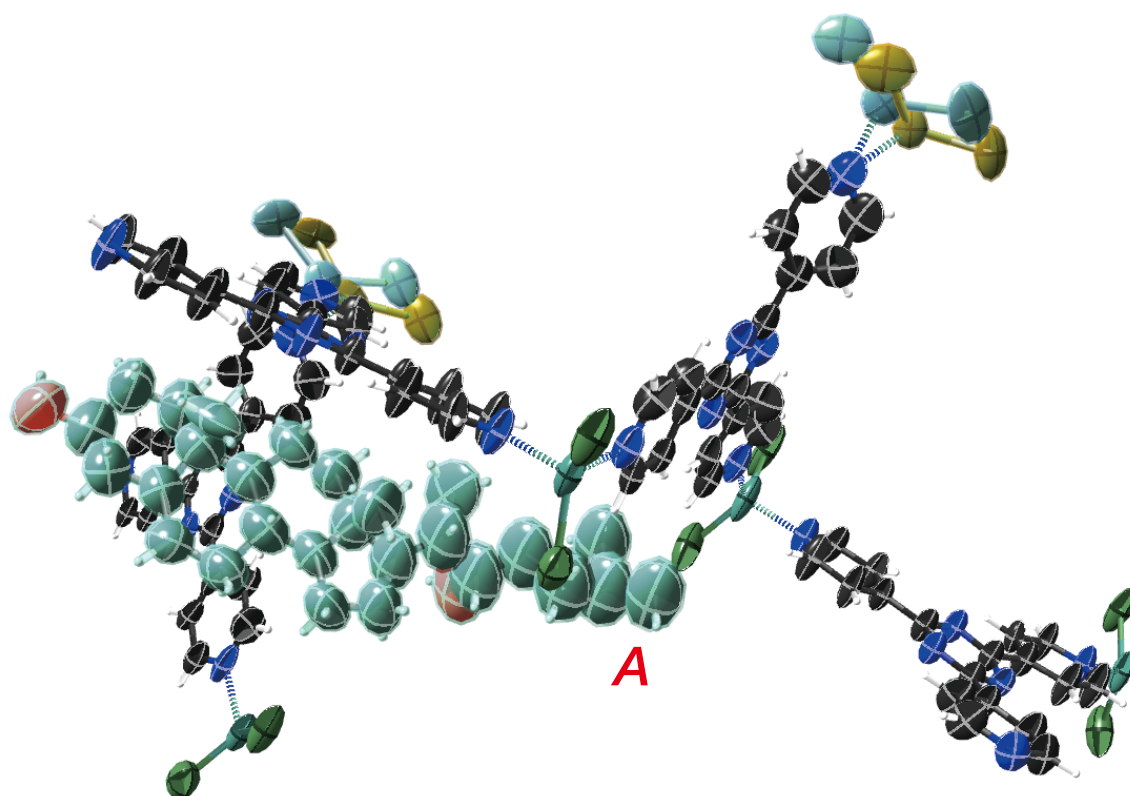
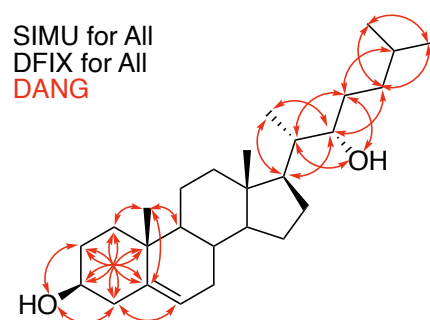


**Fig. 3–25** Thermal ellipsoid plots with 50% probability in an asymmetric unit of **1c·6**.



Guest A (PART -1, Occ. 50%, RESI 1)

**Fig. 3–26** Restraints applied in the refinement of the guest molecule **6**.

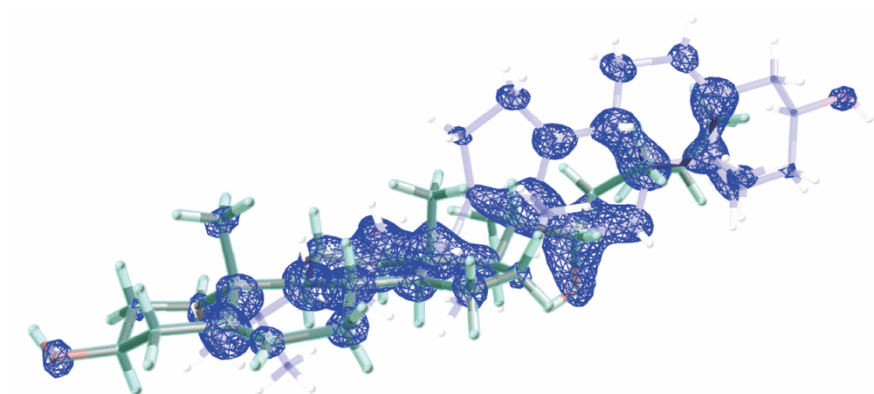


**Fig. 3–27** Electron density ( $F_o$ ) map around **6** drawn at a contour level of  $1.0\sigma$  ( $1.0 \text{ e}\text{\AA}^{-3}$ ).

#### Crystallographic data of **1c·7**

Refined formula:  $\text{C}_{243}\text{H}_{270}\text{Cl}_{24}\text{N}_{48}\text{O}_{18}\text{Zn}_{12}$ , formula weight ( $M_r$ ): 5786.29, crystal system: monoclinic, space group:  $P2_1$ ,  $Z = 2$ ,  $R_{\text{int}} = 0.0905$ , Lattice parameters,  $R$ -factor on  $F^2 > 2\sigma(F^2)$ , and weighted  $R$ -factor are as follows:  $a = 31.0167(15) \text{ \AA}$ ,  $b = 14.3695(6) \text{ \AA}$ ,  $c = 31.6044(16) \text{ \AA}$ ,  $\beta = 98.544(3)^\circ$ ,  $V = 13929.6(11) \text{ \AA}^3$ ,  $\text{GoF} = 1.237$ ,  $R_1 = 0.1034$ ,  $wR_2 = 0.3058$ , Flack parameter calculated by Parsons' method<sup>[17]</sup>;  $0.120(5)$ . CCDC deposit number 1899808.

The ORTEP diagram of the asymmetric unit of **1c·7** is shown in Fig. 3–28. Three guest molecules (**A–C**) were found in the asymmetric unit. The restraints used for the refinement are summarized in Fig. 3–29.

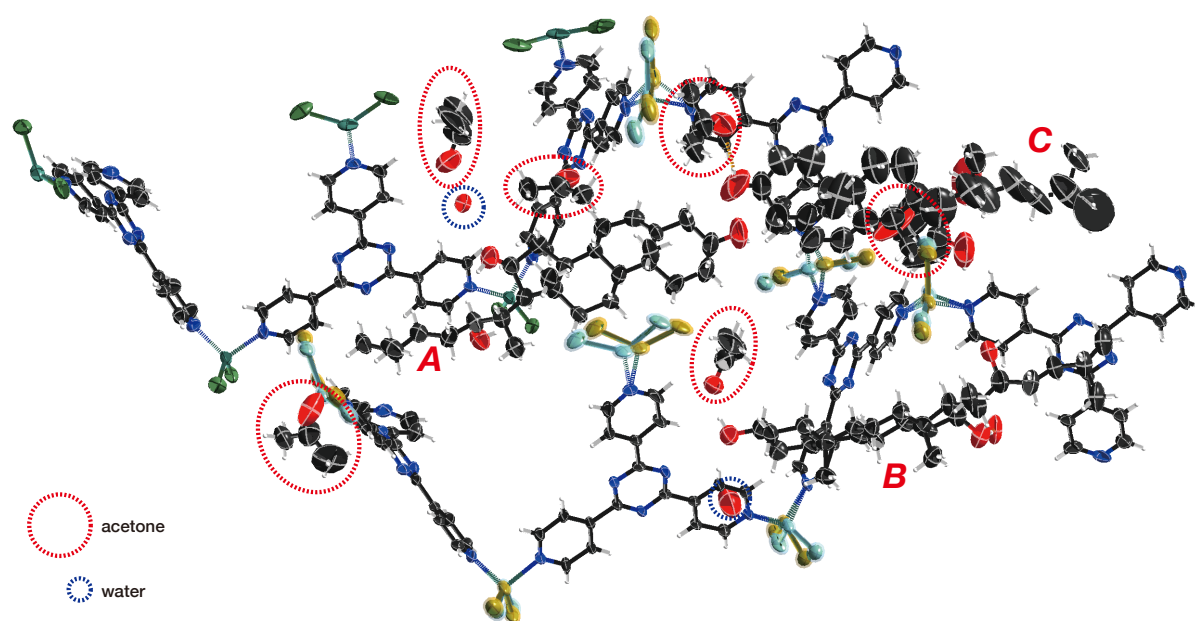


**Fig. 3–28** Thermal ellipsoid plots with 50% probability in an asymmetric unit of **1c·7**. Solvent acetone and water molecules are highlighted by red and blue circles, respectively.

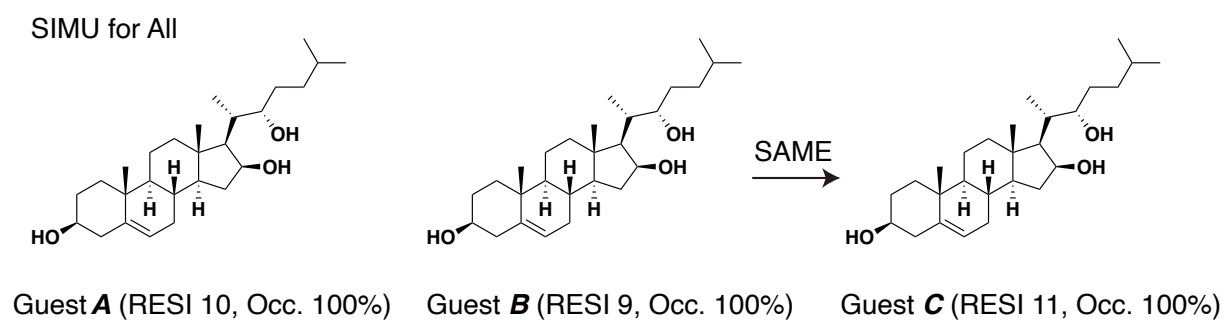


**Fig. 3–29** Restraints applied in the refinement of the guest molecules **7**.

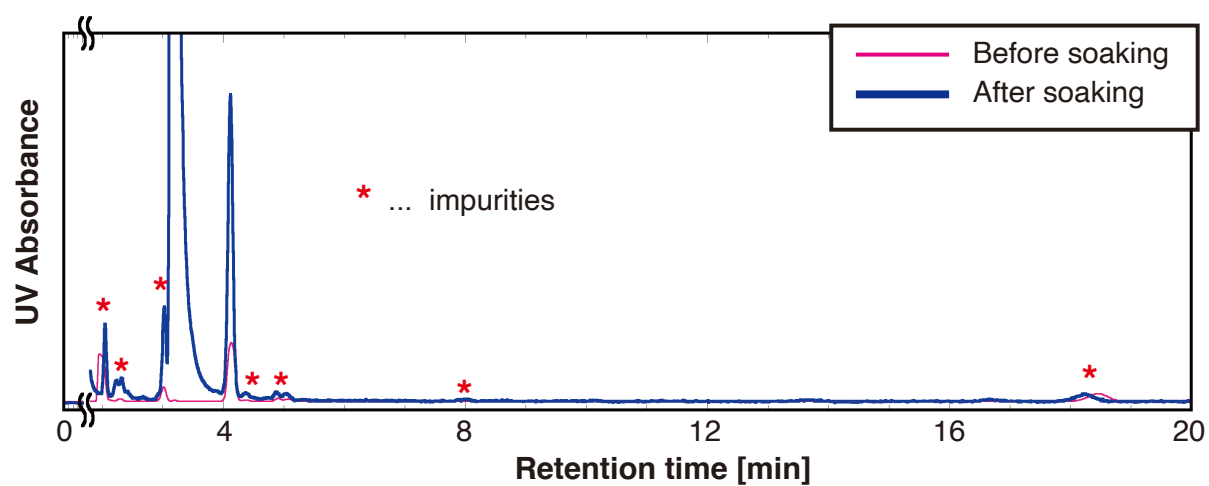


**Fig. 3–30** CSAS using the yeast extract containing **7**. Outline of the HPLC profiling experiments before (magenta) and after (blue) contact with the CS is shown. The intensity is normalized so that summation of the impurity peak at 18.0 min becomes constant.

### 3.7 References

- [1] a) M. Hoshino, A. Khutia, H. Xing, Y. Inokuma and M. Fujita, *IUCrJ* **2016**, *3*, 139-151; b) N. Zigon, V. Duplan, N. Wada and M. Fujita, *Angew. Chem. Int. Ed.* **2021**, *60*, 25204-25222.
- [2] T. R. Ramadhar, S. L. Zheng, Y. S. Chen and J. Clardy, *Chem. Commun.* **2015**, *51*, 11252-11255.
- [3] F. Sakurai, A. Khutia, T. Kikuchi and M. Fujita, *Chem. Eur. J.* **2017**, *23*, 15035-15040.
- [4] a) T. R. Ramadhar, S. L. Zheng, Y. S. Chen and J. Clardy, *Acta Crystallogr. A* **2015**, *71*, 46-58; b) K. Li, D. S. Yang, X. F. Gu and B. Di, *Fitoterapia* **2019**, *134*, 135-140.
- [5] Y. Taniguchi, R. Matsumoto and T. Kadota, *Chem. Eur. J.* **2020**, *26*, 15799-15803.
- [6] T. R. Ramadhar, S. L. Zheng, Y. S. Chen and J. Clardy, *CrystEngComm* **2017**, *19*, 4528-4534.
- [7] Y. Inokuma, S. Yoshioka, J. Ariyoshi, T. Arai and M. Fujita, *Nat. Protoc.* **2014**, *9*, 246-252.
- [8] R. A. Engh and R. Huber, *Acta Cryst. A* **1991**, *47*, 392-400.
- [9] B. Christ, C. Xu, M. Xu, F. S. Li, N. Wada, A. J. Mitchell, X. L. Han, M. L. Wen, M. Fujita and J. K. Weng, *Nat. Commun.* **2019**, *10*, 3206.
- [10] B. Watanabe, K. Makino, M. Mizutani and H. Takaya, *Tetrahedron* **2021**, *91*, 132194.
- [11] M. Kuroda, K. Ori, H. Takayama, H. Sakagami and Y. Mimaki, *Steroids* **2015**, *93*, 96-104.
- [12] K. Kawashima, Y. Mimaki and Y. Sashida, *Chem. Pharm. Bull.* **1991**, *39*, 2761-2763.
- [13] G. M. Sheldrick, *Acta Cryst. A* **2015**, *71*, 3-8.
- [14] G. M. Sheldrick, *Acta Cryst. C* **2015**, *71*, 3-8.
- [15] A. L. Spek, *J. Appl. Crystallogr.* **2003**, *36*, 7-13.
- [16] A. L. Spek, *Acta Cryst. C* **2015**, *71*, 9-18.
- [17] S. Parsons, H. D. Flack and T. Wagner, *Acta Cryst. B* **2013**, *69*, 249-259.





## **Chapter 5**

### **Summary and Perspectives**

This doctoral thesis focuses on establishing a novel research workflow in natural product chemistry on the premise of utilizing the crystalline sponge method. Extraction and structural analyses of chemical compounds from bulk quantities of living materials have remained to be rate-determining steps in natural product chemistry. The crystalline sponge method had facilitated structural analyses by minimizing the quantities of isolated natural products required for compound characterization and enabling single crystal X-ray diffraction (SCXRD) experiments without crystallization. In this thesis, I furthermore demonstrate that structural analysis part can be performed more efficiently (with less quantities of crude extracts

and isolated compounds) by screening the affinity between crystalline sponges and analytes, and that the novel research workflow proposed in this thesis enables structural elucidation of trace amounts of unknown natural products that should be untouchable if the whole research scheme is based on the conventional workflow.

Chapter 2 introduces a new research scheme with the crystalline sponge. Crystalline sponge affinity screening (CSAS) assesses the affinity between the host framework and the guest analytes prior to compound isolation. Absolute structures of six natural products, that showed good affinity to the framework, were successfully characterized with the crystalline sponge method. If CSAS is combined with optimization of the guest-soaking conditions from a mixture of multiple analytes, it would allow high throughput identification of the optimal guest-soaking condition for structural analysis.<sup>[1]</sup>

Chapter 3 describes the application scope of the crystalline sponge method is expanded through optimization of the guest-soaking conditions. Notably, I find that the choice of solvents is an important parameter for ordering the guest molecules in the cavity of the crystalline sponges. Ketone and ester solvents can co-crystallize with the guests and suppress the disorder of a series of steroidal molecules.

Chapter 4 illustrates that novel natural products discovered in a cutting-edge natural product research are completely characterized to absolute structural level from minimal quantities of isolated samples by the crystalline sponge method. Especially, for one compound, haraldol, had it not been for the novel research workflow based on the crystalline sponge

method, the structural elucidation would not be accomplished because of non-crystalline and volatile natures as well as limited isolated quantities.

As a general summary, this thesis work proposed a novel research workflow in structural analysis from natural product extract mixtures and demonstrated that quantities of each isolated natural product can be reduced from (previously) milligram scales to (newly) microgram scales by utilizing the crystalline sponge method.

Future modifications in the crystalline sponge method would potentially reduce the required quantities furthermore. For instance, in this thesis work, SCXRD analysis with the crystalline sponge method is performed from single crystals with ca. 100  $\mu\text{m}$  length using in-house X-ray sources. Currently, SCXRD experiments can be performed with single crystals with 1–10  $\mu\text{m}$  length by high-flux synchrotron radiation. This would bring additional scale-down effects and required compound amounts could be reduced to nanogram-to-picogram scales. One promising application of this workflow may be in combination with pharmacokinetics. Currently, metabolites of medicinal small molecules are typically detected by liquid chromatography - mass spectrometry (LC-MS) from biological samples with ng/mL to  $\mu\text{g/mL}$  amounts. However, as known, MS does not give information of detail chemical structures of target compounds including configurations. If pharmacokinetic research is performed with nanogram-scale preparative LC combined with the synchrotron-based crystalline sponge method, chemical information of medicine metabolism would be obtained to structural level.

The combination of the crystalline sponge method with cryo-microscopy (CryoEM) method microcrystal electron diffraction (MicroED)<sup>[3]</sup> is also considered to bring further scale-down effects. Owing to the recent improvements of electron detectors and measurement techniques, atomic resolution ( $<1$  Å) crystal structures can be obtained from femtogram-scale microcrystals with electron crystallography. Although it is still uncertain whether the crystalline sponge can be physically stable at high-vacuum conditions used in CryoEM experiments and whether the current guest-soaking protocols are effective for sample preparations with microcrystals, the expected scale-down effect should establish a novel structural analysis workflow that provides three-dimensional chemical structures in unprecedented tiny scales.

## References

- [1] L. Rosenberger, C. von Essen, A. Khutia, C. Kuhn, K. Georgi, A. K. H. Hirsch, R. W. Hartmann and L. Badolo, *Eur. J. Pharm. Sci.* **2021**, *164*, 105884.
- [2] S. Suzuki, T. Minamidate, A. Shiga, Y. Ruike, K. Ishiwata, K. Naito, A. Ishida, H. Deguchi, M. Fujimoto, H. Koide, I. Tatsuno, J. I. Ikeda, Y. Yamazaki, H. Sasano and K. Yokote, *BMC Endocr. Disord.* **2020**, *20*, 173.
- [3] D. Shi, B. L. Nannenga, M. G. Iadanza and T. Gonen, *eLife* **2013**, *2*, e01345.

## List of Publications

1. **N. Wada**, R. D. Kersten, T. Iwai, S. Lee, F. Sakurai, T. Kikuchi, D. Fujita, M. Fujita, J.-K. Weng,  
Crystalline-Sponge-Based Structural Analysis of Crude Natural Product Extracts  
*Angew. Chem. Int. Ed.* **2018**, *57*, 3671–3675. [Chapter 2]
2. B. Christ, C. Xu, M. Xu, F.-S. Li, **N. Wada**, A. J. Mitchell, M. Wen, M. Fujita, J.-K. Weng,  
Repeated evolution of cytochrome P450-mediated spiroketal steroid biosynthesis in plants  
*Nat. Commun.* **2019**, *10*, 3206. [Chapter 3]
3. N. Zigon, V. Duplan, **N. Wada**, M. Fujita,  
Crystalline Sponge Method: X-ray Structure Analysis of Small Molecules by Post-Orientation  
within Porous Crystals-Principle and Proof-of-Concept Studies  
*Angew. Chem. Int. Ed.* **2021**, *60*, 25204–25222. [Chapter 1]
4. **N. Wada**, K. Kageyama, Y. Jung, T. Mitsuhashi, M. Fujita,  
Solvent Effects in the Crystalline Sponge Method: Importance of Co-solvents for Ordering  
Absorbed Guests  
*Org. Lett.* **2021**, *23*, 9288–9291. [Chapter 3]
5. **N. Wada**, T. Mitsuhashi, R. D. Kersten, J.-K. Weng, M. Fujita,  
The Crystalline Sponge Method Enables Rapid and Scaled-Down Structural Determination of  
Terpene Synthase Products of Red Algal Origin  
*Manuscript in preparation.* [Chapter 4]

### [Other Publication]

6. **和田直樹**, 藤田誠 「結晶スポンジ法による天然化合物の構造決定」,ファルマシア, **2019**,  
55, 668–670.

## Acknowledgements

My deepest appreciation goes to my supervisor, Professor, Dr. Makoto Fujita for his valuable suggestions and warm encouragement throughout my research life. I am appreciative to Associate Professor, Dr. Jing-Ke Weng (Massachusetts Institute of Technology; MIT and Whitehead Institute for Biomedical Research), Assistant Professor, Dr. Roland Kersten (University of Michigan), and Junior Group Leader, Dr. Tomáš Pluskal (Institute of Organic Chemistry and Biochemistry) for providing valuable algal samples and supervising my biological experiments.

I am also indebted to Project Professor, Dr. Sota Sato, Associate Professors, Dr. Daishi Fujita (Kyoto University) and Dr. Tomohisa Sawada, Assistant Professors, Dr. Yuya Domoto and Dr. Hiroki Takezawa, Research Assistant Professors, Dr. Takaaki Mitsuhashi (Institute for Molecular Science; IMS) and Dr. Takahiro Nakama, former Researchers, Dr. Fumie Sakurai, Dr. Takashi Kikuchi (Rigaku Corporation), Mr. Takahiro Iwai (Japan Tobacco Inc.), and Dr. Shoukou Lee for their constructive mentorship and research suggestions. Especially, I appreciate Dr. Mitsuhashi for kind guidance during my doctoral research.

I thank Chief of Technical Division, Ms. Tomoko Mori (National Institute for Basic Biology; NIBB), Subunit Chief of Technical Division, Ms. Yumiko Makino (NIBB), Assistant Professors, Dr. Maho Yagi (IMS) and Dr. Saeko Yanaka (IMS), and Principal Research Scientist, Dr. Peter Müller (MIT) for helping data collection in Chapter 3 and 4.

I would like to thank Associate Professor, Dr. Tetsuro Kusamoto (IMS), Secretaries Ms. Yukari Ara and Ms. Michiko Masuda (IMS) for their numerous supports for my comfortable life in the laboratory.

I appreciate Mr. Ko Kageyama and Mr. Youngcheol Jung for designing experiments in Chapter 3 and sharing life in Okazaki together. I could share fruitful research life with my colleagues, Dr. Yukari Tamura, Dr. Jiazhao Chen (IMS), Mr. Yuuki Inomata, Ms. Haruka Sunohara, Ms. Anouk Rossen, Mr. Boyu Zhou, Mr. Yikuan Yu, Mr. Chieon Park, Mr. Shingo Funami, Mr. Satoshi Yoshida, and all the former and the current members in Fujita Laboratory.

My appreciation goes to Materials Education program for the future leaders in Research, Industry, and Technology (MERIT) Fellowship and JSPS Research Fellowship for Young Scientists [Grant Number: 19J22015] for the financial supports.

Finally, I wish to express my warmest gratitude to my friends and family members (T.W., M.W., and Y.W.) who continuously supported me throughout my life.

**Naoki Wada**

December 2021